# PARITY-TIME SYMMETRY IN NON-HERMITIAN QUANTUM WALKS

A Dissertation

Submitted to the Faculty

of

Purdue University

by

Franck Assogba Onanga

In Partial Fulfillment of the

Requirements for the Degree

of

Doctor of Philosophy

December 2019

Purdue University

West Lafayette, Indiana

# THE PURDUE UNIVERSITY GRADUATE SCHOOL
# STATEMENT OF DISSERTATION APPROVAL

Dr. Yogesh Joglekar, Chair
Department of Physics
Dr. Ricardo Decca
Department of Physics
Dr. Gautam Vemuri
Department of Physics
Dr. Stephen Wassall
Department of Physics
Dr. Gabor Csathy
Department of Physics

**Approved by:**

Dr. John Finley
Head of the Department Graduate Program

I dedicate this to my family, especially my children, Nadirath Assogba, Faridath Assogba Onanga and Fazeel Assogba Onanga.

# ACKNOWLEDGMENTS

First and foremost, I would like to thank God for giving me the patience and strength to accomplish this modest work.

Next, I would like to express my sincere gratitude to my advisor, Prof. Yogesh N. Joglekar, for the continuous support of my Ph.D study and related research, for his motivation, immense knowledge and faith in my work. His guidance helped me in all the time of research and writing of this thesis. I could not have imagined having a better advisor and mentor for my graduate study.

Besides my advisor, I would like to thank the rest of my thesis committee: Prof. Ricardo Decca, Prof. Gautam Vemuri, Prof. Stephen Wassal, and Prof. Gabor Csathy, for their interest in my research by accepting to be part of my thesis committee and for their insightful comments and encouragement.

I also would like to thank and express my gratitude to all my professors, faculty members and staff from the Physics and Prof. Bruce Kitchens from the Mathematics department for their contribution to my achievement.

I would like thank my research group fellow students for the stimulating discussions we had these years.

Last but not the least, I would like to thank my family: my children for their patience and understanding and my family for giving the support the could throughout my life.

TABLE OF CONTENTS

Page

# LIST OF FIGURES

Figure Page

Figure Page

# LIST OF TABLES

# ABSTRACT

Assogba Onanga, Franck Ph.D., Purdue University, December 2019. Parity-Time Symmetry in Non-Hermitian Quantum Walks. Major Professor: Yogesh N. Joglekar.

Over the last two decades a new theory has been developed and intensively investigated in quantum physics. The theory stipulates that a non-Hermitian Hamiltonian can also represents a physical system as long as its energy spectra can be purely real in certain regime depending on the parameters of the Hamiltonian. It was demonstrated that the reality of the eigenenergy was conditioned by a certain kind of symmetry embedded in the actual non-Hermitian system. Indeed, such systems have a combined reflection (parity) symmetry ($\mathcal{P}$) and time-reversal symmetry ($\mathcal{T}$), $\mathcal{PT}$ symmetry. The theory opens the door to new features particularly in open systems in which there could be gain and/or loss of particle or energy from and/or to the environment. A key property of the theory is the $\mathcal{PT}$-symmetry breaking transition phenomenon which occurs at the exceptional point (EP). The exceptional points are special degeneracies characterized by a coalescence of not only the eigenvalues but also of the corresponding eigenvectors of the system; and the coalescence happens when the gain-loss strength, a measure of the openness of the system, exceeds the intrinsic energy-scale of the system.

In recent years, quantum walks with $\mathcal{PT}$-symmetric non-unitary time evolution have been realized in systems with balanced gain and loss. These systems fall in two categories namely continuous time quantum walks (CTQW) that are characterized by a unitary or non-unitary time evolution Hamiltonian, and discrete-time quantum walks (DTQW) whose dynamic is described by a unitary or non-unitary time evolution operator consisting of a product of shift, coin, and gain-loss operations.

In this thesis, we investigate the $\mathcal{PT}$-symmetric phase of CTQW and DTQW in a variety of non-Hermitian lattice systems with both position-dependent and position-independent, parity-symmetric tunneling functions in the presence of $\mathcal{PT}$-symmetric impurities located at arbitrary parity-symmetric site on the lattice. Moreover, we explore the topological phase diagram and its novel features in non-Hermitian, homogeneous and non-homogeneous, $\mathcal{PT}$-symmetric DTQW with closed or open boundary conditions. We conduct our study using analytical and numerical approaches that are directly and easily implementable in physical experiments. Among others, we found that, despite their non-unitary evolution, open systems governed by parity-time symmetric Hamiltonians support conserved quantities and that the $\mathcal{PT}$-symmetry breaking threshold depends on the physical structure of the Hamiltonian and its underlying symmetries.

# 1. INTRODUCTION

The first two chapters of this thesis interpolate material from four papers by the author [1–4]. Chapter 1 uses material from references [1] and [2], both coauthored with Andrew K. Harter and Yogesh N. Joglekar. Meanwhile, chapter 2 is based on reference [3], coauthored with Yogesh N. Joglekar and Andrew K. Harter and [4], coauthored with Zhihao Bian *et* al..Some material from each of these papers has also been incorporated into this introduction chapter.

From the beginning of the last century, the world has witnessed scientific and technical development as the result of the discovery and study of the field of quantum mechanics. Quantum mechanics is a physical science dealing with the behaviour of matter and energy on the scale of atoms and subatomic particles and waves. The success of quantum mechanics comes from its accuracy on predicting physical behaviour of systems, including systems where Newtonian mechanics has failed. Quantum mechanics has been the foundation of several related disciplines including condensed matter physics [5], quantum chemistry [6, 7], particle physics [8], nanotechnology and electronics [9].

In quantum mechanics the state of a physical system is represented by a vector in a Hilbert space which is a complex vector space with an inner product that makes it a complete, metric space. In the Hilbert space $L^2(\mathbb{R})$ of square-integrable complex-valued functions $\psi : \mathbb{R} \to \mathbb{C}$, the inner product of two wave functions is given by

$$\langle \phi | \psi \rangle = \int_{-\infty}^{+\infty} dx \phi(x)^* \psi(x). \tag{1.1}$$

Additionally in standard quantum mechanics, a Hamiltonian describing a closed physical system is required to possess Hermiticity, sufficient condition that guaranties real

eigenenergy of the system. An operator $A$ defined in the Hilbert space is called Hermitian with respect to the standard inner product if

$$\int (\hat{A}\phi)^* \phi dx = \int \phi^* \hat{A}\phi dx. \tag{1.2}$$

Particularly, the position operator $\hat{x}$ and the momentum operator are Hermitian operators. As a consequence, the Hamiltonian operator is Hermitian. Indeed, computing an inner product involving the position operator $\hat{x}$, we have

$$\int (\hat{x}\phi)^* \phi dx = \int (x\phi)^* \phi dx = \int \phi * x\phi dx = \int \phi * \hat{x}\phi dx,$$

thus, the position operator $\hat{x}$ is Hermitian. Similarly, computing an inner product with the momentum operator $\hat{p}$, we have,

$$\begin{aligned} \int (\hat{p}\phi)^* \phi dx &= \int \left(-i\hbar \frac{d\phi}{dx}\right)^* \phi dx \\ &= i\hbar \int \left(\frac{d\phi}{dx}\right)^* \phi dx \end{aligned}$$

and after integrating by part with the condition that $\phi$ is a smooth complex function rapidly decreasing at infinity, we get on the right-hand side

$$-i\hbar \int \phi^* \frac{d\phi}{dx} dx = \int \phi^* \hat{p}\phi dx,$$

hence, the momentum operator defined by $\hat{p} = -i\hbar d/dx$ is Hermitian. Moreover, the kinetic energy operator $\hat{K} = \hat{p}^2/2m$ is Hermitian since,

$$\begin{aligned} \int (\hat{K}\phi) * \phi dx &= \frac{1}{2m} \int (\hat{p}^2\phi)^* \\ &= \frac{1}{2m} \int (\hat{p}\phi)^* \hat{p}\phi dx \\ &= \frac{1}{2m} \int \phi^* \hat{p}^2 \phi dx \\ &= \int \phi^* \hat{K}\phi dx. \end{aligned}$$

Therefore, the Hamiltonian given by $\hat{H} = \hat{K} + \hat{V}(\hat{x})$ is Hermitian.

Consider a Hamiltonian $\hat{H}$ with an energy eigenvector $|\phi_n\rangle$, such that $\hat{H}|\phi_n\rangle = E_n|\phi_n\rangle$, we have

$$\begin{aligned} \hat{H}|\phi_n\rangle &= E_n|\phi_n\rangle \\ \implies \langle\phi_n|\hat{H}^\dagger &= E_n^*\langle\phi_n| \\ \implies \langle\phi_n|\hat{H} &= E_n^*\langle\phi_n|. \end{aligned} \tag{1.3}$$

Combining the three lines of Eq. 1.3, we get

$$\begin{aligned} \langle\phi_n|\hat{H}|\phi_n\rangle &= E_n^*\langle\phi_n|\phi_n\rangle \\ &= E_n\langle\phi_n|\phi_n\rangle, \end{aligned} \tag{1.4}$$

since $\langle\phi_n|\phi_n\rangle \neq 0$ it follows that

$$E_n^* = E_n. \tag{1.5}$$

Thus, Hermiticity guarantees real energy spectra. Moreover, the eigenvectors of a Hermitian operator are orthogonal. Indeed, by changing the subscript $n$ to $m$ and taking the Hermitian conjugate in the second line of and combining all the lines of Eq. 1.3, we get

$$\begin{aligned} \langle\phi_n|\hat{H}|\phi_m\rangle &= E_n\langle\phi_m|\phi_n\rangle \\ &= E_m\langle\phi_n|\phi_m\rangle, \end{aligned} \tag{1.6}$$

it follows that

$$(E_n - E_m)\langle\phi_n|\phi_m\rangle = 0, \tag{1.7}$$

which implies that the eigenvectors are orthogonal if the energy eigenvalues are non-degenerate. In quantum mechanic, the evolution of a wavefunction forward in time is defined by applying the time evolution operator. For a time independent Hamiltonian, we have

$$|\phi(t)\rangle = \hat{U}|\phi(0)\rangle, \tag{1.8a}$$

$$\hat{U} = e^{-i\hat{H}t/\hbar}, \tag{1.8b}$$

where $\hat{U}$ denotes the time-evolution operator and $\hbar = h/2\pi$ is the reduced Plank constant; without loss of generality, let us set $\hbar = 1$. The Hermiticity of the Hamiltonian guarantees the unitarity, which by extension implies the probability conservation, of the time evolution operator [10]. Actually, $U^{\dagger}(t)U(t) = \exp(+iHt)\exp(-iHt) = 1$.

In reality, except the whole universe there is no such thing as closed system because of an exchange of energy or particles with the environment of the system, in which case the Hamiltonian of the system is no longer Hermitian. Non-Hermitian Hamiltonian have been ideologically used to describe open system with gain and/or loss that result with interaction with the environment. In 1998, Bender and Boettcher [11] showed that a large class of non-Hermitian Hamiltonians can have an entirely real spectra as long as the system possesses parity-time ($\mathcal{PT}$) symmetry, a combined parity symmetry ($\mathcal{P}$) and time-reversal symmetry ($\mathcal{T}$). The parameter space over which the spectrum of the $\mathcal{PT}$-symmetric Hamiltonian is real is called the region of unbroken $\mathcal{PT}$ symmetry, in which case every eigenfunction of the $\mathcal{PT}$-symmetric Hamiltonian is also an eigenfunction of the $\mathcal{PT}$ operator. Broken $\mathcal{PT}$ symmetry occurs when some eigenvalues of the $\mathcal{PT}$-symmetric Hamiltonian become complex; thus, the Hamiltonian and the $\mathcal{PT}$ operator no longer share simultaneous eigenfunctions. $\mathcal{PT}$-symmetric systems can be thought of as intermediate between traditionally closed and open systems. Indeed, an unbroken $\mathcal{PT}$-symmetric system resembles a closed system because it is in equilibrium; however, it is not closed because it is in contact with the external environment. Similarly, a broken $\mathcal{PT}$-symmetric resembles an open system because it is not in equilibrium but unlike most open systems the net probability flux vanishes and the system has $\mathcal{PT}$ symmetry. The parity operator, space-reflection operator, $\mathcal{P}$ operates on a particular state to give the reflection-symmetric version of the original state, and $\mathcal{P}^2 = \mathbf{1}$, where $\mathbf{1}$ is the identity matrix. $\mathcal{P}$ is a linear operator because it satisfies the condition

$$\mathcal{P}(a\,|\Psi\rangle + b\,|\Phi\rangle) = a\mathcal{P}\,|\Psi\rangle + b\mathcal{P}\,|\Phi\rangle\,. \tag{1.9}$$

The time-reversal operator $\mathcal{T}$ is an antilinear operator that performs complex conjugation ($\mathcal{T}^2 = \mathbf{1}$) and it satisfies the condition

$$\mathcal{T}(a\,|\Psi\rangle + b\,|\Phi\rangle) = a^*\mathcal{T}\,|\Psi\rangle + b^*\mathcal{T}\,|\Phi\rangle\,. \tag{1.10}$$

The action of the parity operator $\mathcal{P}$ on the quantum-mechanical coordinate operator $\hat{x}$ and the momentum operator $\hat{p}$ is to change their signs:

$$\mathcal{P}\hat{x}\mathcal{P} = -\hat{x} \qquad \text{and} \qquad \mathcal{P}\hat{p}\mathcal{P} = -\hat{p}. \tag{1.11}$$

The effect of the time-reversal operator on $\hat{x}$ and $\hat{p}$ is given by

$$\mathcal{T}\hat{x}\mathcal{T} = \hat{x} \qquad \text{and} \qquad \mathcal{T}\hat{p}\mathcal{T} = -\hat{p} \tag{1.12}$$

Both, the parity operator $\mathcal{P}$ and the time-reversal operator $\mathcal{T}$ leaves invariant the Heisenberg commutation relation of quantum mechanics,

$$\hat{x}\hat{p} - \hat{p}\hat{x} = \mathrm{i}\hbar\mathbf{1}; \tag{1.13}$$

with the condition,

$$\mathcal{T}\mathrm{i}\mathcal{T} = -\mathrm{i}. \tag{1.14}$$

Moreover, P and T operators commute:

$$\mathcal{P}\mathcal{T} - \mathcal{T}\mathcal{P} = 0, \tag{1.15}$$

it follows that

$$(\mathcal{P}\mathcal{T})^2 = 1. \tag{1.16}$$

For a system described by a (Hermitian or non-Hermitian) Hamiltonian $H$ to have $\mathcal{P}\mathcal{T}$ symmetry, it is required that the Hamiltonian satisfies the following relation:

$$(\mathcal{P}\mathcal{T})H(\mathcal{P}\mathcal{T})^{-1} = (\mathcal{P}\mathcal{T})H(\mathcal{P}\mathcal{T}) = H, \tag{1.17}$$

in which case $H$ and $\mathcal{P}\mathcal{T}$ may share a common set of eigenfunctions [11–14].

$$H\,|\Psi_n\rangle = E_n\,|\Psi_\lambda\rangle\,, \quad \mathcal{P}\mathcal{T}\,|\Psi_n\rangle = \lambda\,|\Psi_n\rangle\,. \tag{1.18}$$

A multiplication of the second equality in Eq. 1.18 by $\mathcal{PT}$ from the right hand side and the use of the property $(\mathcal{PT})^2$ give,

$$\begin{aligned} \mathcal{PT}(\mathcal{PT}\left|\Psi_n\right\rangle) &= \mathcal{PT}(\lambda\left|\Psi_n\right\rangle, \\ (\mathcal{PT})^2\left|\Psi_n\right\rangle &= \lambda^*\mathcal{PT}\left|\Psi_n\right\rangle, \\ \left|\Psi_n\right\rangle &= \lambda^*(\lambda\left|\Psi\right\rangle, \\ \left|\Psi_n\right\rangle &= \left|\lambda\right|^2\left|\Psi_n\right\rangle \end{aligned} \tag{1.19}$$

Therefore, $|\lambda|^2 = 1$ and the eigenvalue $\lambda$ is a pure phase, $\lambda = e^{\mathrm{i}\alpha}$. One can choose the phase $\alpha$ such that $\lambda = 1$; thus, $\mathcal{PT}\left|\Psi_n\right\rangle = \left|\Psi_n\right\rangle$. A multiplication of the first equality in Eq. 1.18 from the right hand side gives,

$$\begin{aligned} \mathcal{PT}(H\left|\Psi_n\right\rangle) &= \mathcal{PT}(E_n\left|\Psi_n\right\rangle, \\ H(\mathcal{PT}\left|\Psi_n\right\rangle) &= E_n^*(\mathcal{PT}\left|\Psi_n\right\rangle, \\ H\left|\Psi_n\right\rangle &= E_n^*\left|\Psi_n\right\rangle, \\ E_n\left|\Psi_n\right\rangle &= E_n^*\left|\Psi_n\right\rangle, \\ E_n &= E_n^*. \end{aligned} \tag{1.20}$$

This confirms that the eigenvalue is real when the Hamiltonian $H$ and $\mathcal{PT}$ share simultaneously the same set of eigenfunctions. The combined symmetry operator $\mathcal{PT}$ is a unitary operator that can still prevail for a non-Hermitian Hamiltonian even if that Hamiltonian has neither parity symmetry ($\mathcal{P}$) nor time-reversal symmetry ($\mathcal{T}$). $\mathcal{PT}$-symmetric Hamiltonians correspond to a particular figures of pseudo-Hermitian operators. A linear operator $O$ is pseudo-Hermitian if there is a Hermitian operator $\eta$ such that $O^\dagger = \eta O \eta^{-1}$. In fact, for $\eta = \mathbf{1}$ and $\eta = \mathcal{P}$ we retrieve the conditions for Dirac Hermiticity and $\mathcal{PT}$ symmetry respectively [12]. With this kind of pseudo-Hermitian design of the Hamiltonian, the eigenfunctions are no longer orthogonal and the structure of the vector space of the eigenmodes is completely changed. A sharp symmetry-breaking transition is established once the non-Hermicity parameter exceeds a certain threshold value. In that regime, the Hamiltonian and the parity-time operator, despite they still commute, have different sets of eigenfunctions and

the eigenvalues of the system are no longer real. Furthermore, there is a creation of singular points, exceptional points (EP), at the $\mathcal{PT}$ breaking region where the eigenvalue branches merge. The number of coalesced eigenvalues will denote the order of the EP. These points have a prominent role in $\mathcal{PT}$-symmetry studies [11–13]. Despite serious challenges posed by decoherence and other factors, the past decade have witnessed a large number of experimental realizations of $\mathcal{PT}$-symmetry systems specially in optical and photonic lattices [15–29]. In general, the parameter space must be investigated analytically or numerically to find the domain where the eigenvalues remain real. As an example, for a $2 \times 2$ non-Hermitian Hamiltonian defined by

$$H = \begin{pmatrix} i\gamma & -J \\ -J & -i\gamma \end{pmatrix}, \tag{1.21}$$

where the energy parameters $J$ and $\gamma$ are non-negative real numbers. Solving the eigenvalue problem gives two energy eigenvalues as

$$\lambda_{\pm} = \pm\sqrt{J^2 - \gamma^2}. \tag{1.22}$$

Figure 1.1 shows the variations of the eigenvalues as a function of $\gamma$ with respect to $J$. The top panel shows the real part of the eigenvalues as a function of $\gamma/J$, where the eigenvalues are purely real (unbroken $\mathcal{PT}$ symmetry) for $\gamma < J$. As the value of $\gamma$ increases toward $J$, the eigenvalues begin to converge until they coalesce at the $\mathcal{PT}$-symmetry-breaking threshold $\gamma_{\mathcal{PT}} = J$, with the emergence of exceptional point of order 2 (EP2). The bottom panel reveals that for $\gamma > J$ the $\mathcal{PT}$ symmetry is broken, and the eigenvalues are purely imaginary. In a similar way to their eigenvalues, the eigenvectors coalesce at the exceptional point $\gamma = J$. In the unbroken region where $\gamma < J$, the normalized eigenvectors are given by

$$u_{\pm} = \frac{1}{\sqrt{2}} \begin{pmatrix} 1 \\ \frac{i\gamma \pm \sqrt{J^2-\gamma^2}}{J} \end{pmatrix}. \tag{1.23}$$

At $\gamma = 0$, the Hamiltonian is Hermitian and the eigenvalues are orthonormal; but as $\gamma \to J^-$ the eigenvectors are still linearly independent but not orthogonal, dynamic

that is justified by a modulation of the Dirac norm in the unbroken region. In the broken region where $\gamma > J$, the normalized eigenvectors are given by

$$v_{\pm} = J\left(2\gamma^2 \mp 2\gamma\sqrt{\gamma^2 - J^2}\right)^{-1/2} \begin{pmatrix} 1 \\ \frac{i\gamma \mp i\sqrt{\gamma^2 - J^2}}{J} \end{pmatrix}. \tag{1.24}$$

The angle between the two eigenvectors in the unbroken and broken $\mathcal{PT}$ symmetry regions are

$$\begin{aligned} < \widehat{u_+, u_-} > &= \cos^{-1}\left(\frac{\mathrm{Re}(u_+ \cdot u_-)}{\|u_+\|\,\|u_-\|}\right) \\ &= \cos^{-1}(\frac{\gamma}{J}) \end{aligned} \tag{1.25a}$$

$$< \widehat{v_+, v_-} > = \cos^{-1}(\frac{J}{\gamma}) \tag{1.25b}$$

respectively. Indeed, when $\gamma = 0$ (Hermitian system), the eigenvectors are orthogonal and as $\gamma$ increases toward $J$, they are closing on each other where the angle between them decreases until they become parallel at $\gamma = J$, then start pulling away from each other as $\gamma$ is becoming larger than $J$.

Although the initial focus of $\mathcal{PT}$ symmetry theory was to develop a complex extension of the quantum mechanics [13], in recent years, the study of $\mathcal{PT}$ symmetric systems has gained much interest for its successful application to open systems with balanced gain and loss [30]. Typically, in such a system, the parity symmetry denotes a reflection symmetry in its spatial arrangement, and when balanced gain and loss (which lead to non-Hermiticity) are introduced, the resultant open system is intrinsically $\mathcal{PT}$-symmetric. For small gain and loss rates, the eigenvalues of the $\mathcal{PT}$-symmetric Hamiltonian describing such a system remain real; but when the strength of the gain/loss exceeds the $\mathcal{PT}$-symmetry breaking threshold, two or more of its eigenvalues become first, degenerate and then complex-conjugate pairs. This emergence of complex conjugate eigenvalues is known as $\mathcal{PT}$ symmetry breaking and leads to unbounded, exponential violation of unitarity in the time-development of the system because one expects the probability defined by the norm of the vector state to remain constant in time.. Thus, below the threshold, the system remains

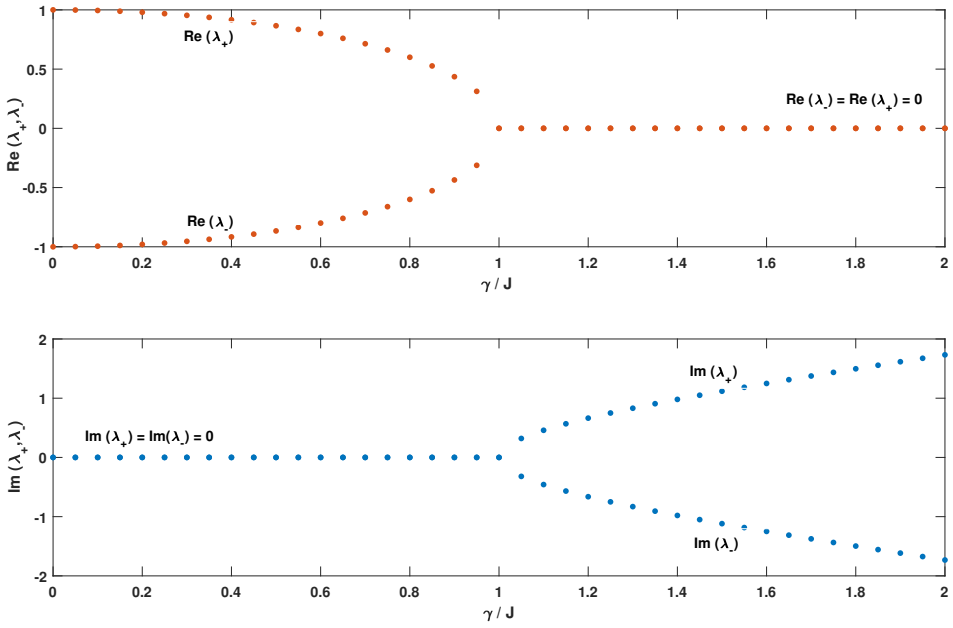


Fig. 1.1. Top panel: Real part of the eigenvalues $\lambda_{\pm}$ as a function of $\gamma$ with respect to $J$, Eq. 1.22. For $\gamma < J$, the eigenvalues are purely real, meaning an unbroken $\mathcal{PT}$ symmetry. Bottom panel: Imaginary part of $\lambda_{\pm}$ as a function of $\gamma/J$. For $\gamma > J$, the $\mathcal{PT}$ symmetry is broken, and the eigenvalues are purely imaginary. At the $\mathcal{PT}$-symmetry-breaking threshold, $\gamma = J$, the eigenvalues coalesce.

in a quasi equilibrium state, and above it, the system is far removed from equilibrium. The existence of a finite threshold is the hallmark of a $\mathcal{PT}$ symmetry breaking transition and the accompanying phenomena that occur at the exceptional point [31]. While $\mathcal{PT}$-symmetric Hamiltonian may, in general, be continuous in their degrees of freedom, it is the discrete $\mathcal{PT}$-symmetric systems that have proven to be the experimentally implementable ones. Recent developments in the fabrication techniques of optical devices have led to the ability to easily create and control arrays of coupled optical waveguides, and the couplings of these arrays can be tuned to match the dynamics of a large variety of different tight-binding Hamiltonians [32–34]. controlled loss and gain can also be implemented relatively straightforwardly, allowing

the observable dynamics to extend into the non-Hermitian realm [18, 35, 36], while cost-effective fabrication processes promise to further boost the importance of such tunable systems [37]. The interactions within theses systems, in one dimension, are dominated by nearest-neighbor hopping; however, for certain one or two dimensional waveguide geometries, higher order (or long-range) hopping can be made relevant. These systems have been greatly successful in demonstrating a variety of quantum phenomena, including localization and the presence of edge modes in a classical, and experimentally viable setting [38].

On the other end, in recent years, quantum walks, which are quantum analogue of classical random walks, with non-unitary evolution have been realized in systems with balanced gain and loss. These systems fall in two categories namely continuous time quantum walks (CTQW), characterized by an Hermitian or non-Hermitian, $\mathcal{PT}$ symmetric Hamiltonian [39], and discrete-time quantum walks (DTQW) which are defined by a unitary or non-unitary time evolution operator consisting of shift, coin, and gain-loss operations [40]. Our study is largely focused on non-Hermitian CTQW and non-unitary DTQW models where gain and loss are located at reflection-symmetric sites.

In this thesis we investigate CTQW described by a time-evolution of a non-Hermitian Hamiltonian with a $\mathcal{PT}$-symmetry, and DTQW models where gain and loss are localized at reflection-symmetric sites, and investigate the interplay between PT breaking transition that is governed by gain-loss strength and topological transitions that are governed by coin operators. In chapter 1, we investigate the $\mathcal{PT}$-breaking phenomena for a real, parity-symmetric, hopping Hamiltonian augmented by a non-Hermitian, balanced, gain-loss potential. Our results are found using a tight-binding model through simulation in Matlab. We present a new class of discrete models in which the tunneling Hamiltonian is not parity-symmetric, yet the models have a nonzero $\mathcal{PT}$-breaking in presence of a pair of gain-loss impurities $\pm i\gamma$ located at reflection-symmetric sites. We uncover a hidden symmetry that is instrumental to the finite threshold strength. Our predictions substantially broaden possible realizations

of a $\mathcal{PT}$ system, particularly in optical waveguide arrays or coupled microstructures, by eliminating the parity-symmetry constraint. In chapter 2, we discuss the dynamics of the wave-function phases in a wide range of $\mathcal{PT}$-symmetric lattice models. In particular, we numerically show that, starting with a random initial state, a universal, gain-site location dependent locking between wave-function phases at adjacent sites occurs in the $\mathcal{PT}$-symmetric-broken region. Our results pave way towards understanding the physically observable implications of time invariance of the $\mathcal{PT}$ product (defined by $\langle\Psi(t)|\Psi(t)\rangle_{\mathcal{PT}} = \langle\Psi(t)|\,\mathcal{PT}\,|\Psi(t)\rangle$) in the nonunitary dynamics produced by $\mathcal{PT}$-symmetric Hamiltonians. Lastly, in chapter 3, we investigate $\mathcal{PT}$ symmetry of the time-evolution operator of nonunitary quantum walks (QW). We provide a necessary and sufficient condition for the time-evolution operator of the nonunitary QW to retain $\mathcal{PT}$ symmetry in various schemes of QW depending on position and coin parameters. We employ DTQW to investigate a nontrivial topological effects.

# 2. PT-SYMMETRY IN PHOTONIC LATTICES

What model of periodic hopping disorder retains a nonzero $\mathcal{PT}$ threshold? To answer that question, we investigate a general theoretical model which exhibits such a disorder in its couplings. First, we review the $\mathcal{PT}$-symmetric, uniform lattice with nearest-neighbor couplings which has been extensively studied and forms the starting point for our model [41, 42].

## 2.1 The Uniform Lattice

Let us consider a system of $N$ waveguides with constant couplings $J > 0$, where $J$ defines the natural energy or frequency scale for the lattice. The system can be described as a tight-binding lattice with a basis which is defined by the waveguide labels $m = 1, 2, \ldots, N$. The constant coupling Hamiltonian is given by

$$H_0 = -J \sum_{k=1}^{N-1} (|k\rangle \langle k+1| + |k+1\rangle \langle k|) = H_0^\dagger, \tag{2.1}$$

where $|k\rangle$ denotes a single-particle state localized at site $k$. The action of the parity operator on such a lattice is given by $\mathcal{P} : k \to \bar{k} = N + 1 - k$, and the time-reversal operator corresponds to complex conjugation, $\mathcal{T} = *$. The system described here is Hermitian. Suppose we introduce a balanced gain and loss, with strength $\gamma$, at parity symmetric sites $k$ and $\bar{k}$ respectively. This corresponds, in the description of a tight-binding Hamiltonian, to a pair of complex-conjugate imaginary potentials located at the parity-symmetric locations with Hamiltonian given by

$$\Gamma = i\gamma(|m_0\rangle \langle m_0| - |\bar{m}_0\rangle \langle \bar{m}_0|) = -\Gamma^\dagger. \tag{2.2}$$

In this system, the underlying pattern of couplings $H_0$ is uniform and real, and thus commutes with $\mathcal{PT}$. Because the gain and loss are complex conjugates and located at parity-symmetric locations, they also commute with $\mathcal{PT}$, and the full non-Hermitian Hamiltonian $H(\gamma) = H_0 + \Gamma$ is, too, $\mathcal{PT}$-symmetric; that is, $\mathcal{PT}H\mathcal{PT} = H$. A representation of the lattice system is shown in Fig. 2.1. Starting from zero, the gain-loss strength $\gamma$ is increased, the eigenvalues of $H(\gamma)$ remain real and its eigenfunctions are simultaneous eigenfunctions of $\mathcal{PT}$ until the $\mathcal{PT}$ symmetry is broken at $\gamma = \gamma_{PT}$, resulting in complex conjugate eigenvalues for $H(\gamma)$. The $\mathcal{PT}$-phase marked by the reality of the spectrum happens when $\gamma \leq \gamma_{PT}(m_0)$ where the gain-location dependent $\gamma_{PT}$ is the $\mathcal{PT}$-symmetry breaking threshold. For an odd size lattice $N$, $\gamma_{PT} \to J/2$ ($\gamma_{PT} \to J$) when $d = 2$ ($d = N - 1$). For an even size lattice, the maximum threshold $\gamma_{PT}$ occurs when the distance $d$ between the gain and loss potentials is minimum or maximum at $d = 1$ or $d = N - 1$, Fig. 2.2. It worth mentioning that the unexpected robustness of the $\mathcal{PT}$-symmetry-breaking threshold is the largest gain-loss distance is due to open boundary conditions [42, 43].

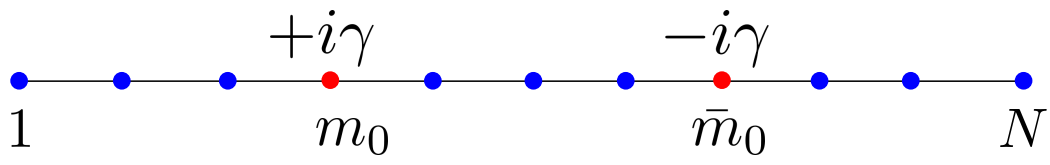


Fig. 2.1. A representation of $N$-site tight-binding lattice with uniform coupling $J$; gain and loss represented by $\pm\gamma$ are located at sites $m_0$ and $\bar{m}_0$ respectively.

## 2.2 Disordered Lattice

The elements of the Hamiltonian can be altered with a random, uncorrelated disorder; in which case the threshold is suppressed to zero because a random disorder does not preserve the symmetries of the Hamiltonian. But this problem can be

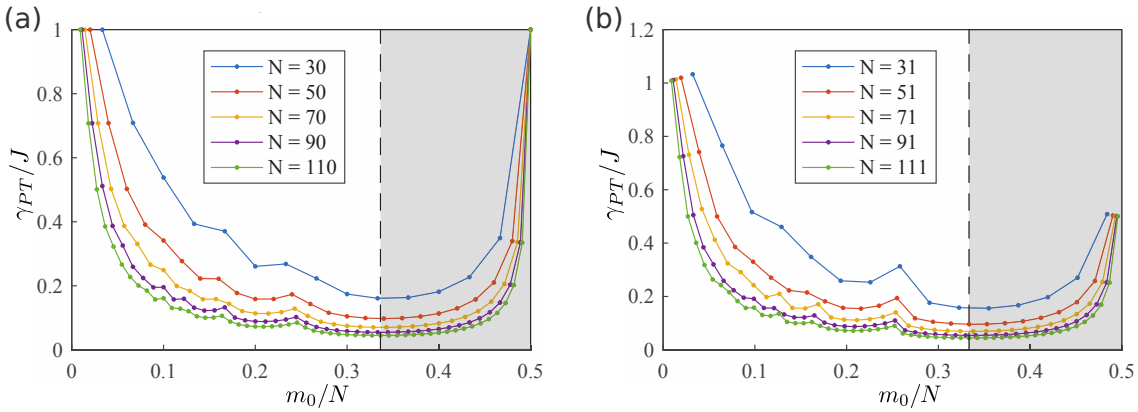


Fig. 2.2. $\mathcal{PT}$-symmetry-breaking threshold $\gamma_{\mathcal{PT}}$ in unit of $J$ for even (a) and odd (b) cases as a function of gain location $m_0/N < 0.5$ for different system size $N$. The shaded area indicates the fraction of the lattice for which the $\mathcal{PT}$-threshold decays monotonically with $d$, thus the results are the expectation in an infinite lattice. In the non-shaded area, $m_0/N \leq 0.35$, due to the boundary,the $\gamma_{\mathcal{PT}}$ increases as a function of $d$, [1].

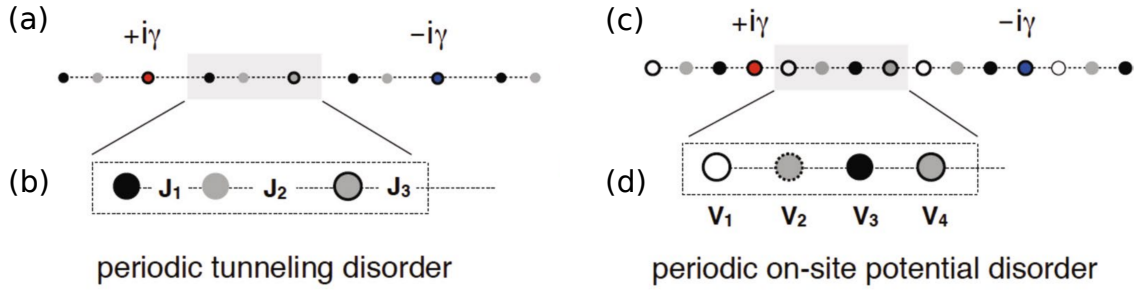


Fig. 2.3. Disordered $\mathcal{PT}$-symmetric lattices with open boundary conditions. (a) For a lattice size $N = 11$ with $m_0 = 3$ and random periodic tunneling $J_k = J(1 + \lambda_1 r_k)$; $\lambda_1 = 1$ is the strength of the disorder and $r_1, \ldots, r_p$ are $p$ random numbers from a standard normal distribution. (b) The tunneling disorder with period $p = 3$. (c) $N = 15$ uniform lattice with a gain site $m_0 = 4$ and random on-site potentials $V_k = J_0 r_k$ with $_0 = 1$. (d) The potential disorder has period $p = 4$, [2].

circumvented by a choice of a periodic disorder. For an inquiry in that claim, let

consider two classes of Hamiltonian disorders in a periodic lattice of period $p$, one in the tunneling amplitude and other in the on-site potential, given respectively by,

$$H_T = J\lambda_1 \sum_{k=1}^{N-1} r_k(|k\rangle \langle k+1| + |k+1\rangle \langle k|), \tag{2.3a}$$

$$V_O = J\lambda_0 \sum_{k=1}^{N} r_k |k\rangle \langle k|, \tag{2.3b}$$

where the dimensionless number $\lambda_1$ and $\lambda_0$ represent the strength of tunneling and on-site disorder respectively. $r_1, \ldots, r_p$ are independent, identically distributed (i.i.d.) random numbers drawn from a standard normal distribution with zero mean and unit variance, and the periodic nature of disorder implies that $r_{k'} = r_k$ if $k' - k = 0$ mod $p$. We emphasize that although the randomness of disorder is only confined to a unit-cell of size $p$, the lattice with $N$ sites may or may not contain integer number of such unit cells. The existence of a finite threshold depends critically on these details and, thus, cannot be obtained via the Bloch-theorem approach. Figure 2.3 (panels a and b) shows an illustration of a disordered lattice chain with $N = 11$ sites with gain potential $i\gamma$ at $m_0 = 3$. The chain has a periodic tunneling disorder of period $p = 3$ with three independent, random tunnelings within a unit cell given by $J_k = J(1 + \lambda_1 r_k)$. Figure 2.3 (panels c and d) shows an on-site potential disordered lattice with $N = 15$ sites, gain potential $m_0 = 4$, and disorder period $p = 4$; the four independent random potentials are given by $V_k = J\lambda_0 r_k$. In each of the above cases, the potential is not $\mathcal{PT}$-symmetric. So, at first hand, it is reasonable to expect a zero $\mathcal{PT}$-symmetry breaking threshold for the disordered Hamiltonian. However after investigation , we detected that the Hamiltonian has a non-zero $\mathcal{PT}$-symmetry breaking for some specific choices of the system size and location of the gain potential accordingly with the periodicity $p$ of the tunneling amplitude or of the on-site potential. Indeed The Hamiltonian has a finite nonzero threshold when the system

size $N$, the gain location $m_0$, and the periodicity $p$ of the tunneling amplitude (or on-site potential) are described by

$$\begin{aligned} N+1 &= 0 \mod p, \\ m_0 &= 0 \mod p. \end{aligned} \tag{2.4}$$

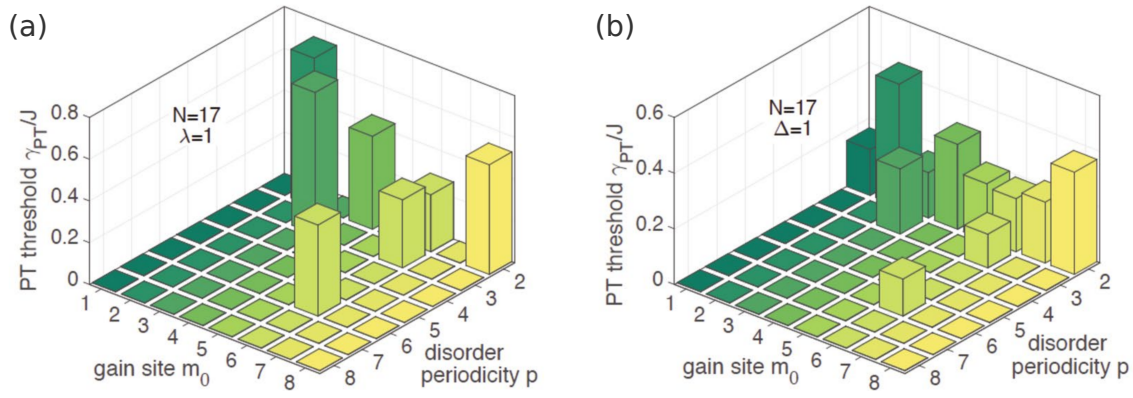


Fig. 2.4. (a) $\mathcal{PT}$-symmetry breaking threshold $\gamma_{\mathcal{PT}}$ as a function of gain location $m_0 < N/2$ and tunneling disorder period $p \leq N/2$ for an $N = 17$ site lattice shows that $\gamma_{\mathcal{PT}} > 0$ if only $N + 1 = 0 \mod p$ and $m_0 = 0 \mod p$; otherwise it is zero. (b) $\gamma_{\mathcal{PT}}$ as a function of $m_0$ and on-site disorder period $p$; at $p = 2$, $\gamma(m_0) > 0$ for all $m_0$.

Figure 2.4a shows, for a system size $N = 17$, a phase diagram of the $\mathcal{PT}$-symmetry breaking threshold $\gamma_{\mathcal{PT}}$ as a function of the gain location $m_0$ and the disorder period $p$ of the tunneling amplitude with tunneling strength $\lambda_1 = 1$. Precisely, it is shown that $\gamma_{\mathcal{PT}}$ is nonzero only when $N + 1$ and $m_0$ are multiples of the disorder period $p$. Indeed, for $p = 2$ the threshold $\gamma_{\mathcal{PT}}$ is nonzero only when $m_0$ is even, for $p = 3$ it is nonzero for $m_0 \in 3, 6$, and for $p = 6$ it is nonzero for $m_o = 6$. It is definitely zero for periods $p \in \{4, 5, 7, 8\}$ for any gain-site location $m_0$. These result confirm that an appropriate choice of the tunneling disorder period, gain-site location, and a system size leads to a positive $\mathcal{PT}$-symmetry breaking threshold. Similarly in Fig. 2.4b, the plot of $\gamma_{\mathcal{PT}}$ as a function of the gain-site location $m_0$ and the on-site disorder period $p$ with strength $\lambda_0$, where we have a nonzero $\gamma_{\mathcal{PT}}$ only when $p \in \{2, 3, 6\}$ and

it zero when $p \in \{4, 5, 7, 8\}$. There is a singularity with the on-site periodic disorder for the case $p = 2$ when the $\gamma_{\mathcal{PT}}$ is positive for odds $m_0$ as well. In fact, for an odd lattice size, which is the case for $N = 17$, the on-site disorder is always $\mathcal{PT}$-symmetric.

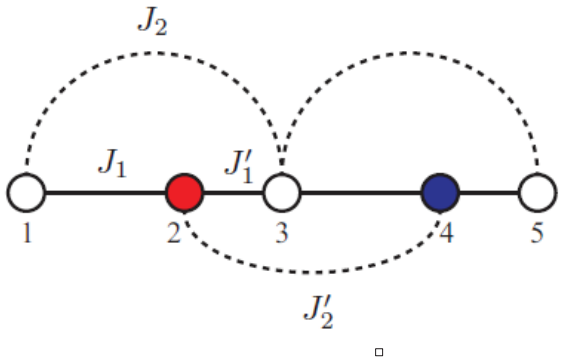


Fig. 2.5. Illustration of a 1D lattice with nearest neighbor couplings $J + \lambda_{11}A_1 \in \{J_1, J_1'\}$ and next-nearest neighbor couplings $\lambda_{12}A_2 \in \{J_2, J_2'\}$. This corresponds to a periodicity $p = 2$ and $p' = 2$ along the first and second off-diagonals of the Hamiltonian respectively.

We also study systems with higher order of connectivity in a lattice model where hopping or tunneling processes arise between sites $k$ and $k + n$ with $n \geq 1$. Let consider a system with both nearest-neighbor and next-nearest-neighbor couplings defined by $A_1(n)$ and $A_2(n)$ respectively. Thus, the Hamiltonian is given by

$$H_{1,2} = \sum_{k=1}^{N-1} \left(\lambda_{11}A_1 \left|k\right\rangle\!\left\langle k+1\right| + \lambda_{12}A_2 \left|k\right\rangle\!\left\langle k+2\right| + h.c\right), \tag{2.5}$$

where in system with couplings periodicity $p = 2$ we have $A_1 \in \{J_1, J_1'\}$ and $A_2 \in \{J_2, J_2'\}$ as described in fig 2.5, and $h.c$ stands for Hermitian conjugate. Note that if $A_1 = 0$, the system would transform into two independent, isolated systems with nearest neighbor couplings. This can be interpreted as a simple rearrangement of the on-site labels which could corresponds to a transformation of pentadiagonal matrix to

a tridiagonal matrix. Adding the effect of the on-site potential, the full non Hermitian and non-$\mathcal{PT}$-symmetric Hamiltonian is

$$H(\gamma) = H_0 + H_{1,2} + \Gamma. \tag{2.6}$$

Figure 2.6 shows the $\mathcal{PT}$-symmetric breaking threshold $\gamma_{PT}/J$ as a function of gain location $m_0$ and disorder period $p$ for a lattice system of size $N = 23$. The left-hand panel shows that when a uniform lattice is perturbed by random, periodic next-nearest-neighbor hopping, the $\mathcal{PT}$ symmetry breaking threshold remains positive for $(m_0, p)$ that satisfy Eq. 2.4. The center panel shows the same pattern for a positive $\mathcal{PT}$ symmetry breaking threshold in the presence of both $n = 1$ and $n = 2$ pertubations. The right-hand panel shows that the $\mathcal{PT}$-symmetric phase of the Hamiltonian $H(\gamma) = H_0 + \Gamma$ is robust against random, periodic, long-range hopping pertubations for specific periodicities and gain locations. Note that the positive threshold values $\gamma_{PT}/J$ obtained in Fig. 2.6 are for specific realizations of the disordered Hamiltonian; accordingly, different disorder realizations will lead to different threshold values. However the locations in the $(m_0, p)$-plane that lead to a positive threshold do not change.

In summary, we have explored the actions of random, periodic, long-range disorder on the outcome of the $\mathcal{PT}$-symmetric phase in a uniform lattice with a pair of balanced gain-loss potentials. Despite the sensibility of the $\mathcal{PT}$ symmetry of the underlying Hermitian Hamiltonian, we discover that there exists a positive $\mathcal{PT}$ symmetry breaking threshold when the lattice size $N$ and the gain location $m_0$ are both related to the disorder period $p$ as defined in Eq. 2.4.

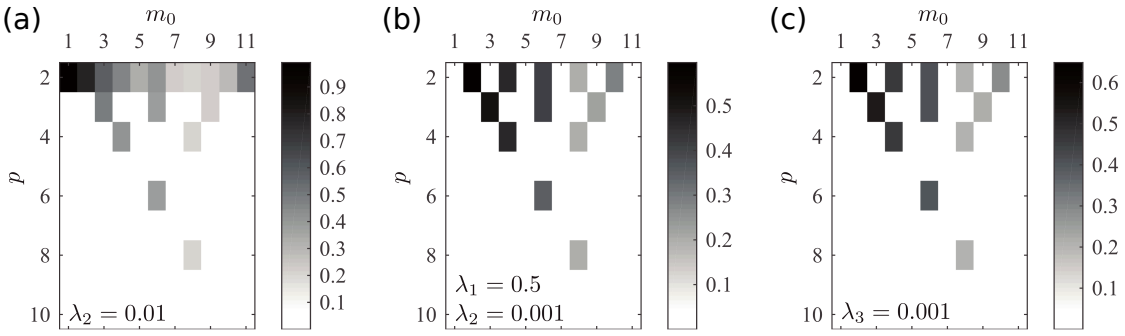


Fig. 2.6. Phase diagram showing the $\mathcal{PT}$-breaking threshold corresponding to periodicity $p$ and gain location $m_0$, results are shown averaged over 100 random realizations; the colorbar indicates the scale of the results for each panel and is measured relative to $J$, the uniform coupling frequency. In (a), we have uniform nearest-neighbor coupling combined with periodic disorder in next-nearest-neighbor coupling modulated by $\lambda_{12}$; in (b), periodic disorder is introduced in both nearest-neighbor and next-nearest-neighbor couplings (same periodicity), modulated by $\lambda_{11}$ and $\lambda_{12}$ respectively; in (c), we have uniform nearest-neighbor coupling combined with periodic disorder in third-nearest-neighbor coupling modulated by $\lambda_{13}$, [1].

# 3. TIME-INVARIANTS AND FOURTH-ORDER EXCEPTIONAL POINT IN A PARITY-TIME SYMMETRIC QUDIT

## 3.1 Time-Invariant in PT-Symmetric System

After the discovery of $\mathcal{PT}$ symmetry theory, the research has progressed along two non overlapping lines. The first approach, fiercely researched initially, was to develop a complex extension of quantum mechanics [13]. Because $[\mathcal{PT}, H_{\mathcal{PT}}] = 0$, the $\mathcal{PT}$ product, defined as $\langle\psi(t)|\phi(t)\rangle_{\mathcal{PT}} \equiv [\mathcal{PT}\,|\psi\rangle\,(t)]^{\mathrm{T}}\,|\phi(t)\rangle$, remains constant with time [44]. However, it is not positive-definite and therefore cannot be used to construct a self-consistent quantum theory. To bypass that obstacle an Hamiltonian-dependent, commuting operator $\mathcal{C}$ is defined such that the $\mathcal{CPT}$ product defined similarly, is positive-definite and leads to a unitary time evolution [12, 44]. This approach leads to the formulation of the pseudo-Hermiticity [14, 45–47] of the non-Hermitian Hamiltonian and it has been extensively studied also in the language of general intertwining operators. But its validity is limited to the $\mathcal{PT}$-symmetric region where the eigenvalues of $H_{\mathcal{PT}}$ are purely real.

The second approach, started about a decade ago [35, 48], treats $H_{\mathcal{PT}}$ as an effective Hamiltonian for an open system, classical or quantum, where a unitary time evolution is neither required nor expected. In this interpretation, the anti-symmetric potential $i\gamma V$ represents a gain for the system when $V > 0$ and is accompanied by an equal loss with $V < 0$ at the parity-symmetric location. The development of complex-conjugate eigenvalues corresponds to the emergence of two eigenmodes, one of which amplifies with time and the other one decays. This approach does not change the fundamental, Dirac inner product of quantum theory, and is applicable in both $\mathcal{PT}$-symmetric and $\mathcal{PT}$-broken (complex conjugate spec-

trum) phases. It has been immensely successful in predicting a multitude of novel phenomena in $\mathcal{PT}$-symmetric systems and explaining the subsequent experimental observations [17, 18, 22–24, 49–54]. But, in this case, the constants of motion for such a system [55] are not clear. The two approaches can be bridged by connecting the time-invariant $\mathcal{PT}$ product mentioned in the first approach with the nonunitary evolution of a physical system in the second approach. This can be done by showing that, deep in the $\mathcal{PT}$-broken state, the exponentially-in-time growth of the Dirac norm, combined with the constant-in-time constraint on the $\mathcal{PT}$ product (and expectation values of other intertwining operators), leads to phase locking that is independent of the initial state. In the following sections, we investigate the time evolution of the phase difference for systems with uniform and periodic coupling in open boundary conditions settings.

### 3.1.1 $\mathcal{PT}$-Symmetric Dimer and Trimer

A $\mathcal{PT}$-symmetric dimer is a two level system (qubit) represented by two sites $|1\rangle$ and $|2\rangle$ having tunneling amplitude $J > 0$ and gain/loss potentials $\pm i\gamma$. The Hamiltonian of a dimer is given by Eq. 1.21 and it can be defined in a compact form by $H_2 = -J\sigma_1 + i\gamma\sigma_3 \neq H_2^\dagger$ where $\sigma_1$ and $\sigma_3$ are standard Pauli matrices. $H_2$ have a $\mathcal{PT}$ symmetry (a combined parity symmetry $\mathcal{P} = \sigma_1$ and time-reversal symmetry $\mathcal{T} = *$) and its spectrum undergoes a $\mathcal{PT}$ transition at $\gamma_{\mathcal{PT}} = J$ where the two eigenvalues $\pm\lambda_2 = \pm\sqrt{J^2 - \gamma^2}$ coalesce same as the corresponding eigenfunctions. From its definition,

$$H_2 = -J\sigma_1 + i\gamma\sigma_3 = \begin{pmatrix} i\gamma & -J \\ -J & -i\gamma \end{pmatrix}, \tag{3.1}$$

and

$$H^2 = (J^2 - \gamma^2)\begin{pmatrix} 1 & 0 \\ 0 & 1 \end{pmatrix}. \tag{3.2}$$

Thus, the nonunitary time evolution operator $\exp(H_2 t)$ is defined by

$$G_2 = \cos(\lambda_2 t)\mathbf{1} - i(H_2/\lambda_2)\sin(\lambda_2 t). \tag{3.3}$$

In the $\mathcal{PT}$-symmetric state, the norm of the evolved wavefunction oscillates with time. At the exceptional point $\gamma = J$, it grows algebraically with time as $t^2$ ( Since $H_2^2 = 0$ at $\gamma = J$), and in the $\mathcal{PT}$-broken state it grows exponentially as $\exp(+\Lambda_2 t)$ where $\Lambda_2 = \sqrt{\gamma^2 - j^2} > 0$. Let consider a random initial state $(\phi_1(0), \phi_2(0))^{\mathrm{T}}$. The time invariance of the $\mathcal{PT}$ product of the two two-state $\mathcal{PT}$-symmetric system $(\phi_1(t), \phi_2(t))^{\mathrm{T}} = \left(r_1(t)e^{i\theta_1(t)}, r_2(t)e^{i\theta_2(t)}\right)^{\mathrm{T}}$ is given by

$$N_{\mathcal{PT}} = 2r_1(t)r_2(t)\cos(\theta_2(t) - \theta_1(t)) = \text{const.} \tag{3.4}$$

For $N_{\mathcal{PT}} = 0$, in which case the initial state is localized only on one site or has an initial $\pi/2$ phase difference between the two sites, it implies that the phase difference between the two sites remains fixed, $\theta_2 - \theta_1 = \pm\pi/2$. This result holds in the Hermitian limit, $\gamma = 0$, as well.

For $N_{\mathcal{PT}} \neq 0$, in which case the initial state is spread over the two sites and complex, thus the time invariance of $N_{\mathcal{PT}}$ implies that the phase difference $\theta_2 - \theta_1$ evolves with time and is not stationary. However, in the $\mathcal{PT}$-broken state, at advanced times ($\Gamma_2 t >> 1$), the weights $r_{1,2}(t)$ grow exponentially. Thus, the time invariance of Eq. 3.4 requires that $\cos(\theta_2(t) - \theta_1(t)) \approx \cos(\theta_2(0) - \theta_1(0))e^{-2\Lambda_2 t} \to 0^{\pm}$ depending on the initial sign of $N_{\mathcal{PT}}$. That is, for an arbitrary initial state, the phase difference $\theta_2(t) - \theta_1(t) \to \pm\pi/2$, Fig. 3.1a. This result is completely different from the dynamic in Hermitian case or $\mathcal{PT}$-symmetric region.

For a $\mathcal{PT}$-symmetric trimer (three-level) system with Hamiltonian, in compact form, given by $H_3 = -JS_x + i\gamma S_z$, where $S_x$ and $S_z$ are spin-1 representations of angular momentum operators [56]. The eigenvalues of the trimer are given by $0, \pm\lambda_3$ with $\lambda_3 = \sqrt{J^2 - \gamma^2}$, which become degenerate at $\gamma_{\mathcal{PT}} = J$ and complex for $\gamma > J$. The constant-in-time of the $\mathcal{PT}$ product is given by

$$r_2^2 + 2r_1(t)r_3(t)\cos(\theta_3(t) - \theta_1(t)) = \text{const.} \tag{3.5}$$

From Eq. 3.5, one can notice that the $\mathcal{PT}$ product of a trimer has information about the wave-function phases only at the gain and loss locations, but not about the neutral

location. This makes impossible to obtain any definitive conclusions about the phase locking in the $\mathcal{PT}$-broken state based solely on Eq. 3.5, despite the numerical result Fig. 3.1b.

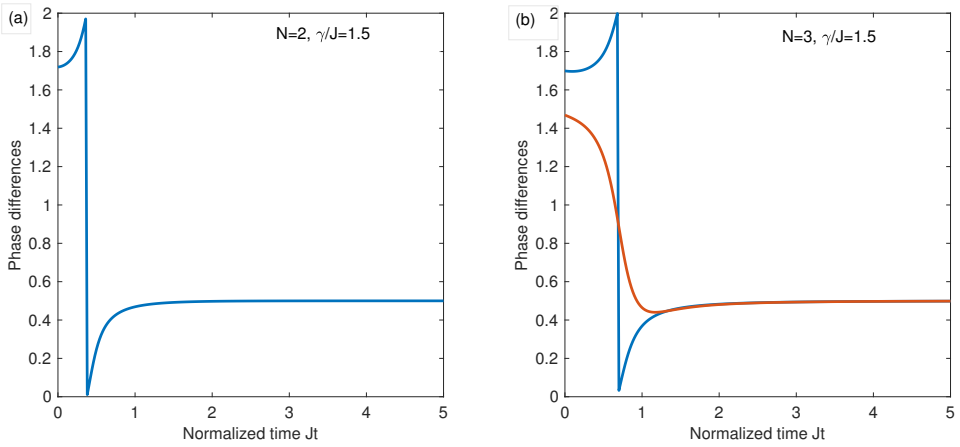


Fig. 3.1. (a) the phase difference for a two-level system, with gain and loss, locks to $\pi/2$, (b) the two phase differences for a trimer, with gain at first site and loss at third site, lock to $\pi/2$.

### 3.1.2 $\mathcal{PT}$ Product of a Uniform Tunneling Lattice Chain

Let consider an $N$-site tight-binding lattice with tunneling $J > 0$ and two impurities defined by imaginary potentials; the Hamiltonian can be defined by

$$H(\gamma) = -J \sum_{k=1}^{N-1} (|k\rangle \langle k+1| + |k+1\rangle \langle k|) + i\gamma(|m_0\rangle \langle m_0| - |\bar{m}_0\rangle \langle \bar{m}_0|), \tag{3.6}$$

where $|k\rangle$ denotes a single-particle state localized at site $k$, $m_0 \leq N/2$, and $\bar{m}_0 = (N + 1 - m_0) > N/2$ is the reflection-counterpart of site $m_0$. The nonunitary time evolution operator of the Hamiltonian is defined by

$$G(t) = e^{-iHt}, \tag{3.7}$$

and its action on a random initial state $|\phi(0)\rangle$ is given by

$$G(t)\,|\phi(0)\rangle = |\phi(t)\rangle = \sum_{k=1}^{N} a_k(t) e^{i\theta_k(t)}\,|k\rangle\,. \tag{3.8}$$

The Dirac norm of the state $\phi(t)$ and its time invariant $\mathcal{PT}$ product with itself are given by,

$$\langle\phi(t)|\phi(t)\rangle = \sum_{k=1}^{N} a_k^2(t), \tag{3.9a}$$

$$\langle\phi(t)|\phi(t)\rangle_{\mathcal{PT}} = \sum_{k}^{N} a_k(t) a_{\bar{k}}(t) e^{i[\theta_k(t)-\theta_{\bar{k}}(t)]}, \tag{3.9b}$$

respectively.

The Dirac norm Eq. 3.9a is not constant in time. Indeed, it undergoes bounded oscillations in $\mathcal{PT}$-symmetric region, grows algebraically with time as a power that depends on the order of the exceptional point at $\mathcal{PT}$ breaking transition point, increases exponentially with time in the $\mathcal{PT}$-broken regime.

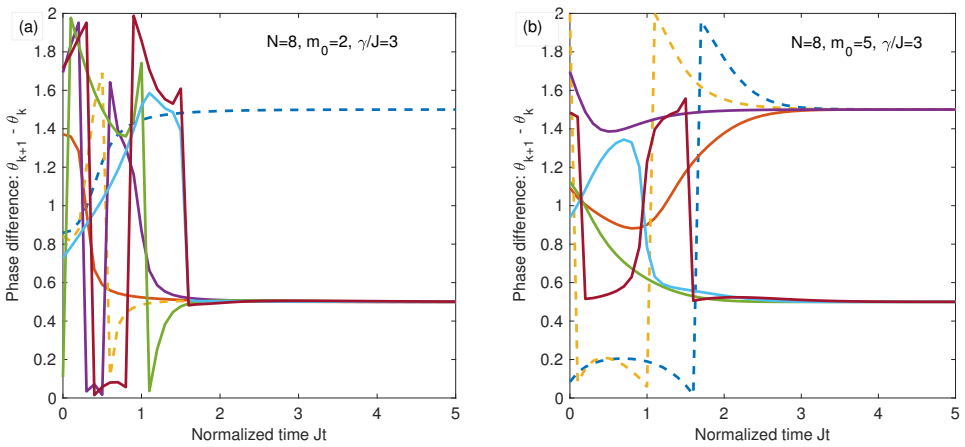


Fig. 3.2. Time evolution of neighboring site phase differences deep in the $\mathcal{PT}$-broken region with $\gamma/J = 3$, measured in unit of $\pi$, for N = 8 site lattice . (a) Gain location $m_0 = 2$ implies one phase difference saturate to $3\pi/2$ and the remaining saturate to $\pi/2$, (b) gain location $m_0 = 5$ implies four phase difference saturate to $3\pi/2$ and the remaining three saturate to $\pi/2$.

Figure 3.2 shows the time evolution of adjacent phase difference in a deep $\mathcal{PT}$-broken phase ($\gamma/J = 3 >> \gamma_{\mathcal{PT}}$) [43] of a chain system of $N = 8$, meaning $N - 1 = 7$ phase differences. Figure 3.2a shows the case when the gain is located at $m_0 = 2$, which reveals one phase difference saturate to $3\pi/2$ while the rest are locked to $\pi/2$. Fig. 3.2b describes the case when the gain is located at location $m_0 = 3$ showing two phase differences saturate to $3\pi/2$ and the remaining saturate to $\pi/2$. The dynamic shown by the figures is that all phase differences of the time evolved wave function up to the gain site are locked to $3\pi/2$ while the remaining saturate to $\pi/2$, independently of the initial state. While Fig. 3.3 confirms the phase locking phenomenon it also highlights the dependence of the $\mathcal{PT}$-breaking threshold on the gain location. For the same gain $\gamma/J = 1.5$ and different gain location $m_o$, the time evolved of the phase difference of the wave function behaves differently. Indeed with the gain location at $m_0 = 2$, Fig. 3.3a, the system is still in $\mathcal{PT}$ regime and the time evolution of the phase difference undergoes oscillations while in Fig. 3.3b, where the gain location is at $m_0 = 3$, the system is in $\mathcal{PT}$-broken regime with appearance of the phase locking phenomena. Thus, Figs. 3.2 and 3.3 show that the gain site $m_0$ is the location where, deep in $\mathcal{PT}$-broken regime, the locked time evolved phase difference changes from $3\pi/2$ to $\pi/2$.

### 3.1.3 Periodic Tunneling Lattice Chain

A periodic tunneling lattice is a system chain with site-dependent tunneling amplitude $J(k)$; and without a loss of generality, its Hamiltonian can be defined by Eq. 2.3a. Let consider an open $N$-site system with a single pair gain-loss potentials $\pm\gamma$ located at $m_0$ and $\bar{m}_0$ respectively with a tunneling amplitude with period $p = 2$. Such a system bears the name of Su-Schrieffer-Heeger (SSH) [1, 57] model and its coupling structure is given by

$$J(k) = \begin{cases} J & k = 0 \mod 2, \\ J(1-\delta) & k = 1 \mod 2, \end{cases} \tag{3.10}$$

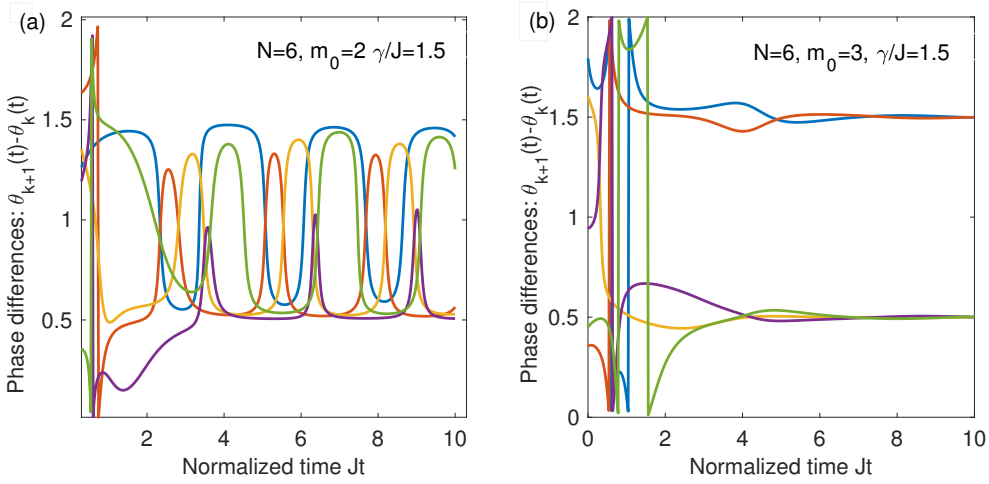


Fig. 3.3. Time evolution of neighboring site phase differences deep in the $\mathcal{PT}$-broken regime with $\gamma/J = 3$, measured in unit of $\pi$, for N = 6 site lattice . (a) With gain location at $m_0 = 2$, the system is in $\mathcal{PT}$ breaking transition phase, (b) with gain location at $m_0 = 3$, the system is in $\mathcal{PT}$-broken regime which implies two phase difference saturate to $3\pi/2$ and the remaining three saturate to $\pi/2$.

where $\delta \leq 1$ defines the coupling relationship strength between the periodic couplings [57, 58]. The SSH model Hamiltonian ($H_{SSH}$) described here is parity symmetric for an even $N$ and the $\mathcal{PT}$-breaking threshold depends on the strength $\delta$ for a fixed gain location $m_0$. Indeed, the $\gamma_{\mathcal{PT}}$ monotonically increases as a function of the coupling relationship strength $\delta$. Figure 3.4 shows the phase locking phenomenon for a SSH chain model with the gain strength of $\gamma/J = 2.3$ locates at $m_0 = 2$. In both cases of Fig. 3.3, the time evolved of the only phase difference $\theta_2(t) - \theta_1(t)$ (number of phase differences up to the gain location) saturates to $3\pi/2$ whereas the rest saturate to $\pi/2$. For a small coupling relationship $\delta = 0.2$, Fig. 3.3.a shows a fast phase locking process i.e. the system reaches the $\mathcal{PT}$-broken regime faster than in Fig. 3.3.b where the coupling strength is $\delta = 0.8$. Again, the phase locking phenomenon is independent of the random initial state, the gain-loss strength threshold and the coupling relationship strength.

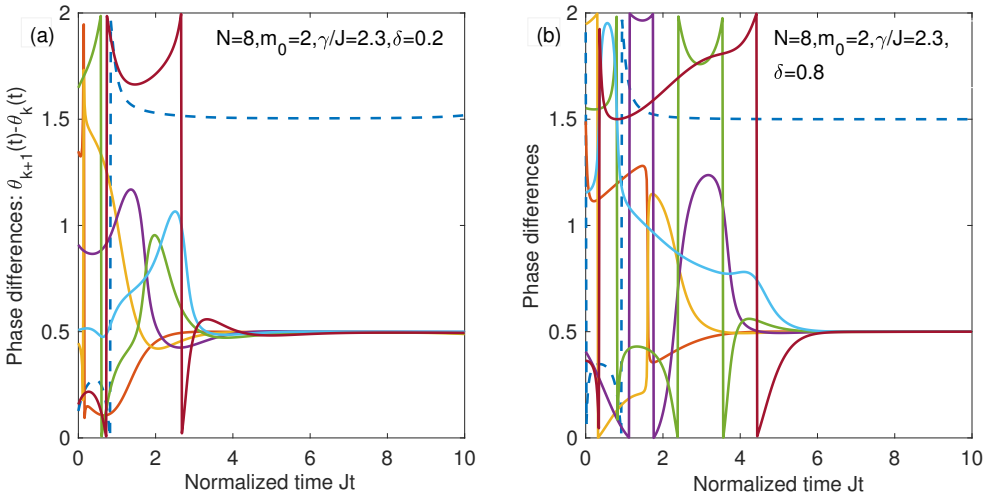


Fig. 3.4. Time evolution of neighboring site phase differences deep in $\mathcal{PT}$-broken phase with $\gamma/J = 3$, measured in unit of $\pi$, for N = 8 SSH chain with gain located at $m_0 = 2$. (a) For small strength = 0.2, the phase difference $\theta_2(t) - \theta_1(t)$ saturates at $3\pi/2$ while the rest saturate at $\pi/2$ (b) with gain location at $m_0 = 3$, the system is in $\mathcal{PT}$-broken regime which implies two phase difference saturate to $3\pi/2$ and the remaining three saturate to $\pi/2$.

For a period $p \geq 3$, the tunneling lattice is labelled AAH model after the authors Aubry-Andre Harper [59,60]. Unlike in SSH model where the tunneling profile shows a parity symmetry for an even lattice number $N$, the tunneling profile of a AAH model has no parity symmetry at all. As it has been explained above in section 2.2, the full Hamiltonian of the lattice chain does sustain a $\mathcal{PT}$ symmetry when the $N + 1 = 0$ mod $p$ and $m_0$ mod $p$. Figure 3.5 shows the time evolution of neighboring site phase difference for $N = 8$ AAH model with period $p = 3$. When the gain location is $m_0 = 3$ and the loss site is $\bar{m}_0 = 6$, the two phase differences up to the gain location saturate to $3\pi/2$ while the remaining saturate to $\pi/2$ (left panel). Interchanging the gain and loss locations ($m_0 = 6$ and $\bar{m}_0 = 2$) leads to two phase differences saturate to $\pi/2$ and the rest saturate to $3\pi/2$ as expected. These results reveal that when the initial state is confined to a single site, then the evolved wave-function phase differences of

neighboring sites, deep in $\mathcal{PT}$-broken phase, are locked at $3\pi/2$ up to the gain site, and the remaining are locked at $\pi/2$.

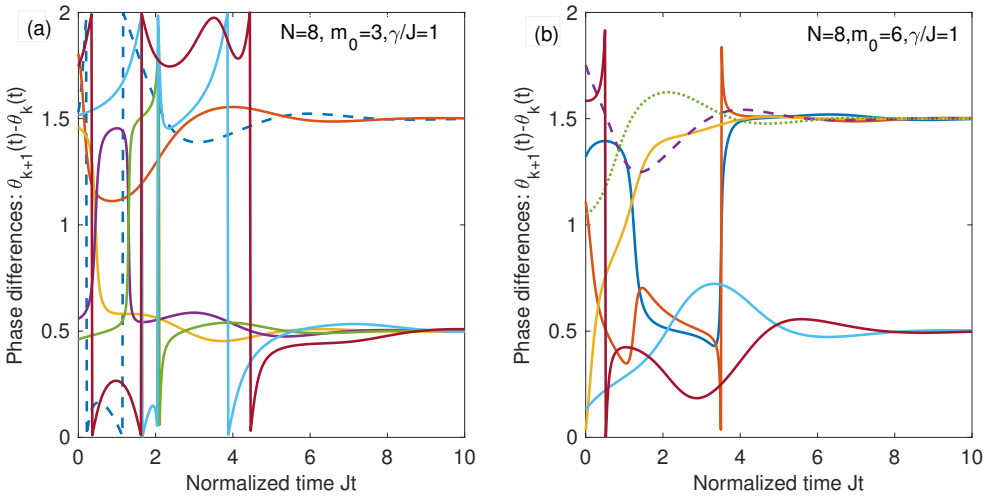


Fig. 3.5. Time evolution of neighboring site phase differences deep in $\mathcal{PT}$-broken phase with $\gamma/J = 1$ for an AAH chain with $N = 8$. (a) for $m_0 = 3$, two phase differences saturate to $3\pi/2$ and the phase differences after the gain site saturate to $\pi/2$. (b) For $m_0 = 6$, the two phase difference after the gain site saturate at $\pi/2$.

Figure 3.5 shows the dynamic of the time evolution of the phase difference of the wave functions of a AAH model of lattice chain with a period $p = 3$; where the repeated tunneling coupling and the gain-loss strength are given by $\{J_1, J_2, J_3\} = J\{1, 0.7, 0.4\}$ and $\gamma/J = 1$ respectively. Here again, the phase locking phenomenon is manifested in $\mathcal{PT}$-broken regime independently of the random initial state of the system.

## 3.2 Extended $\mathcal{PT}$-Symmetric Gain-Loss Potentials

The Hamiltonian of a lattice chain ($N > 3$) with an extended $\mathcal{PT}$-symmetric gain-loss potentials is given in a compact form by

$$H(\gamma) = -JS_x + i\gamma S_z, \tag{3.11}$$

where $S_x$ and $S_z$ are spin $S = (N-1)/2$ dimensional representations of the angular momentum algebra, and the site index $k$ in this chain maps on to the $S_z$ angular momentum projection index. Moreover, the tunneling amplitude between sites $k$ and $k+1$ is given by $\sqrt{k(N-k)/2}$ and the $\mathcal{PT}$-symmetric gain-loss potential changes linearly from $-i\gamma S$ to $+i\gamma S$ in steps of $i\gamma$. Despite having an algebraically fragile $\mathcal{PT}$-symmetric phase, this type of Hamiltonian does model a perfect state transfer phenomenon. The equidistant energy spectrum of the Hamiltonian shows a particle-hole symmetry described by

$$\epsilon_m = m\sqrt{J^2 - \gamma^2}, \tag{3.12a}$$

$$-S \leq m \leq S. \tag{3.12b}$$

This Hamiltonian has an exceptional point of order $N$ at the $\mathcal{PT}$-symmetry breaking threshold $\gamma_{\mathcal{PT}} = J$. Figure 3.6 shows the dynamic of the time evolution of the adjacent phase differences. When the gain strength parameter $\gamma$ is less than the threshold $\gamma_{\mathcal{PT}}$, the phase differences undergo a periodic oscillations with period $T_{os} = \pi/\sqrt{J^2 - \gamma^2}$ (left panel). For $\gamma = 1.1$, the system is in $\mathcal{PT}$-broken phase and all adjacent phase differences are locked at $3\pi/2$ (right panel). For the extended $\mathcal{PT}$-symmetric potential, the larger gain potential site plays the role gain location in controlling the dynamic of the phase locking. This leads, in the broken phase, to all adjacent phase differences being locked at $3\pi/2$ when the larger gain potential site is located at the end of the chain, whereas they all saturate at $\pi/2$ when the larger gain site is located at the beginning of the chain. These results reveal that the phase-locking phenomenon is robust in a wide different settings of finite lattices with open boundary conditions. However, the investigation in the phase locking phenomenon was motivated by the time-invariant $\mathcal{PT}$ product which from its definition provides only one phase differences dependent equation while there are $N-1$ phase differences. Thus, additional equations, in the form of other time invariants, are needed to fully characterize the phase locking phenomenon.

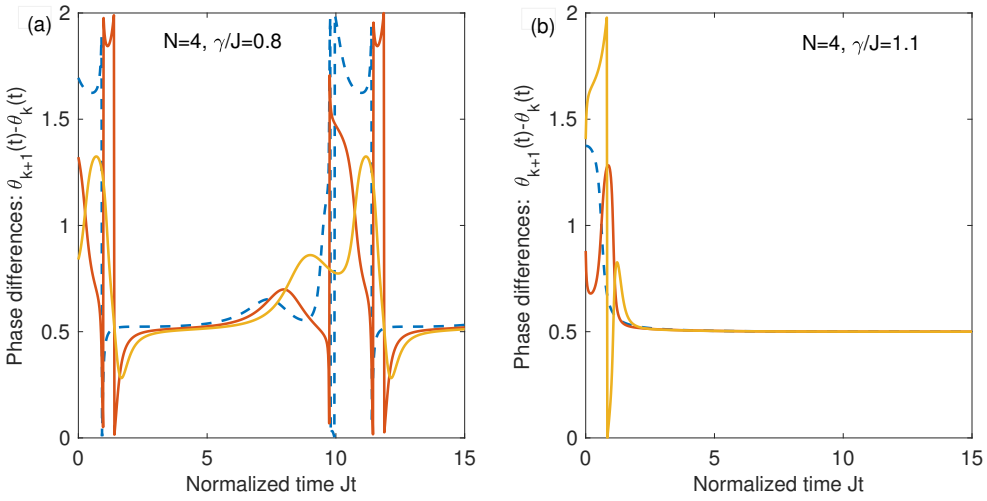


Fig. 3.6. (a) In $\mathcal{PT}$-symmetric phase where $\gamma <_{\mathcal{PT}}$, the phase differences oscillate with period $T_{os} = \pi/\sqrt{J^2 - \gamma^2}$. For $\gamma > \gamma_{\mathcal{PT}}$, all the phase differences are locked at $3\pi/2$ in this configuration where the gain region is in the second half of the lattice chain.

### 3.3 Other Time-Invariants for $H_{\mathcal{PT}}$

By definition, a Hermitian operator $\hat{\eta}$ is said to be an intertwining operator [14,47] for a $\mathcal{PT}$-symmetric Hamiltonian $H_{\mathcal{PT}}$ with an energy scale $J$ if it satisfies

$$H_{\mathcal{PT}}^{\dagger}\hat{\eta} = \hat{\eta}H_{\mathcal{PT}}, \tag{3.13}$$

It follows that $\hat{\eta}$ is invariant under a transformation by the non-unitary time evolution operator of $H_{\mathcal{PT}}$ given by $G(t) = \exp(-iH_{\mathcal{PT}}t)/$, i.e

$$G^{\dagger}(t)\hat{\eta}G(t) = \hat{\eta}. \tag{3.14}$$

Indeed, taking a power expansion of the propagator $G(t)$ in the right hand side of the 3.14, we have,

$$\begin{aligned} G^{\dagger}(t)\hat{\eta}G(t) &= (1 + iH^{\dagger}_{\mathcal{PT}} + \frac{(iH^{\dagger}_{\mathcal{PT}}t)^2}{2!} + \dots)\eta(1 - iH_{\mathcal{PT}}t + \frac{(-iH_{\mathcal{PT}}t)^2}{2} + \dots) \\ &= \eta - i\eta H_{\mathcal{PT}} - \eta\frac{H^2_{\mathcal{PT}}t^2}{2} + \dots + iH^{\dagger}_{\mathcal{PT}}\eta t + \frac{H^{\dagger}_{\mathcal{PT}}\eta H_{\mathcal{PT}}t^2}{2} + \dots \\ &= \eta - i\eta H_{\mathcal{PT}} - \eta\frac{H^2_{\mathcal{PT}}t^2}{2} + \dots + i\eta H_{\mathcal{PT}} + \eta\frac{H^2_{\mathcal{PT}}t^2}{2} + \dots \\ &= \eta. \end{aligned}$$

Equation 3.14 implies that the expectation value of the operator $\hat{\eta}$ in an arbitrary state is time invariant. In principle, all time invariants can be derived by solving the system of $n^2$ linear Eqs. 3.14, where $n$ denotes the dimension of $H_{\mathcal{PT}}$.

Most of theoretically studied lattice models and all experimentally investigated $\mathcal{PT}$-symmetric systems have transpose and $\mathcal{PT}$ symmetries. The transpose symmetry of the Hamiltonian $H_{\mathcal{PT}}$ implies its time-reversal symmetry is defined by

$$\mathcal{T}H_{\mathcal{PT}}\mathcal{T} = H^{\dagger}_{\mathcal{PT}}. \tag{3.15}$$

Composing Eq. 3.15 on the left by the parity operator $\mathcal{P}$ and rearranging the equality we get,

$$\begin{aligned} & \mathcal{PT}H_{\mathcal{PT}}\mathcal{T} = \mathcal{P}H^{\dagger}_{\mathcal{PT}} \\ \Longrightarrow \quad & H_{\mathcal{PT}}\mathcal{PTT} = \mathcal{P}H^{\dagger}_{\mathcal{PT}} \\ & H_{\mathcal{PT}}\mathcal{P} = \mathcal{P}H^{\dagger}_{\mathcal{PT}} \end{aligned} \tag{3.16}$$

Thus, the parity operator $\mathcal{P}$ is an intertwining operator and we can set $\hat{\eta}_1 = \mathcal{P}$. Using a recursion relation, we can construct a sequence of dimensionless, linearly independent operators such that $\hat{\eta}_k = \hat{\eta}_{k-1}H_{\mathcal{PT}}/J$ for $k = 2, \dots, n$, See box below. Due to the characteristic equation of the $H_{\mathcal{PT}}$, the sequence stops at $\hat{\eta}_n$; and $\mathcal{P}(H_{\mathcal{PT}}/J)^n$ is a linear combination of lower-order intertwining operators. The construction of sequence leads to a maximal set of $n$ linearly independent constants of motion for a $n$-dimensional Hamiltonian.

$\hat{\eta}_1$ intertwining operator $\Longrightarrow \hat{\eta}_1 H_{\mathcal{PT}} = H^\dagger_{\mathcal{PT}} \hat{\eta}_1$

Define $\hat{\eta}_2 = \hat{\eta}_1 H_{\mathcal{PT}}/J$. We have,

$$\begin{aligned} H^\dagger_{\mathcal{PT}} \hat{\eta}_2 &= H^\dagger_{\mathcal{PT}} \left(\hat{\eta}_1 H_{\mathcal{PT}}/J\right) \\ &= \left(\hat{\eta}_1 H_{\mathcal{PT}} \hat{\eta}_1\right) \left(\hat{\eta}_1 H_{\mathcal{PT}}/J\right) \\ &= \left(\hat{\eta}_1 H_{\mathcal{PT}}/\,J\right) \left(H_{\mathcal{PT}}\right) \\ &= \hat{\eta}_2 H_{\mathcal{PT}}. \end{aligned}$$

Thus, $\hat{\eta}_2$ is an intertwining operator of $H_{\mathcal{PT}}$.

Suppose $\hat{\eta}_{k-1}$ is an intertwining operator, we have $\hat{\eta}_{k-1} H_{\mathcal{PT}} = H^\dagger_{\mathcal{PT}} \hat{\eta}_{k-1}$

$$\begin{aligned} H^\dagger_{\mathcal{PT}} \hat{\eta}_k &= H^\dagger_{\mathcal{PT}} \left(\hat{\eta}_{k-1} H_{\mathcal{PT}}/J\right) \\ &= \left(\hat{\eta}_{k-1} H_{\mathcal{PT}} \hat{\eta}_{k-1}\right) \left(\hat{\eta}_{k-1} H_{\mathcal{PT}}/J\right) \\ &= \left(\hat{\eta}_{k-1} H_{\mathcal{PT}}/J\right) \left(H_{\mathcal{PT}}\right) \\ &= \hat{\eta}_k H_{\mathcal{PT}}. \end{aligned}$$

Therefore, $\eta_k$ is an intertwining operator for $H_{\mathcal{PT}}$

For instance, let consider a qudit system, system with extended $\mathcal{PT}$-symmetric gain-loss potentials, whose Hamiltonian is given in compact form by $H_Q = -JS_x + i\gamma S_z$. Here $S_x$ and $S_z$ are spin-3/2 representation representations of the SU(2) group. The $\mathcal{PT}$-symmetric Hamiltonian has an antidiag(1,1,1,1) as a parity operator. Explicitly, $H_{\mathcal{PT}}$ is given by

$$H_Q = \frac{1}{2} \begin{pmatrix} 3i\gamma & -\sqrt{3}J & 0 & 0 \\ -\sqrt{3}J & i\gamma & -2J & 0 \\ 0 & -2J & -i\gamma & -\sqrt{3}J \\ 0 & 0 & -\sqrt{3}J & -3i\gamma \end{pmatrix} \tag{3.17}$$

From Eq. 3.12, the four equidistant eigenvalues are given by

$$\lambda_k = \{-3/2, -1/2, +1/2, +3/2\} \sqrt{J^2 - \gamma^2}, \tag{3.18}$$

which leads to an exceptional point of order 4, EP4, at the $\mathcal{PT}$-symmetry breaking threshold at $\gamma = J$. It worth mentioning the fact that the order of the exceptional point equals the dimension of the system makes the qudid a prototype choice that can be generalised to an arbitrary dimensional system.

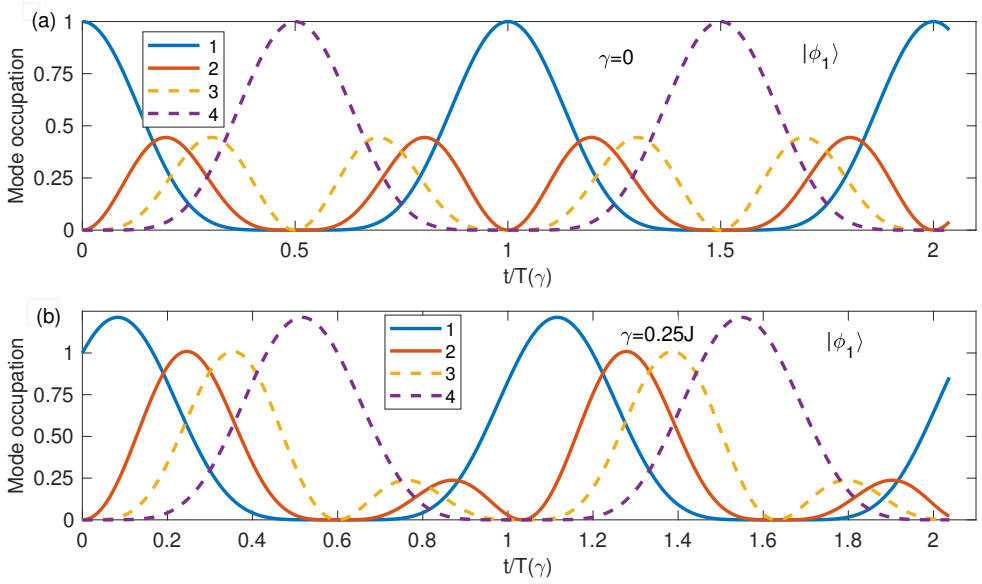


Fig. 3.7. (a) In the Hermitian limit, mode occupation numbers are periodic with period $T_{os} = 2\pi/J$, and a perfect state transfer manifest by a mirror of mode $k$ to mode $5-k$ at time $T_{os}/2$. (b) $\mathcal{PT}$-symmetric phase with $\gamma = 0.25J$, the occupation numbers are still periodic but no state transfer due the nonunitary dynamic of the qudit. In both cases, the initial state is given by $|\phi_0\rangle = (1, 0, 0, 0)^{\mathrm{T}}$.

Figure 3.7 shows the time evolution of the mode occupation numbers. In the top panel (a), for $\gamma = 0$, the occupation numbers of the four modes undergo a perfect state transfer characterised by $P_k(t) = P_{5-k}(t+\pi/J)$, where $P_k(t) = |\langle k|\phi(t)\rangle|^2$; that is, a perfect state transfer of the first (solid blue) and second (solid red) modes to the fourth (dash blue) and third (dash orange) modes respectively at time $T_{os}/2 = \pi/J$. The lower panel (b) shows the periodic occupation numbers with time period $T_{os}(\gamma) = 2\pi/\sqrt{J^2-\gamma^2}$ in the $\mathcal{PT}$-symmetric phase with $\gamma = 0.25J$; there is no perfect state

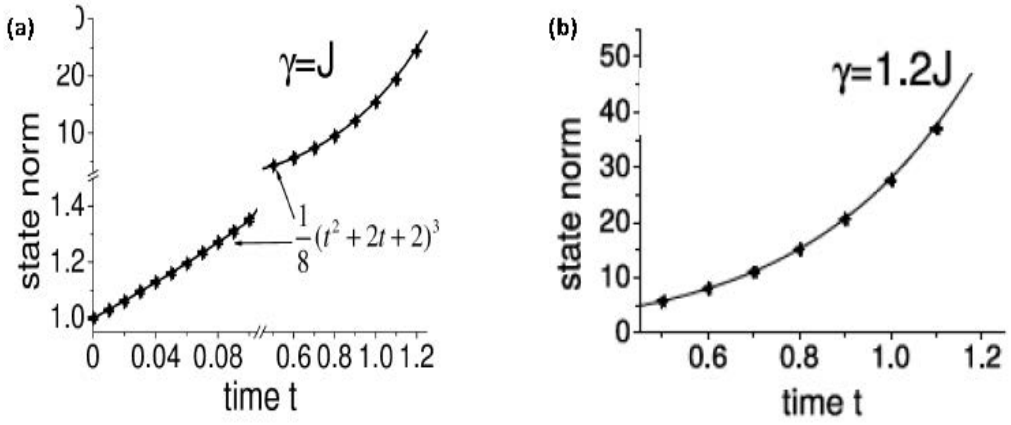


Fig. 3.8. (a) At the $\mathcal{PT}$-breaking threshold $\gamma_{\mathcal{PT}} = J$, the norm of the state $|\phi(t)\rangle$ grows with time as $t^6$ showing that the exceptional point is of order six. (b) Exponential growth with time of the time dependent norm in the $\mathcal{PT}$-broken phase with $\gamma = 1.2J$. In both cases, the initial state is localized in the first mode, i.e $|\phi_1\rangle = (1, 0, 0, 0)^{\mathrm{T}}$, [4].

transfer in this case due the nonunitary dynamic of the system.

The development of an exceptional point of order four (EP4) at $\gamma = J$ is characterised by $H^4_{\mathcal{PT}}(\gamma = J) = 0$. Thus from the power series expansion, the propagator $\mathcal{G}(t)$ vanishes starting at the fourth order and the observed time-dependent norm $P(t) = \sum_k P_k(t)$ increases algebraically with time as $t^6$, Fig. 3.8a.

Furthermore, the existence of the fourth order exceptional point can be demonstrated by studying the spectrum of a perturbed $\mathcal{PT}$-symmetric Hamiltonian from the exceptional point; where the complex eigenvalues in the vicinity of EP$n$ (exceptional point of order $n$) follow a Puiseux series in $\delta^{1/n}$. Thus, for a perturbation of the qudid Hamiltonian $H_Q$ in the vicinity of the exceptional point given by $H_\delta(\gamma) = H_{\mathcal{PT}}(\gamma) - i\delta\,|1\rangle\langle 1|$, the expected eigenvalues should scale as $\delta^{1/4}$. Figure 3.9a shows the plots of the real part of the eigenvalues $\lambda_{1,2,3,4}$ as a function of the perturbation $\delta$ (dot lines); plots that indeed scale as $\delta^{1/4}$ (green solid line). Similar

trend in Fig. 3.9b for the plot of the imaginary part of $\lambda_{1,2,3,4}$ as a function of the perturbation $\delta$.

Additionally, a numerical study of the intertwining operators reveals that, despite generically dependent on $\gamma$, its expectation values $\eta_k(t) = \langle\phi(t)|\,\hat{\eta}_k\,|\phi(t)\rangle$ remain constant regardless of the regime of the systems. In fact the expectation values $\eta_{1,2}$ remain time invariants for different values of $\gamma$ across all the phases of the system. The constant in time of the expectation value of $\eta_1(t)$ is illustrated in figure 3.10(a) in Hermitian case ($\gamma = 0$), in $\mathcal{PT}$ symmetry regime ($\gamma = 0.3J$), at the EP4 ($\gamma = J$) , and in $\mathcal{PT}$-broken phase ($\gamma = 1.3$), for a symmetric initial state given by $|\phi_0\rangle = (|1\rangle + |2\rangle + |3\rangle + |4\rangle)/2$. In figure 3.10 (b), deep in $\mathcal{PT}$-broken phase ($\gamma = 1.3J$) where the norm of the wave function grows exponentially with time, the expectation value of $\eta_2(t)$ remain constant in time independently of the initial state ($|1\rangle\,, |2\rangle$). Although being constant in time, the expectation value $\eta_2$ is not positive definite for the initial state $|2\rangle$. This suggests that an appropriate choice of the initial state does matter for a meaningful measurement of the expectation values.

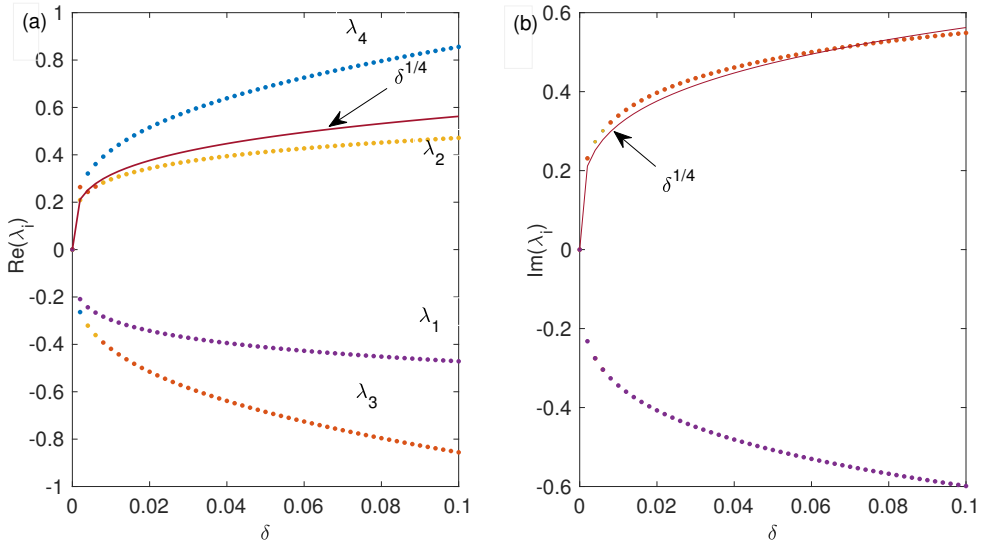


Fig. 3.9. (a) Real part of $\lambda_i$ (dot line) of the perturbed Hamiltonian $H_\delta(\gamma) = H_{\mathcal{PT}}(\gamma) - i\delta\,|1\rangle\langle 1|$ as a function of perturbation $\delta$ show a $\delta^{1/4}$ (solid green line) dependence. (b) Likewise for the imaginary part of the eigenvalues $\lambda_i$.

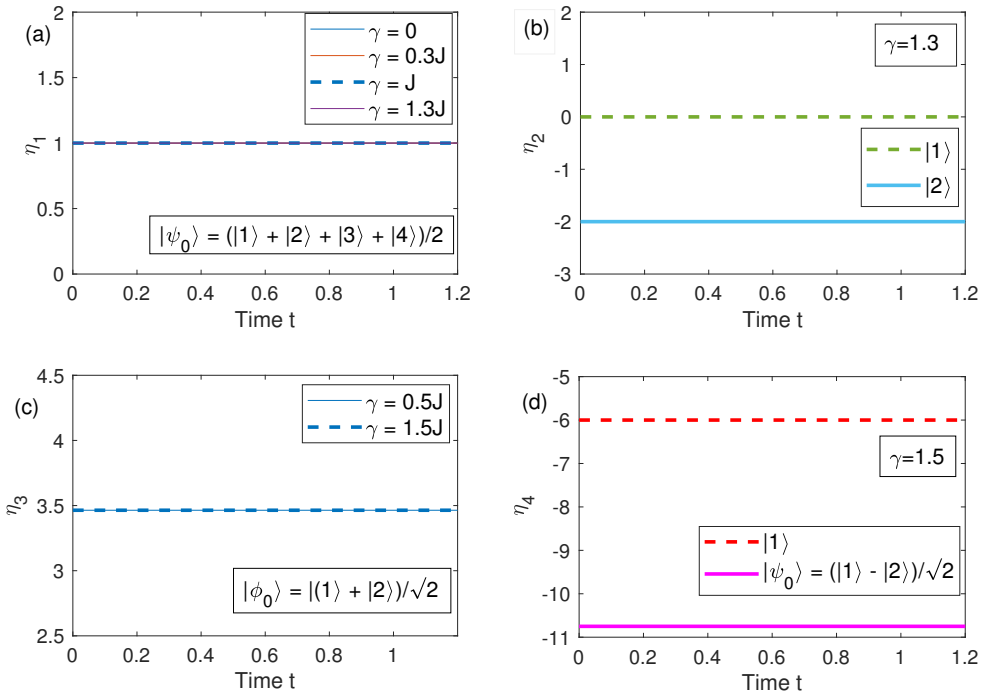


Fig. 3.10. Expectation values of dimensionless intertwining operators. (a) For a symmetric initial state $|\phi_0\rangle = (|1\rangle + |2\rangle + |3\rangle\,|4\rangle)/2$, the expectation value $\eta_1(t)$ remains constant with time when $\gamma = 0, 0.3J, J, 1.3J$. (b) For $\gamma = 1.3J$, the expectation value of $\eta_2(t)$ remains constant in time starting with different initial state $|1\rangle$ and $|2\rangle$. (c) For a initial state $|\psi_0\rangle = (|1\rangle + |2\rangle)\sqrt{2}$, the spectattion value $\eta_4$ remains constant in time for $\gamma = 0.5J, 1.5J$. (d) For $\gamma = 1.5$, the expectation value of $\eta_4$ remains constant in time with different initil $|1\rangle$ and $|\psi_0\rangle = (|1\rangle - |2\rangle)/\sqrt{2}$

# 4. RANDOM WALKS

## 4.1 Classical Random Walks

The classical random walk is the mathematical description of a movement consisting of random steps on some mathematical space such as integers. Classical random walks have applications in various fields including biology, chemistry, computer science, ecology, economy, and physics. An elementary example of classical random walk is a random walk on the integer number line, $Z$, which starts at 0 and moves to the right or to the left with equal probability depending on the coin flip. In that scenario of an unbiased process, for a large number of time step $t$, the one dimensional classical random walk has a symmetric probability distribution that approaches a Gaussian distribution (independently of its starting point) with a deviation from origin approaching $\sqrt{t}$. Table. 4.1 shows a table of the probability distribution for a 5 steps classical random walk on the line starting at 0.

Table 4.1.
Table of the probability distribution of a classical random walk on the line starting at 0.

| t \ $n$ | -5 | -4 | -3 | -2 | -1 | 0 | 1 | 2 | 3 | 4 | 5 |
|---|---|---|---|---|---|---|---|---|---|---|---|
| 0 | | | | | | 1 | | | | | |
| 1 | | | | | $\frac{1}{2}$ | | $\frac{1}{2}$ | | | | |
| 2 | | | | $\frac{1}{4}$ | | $\frac{1}{2}$ | | $\frac{1}{4}$ | | | |
| 3 | | | $\frac{1}{8}$ | | $\frac{3}{8}$ | | $\frac{3}{8}$ | | $\frac{1}{8}$ | | |
| 4 | | $\frac{1}{16}$ | | $\frac{1}{4}$ | | $\frac{3}{8}$ | | $\frac{1}{4}$ | | $\frac{1}{16}$ | |
| 5 | $\frac{1}{32}$ | | $\frac{5}{32}$ | | $\frac{5}{16}$ | | $\frac{5}{16}$ | | $\frac{5}{32}$ | | $\frac{1}{32}$ |

As an illustration, let us consider a classical random walk on the integers line starting at 0 with equal $\frac{1}{2}$ probability to move to the right or to the left. Let us denote by $n_R$, $n_L$, and $t$ the number of steps to the right, number of steps to the left, and the total number of steps respectively. If $n$ denotes the position of the walker after $T$ steps, we have

$$n_R - n_L = n, \qquad n_R + n_L = T, \tag{4.1}$$

from which, it follows that

$$n_R = \frac{1}{2}(T+n), \qquad n_L = \frac{1}{2}(T-n). \tag{4.2}$$

For a walk of $T$ steps, the total number of possible $T$-step walks is $2^T$, and the total number of possible paths ending at $n$ is given by

$$\frac{T!}{(n_R)!(n_L)!} = \frac{T!}{(\frac{1}{2}(T+n))!(\frac{1}{2}(T-n))!}. \tag{4.3}$$

So the probability of walker ending at $n$ is given by,

$$P(n) = \frac{T!}{(\frac{1}{2}(T+n))!(\frac{1}{2}(T-n))!} \cdot \frac{1}{2^T}. \tag{4.4}$$

Using Stirling's formula for large $T$, we have $\ln T! \cong T\ln T - T$. Thus,

$$\begin{aligned}
\ln P(n) &= \ln\left(\frac{T!}{(\frac{1}{2}(T+n))!(\frac{1}{2}(\mathbf{T}-n))!} \cdot \frac{1}{2^T}\right) \\
&\cong T\ln T - T - \left(\frac{T+n}{2}\right)\ln\left(\frac{T+n}{2}\right) + \left(\frac{T+n}{2}\right) - \left(\frac{T-n}{2}\right)\ln\left(\frac{T-n}{2}\right) \\
&+ \left(\frac{T-n}{2}\right) - T\ln 2 \\
&= T\ln T - \left(\frac{T+n}{2}\right)\ln\left(\frac{T+n}{2}\right) - \left(\frac{T-n}{2}\right)\ln\left(\frac{T-n}{2}\right) - T\ln 2,
\end{aligned} \tag{4.5}$$

but

$$\ln\left(\frac{T\pm n}{2}\right) = \ln\frac{T}{2} + \ln\left(1 \pm 2\frac{n}{T}\right) \cong \ln\frac{T}{2} \pm 2\frac{n}{T} - \frac{1}{2}\left(\frac{n}{T}\right)^2, \tag{4.6}$$

which gives

$$\ln P(n) = -\frac{n^2}{2T}, \tag{4.7}$$

thus,

$$P(n) \propto e^{-\frac{n^2}{2T}}, \tag{4.8}$$

which indeed proves that for a large $t$, the probability distribution approaches a Gaussian distribution, see Fig. 4.1. In higher dimension, an example of classical random walks on a graph can be described by a particle moving on a lattice where a node has 6 vertices, and the particle moves according to the outcomes from tossing a dice. Particularly the classical random walks on a d-dimensional hypercube (where in each step a neighboring vertex is chosen with probability $1/d$) can be reduced to a walk on a line of $d+1$ vertices, where the transition probability from vertex $i$ to vertex $i+1$ in the general case is given by $p_{i,i+1} = \frac{d-i}{d}$ and from $i+1$ to $i$ by $p_{i+1,i} = \frac{i+1}{d}$ [61].

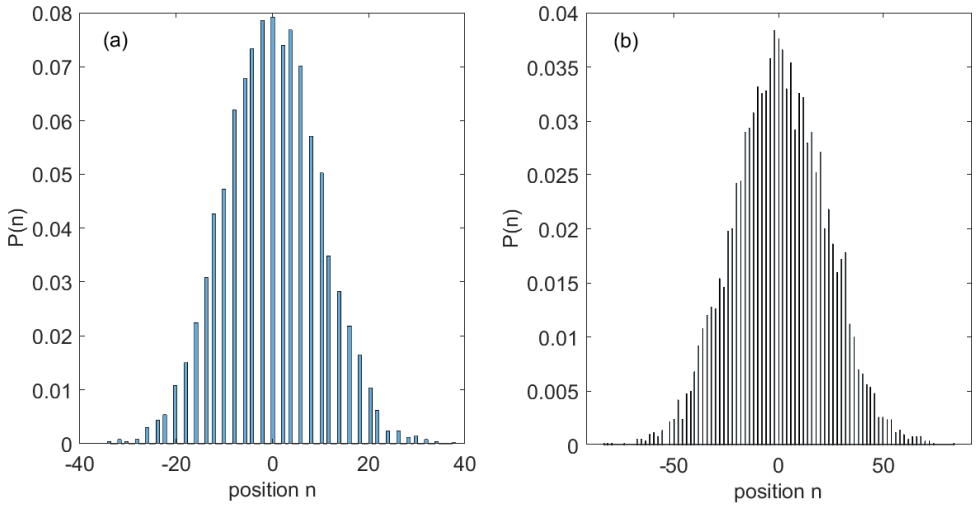


Fig. 4.1. (a) and (b), probability distribution after $T = 100$ and $T = 500$ respectively of a classical random walk.

## 4.2 Quantum Random Walk

The notion of a quantum walk was originally discovered by Aharonov *et al.* in 1993 [40]. The quantum random walks are quantum analogue of classical random walks. But unlike its classical counterpart in one-dimensional lattice where the walker can take one direction only with a defined probability at a specific time step, a quantum random walker can take both directions at each time step with a specified probability. The shape of the probability distribution of a quantum random walk depends on its initial state [61, 62]. Moreover, the deviation of the quantum random walk is about the time step $T$ meaning the walk spreads quadratically faster. Properties, such as diffusion time, hitting time (the expected number of steps before node $j$ is visited, starting from node $i$), mixing time (measure of how fast the discrete ransom walk converges to its limiting distribution), etc make the quantum random walks a subject of intense and interesting studies in the past decade where they have been widely used in study and realization of quantum computing, quantum information and quantum cryptography [63]. They have also been realized in nuclear magnetic resonance systems, optical cavities, optical lattices, ions trap, etc [61]. There are two kind of quantum random walks, the continuous-time quantum walk defined on a Hilbert space $\mathcal{H}$ composed exclusively of position space $\mathcal{H}_{\mathcal{P}}$, and the discrete-time quantum walk whose Hilbert space is a combination of the position space $\mathcal{H}_{\mathcal{P}}$ and the coin space $\mathcal{H}_{\mathcal{C}}$, $\mathcal{H} = \mathcal{H}_{\mathcal{P}} \otimes \mathcal{H}_{\mathcal{C}}$.

### 4.2.1 Continuous-Time Quantum Walk

CTQW was initially proposed by Farhi and Gutmann [39], and its formalism is derived from its classical counterpart fairly from the Markov process [64]. The dynamic of the continuous-time quantum walk (CTQW) consists of a walker and a generator (Hamiltonian) operator of the system that can be applied at any time. The mathematical structure of the model is a diffusion-type differential equations. Suppose we have a graph with $N$ vertices indexed by integers $n = 1, 2, \cdots, N$. A

vertex may be connected to other vertices by an edge. Let $\mu$ denote the jumping rate per unit time between vertices and impose the requirement that a walk is only possible between nodes connected to an edge. Thus, the random walk can be described by a stochastic generator matrix $M$ whose matrix element $M_{ab}$, probability to go from $a$ to $b$, equal to $\frac{1}{d_a}$ ($d_a$ is the degree of $a$), is defined by

$$M_{ab} = \begin{cases} -\mu & a \neq b \\ 0 & a \neq b \\ d_a\mu & a = b \end{cases} \tag{4.9}$$

In infinitesimal time $\epsilon$ limit such that $\mu\epsilon \approx 1$ is the probability of jumping from one vertex to its neighbor, then the probability of being at vertex $a$ at a given time $t$ is [64]

$$\frac{dp_a}{dt} = -\sum_b M_{ab}p_b(t), \tag{4.10}$$

with

$$\sum_a p_a(t) = 1. \tag{4.11}$$

To transition to the continuous-time quantum walk from its classical counterpart, let us construct an $N$-dimensional Hilbert space $\mathcal{H}$, a set of the vectors $|a\rangle$ where $a = 1, 2, \cdots, N$ denote the vertices of the graph G, and define a Hamiltonian $\hat{H}$ with matrix elements given by

$$\langle a|\,\hat{H}\,|b\rangle = M_{ab}. \tag{4.12}$$

Thus, the Schroedinger equation of a quantum state $|\Psi\rangle \in \mathcal{H}$ is defined by

$$i\frac{d\,\langle a|\Psi(t)\rangle}{dt} = \sum_b \langle a|H|b\rangle\,\langle b|\Psi(t)\rangle \tag{4.13}$$

Combining Eqs. 4.12 and 4.13, the unitary evolution operator defining a CTQW on the graph G is given by [64],

$$\hat{U}(t) = e^{-i\hat{H}t/\hbar}. \tag{4.14}$$

Starting at an initial state $|\Psi_0\rangle$ the state of the walker at time $t$ is $|\Psi(t)\rangle = \hat{U}\,|\Psi_0\rangle$, from which the state $|\Psi(t)\rangle$ can be expressed as a complex superposition of basis

states corresponding to the vertices. Figure 4.2a shows the time evolution of a CTQW starting at $\Psi(n,0) = \delta_{n,0}$ and spreading over a discrete position space. Figure 4.2 (panels b and c) shows a symmetric spread of the probability distribution at a half and the end of the propagation time respectively.

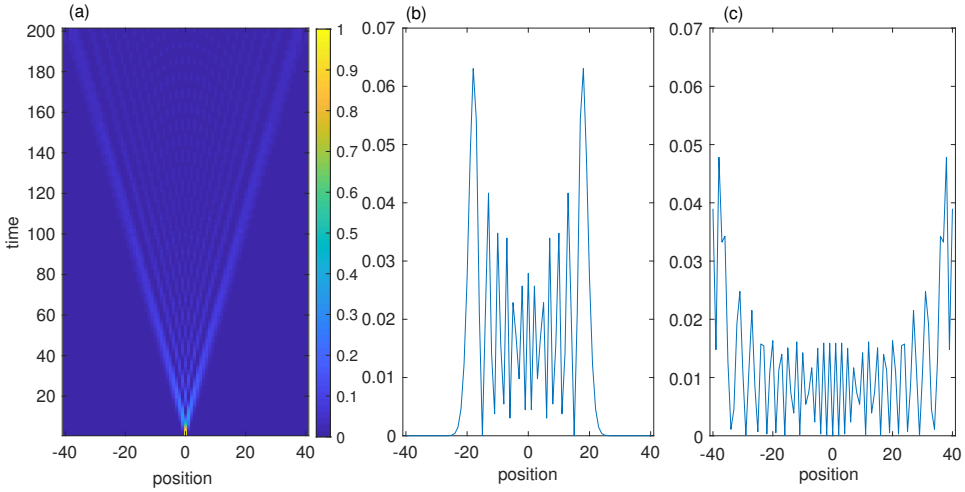


Fig. 4.2. (a) Probability distribution of a CTQW starting at $\Psi(n,0) = \delta_{n,0}$. (b) and (c) Instantaneous probability distribution at half and end of the propagation time respectively.

### 4.2.2 Discrete-Time Quantum Walk

A DTQW on a one-dimensional lattice can be described by an ordered sequence of coin and shift operations. The coin operator acts on the internal states of the walker with an outcome that decides the action of the shift operator. To illustrate this, let us consider a walker at an arbitrary position of $|n_0\rangle$ on a one-dimensional lattice. The walker flips a coin (with outcomes R and L) to decide which way to move on the lattice, with a R (L) outcome corresponding to the right (left) direction of the motion. These outcomes of the 'quantum coin' represent the eigenstates of the coin operator with $|R\rangle = (1,0)^{\mathrm{T}}$and $|L\rangle = (0,1)^{\mathrm{T}}$. Unlike in classical random walk, an outcome of the coin can also be a superposition of the two eigenstates. Basically,

a coin operation is a rotation operation on the internal space of the walker, and can be designed depending on the model of quantum random walk one desires. From the results of the coin operator on the internal states of the walker, the shift operator moves the walker on the position space spanned by $|n\rangle$ where $n \in \mathbb{Z}$; and is a unitary operator defined in this context by

$$S = \left(\sum_n |n+1\rangle \langle n|\right) \otimes |R\rangle \langle R| + \left(\sum_n |n-1\rangle \langle n|\right) \otimes |L\rangle \langle L| . \tag{4.15}$$

One frequently used coin operator is the Hadamard coin operator defined by

$$H = \frac{1}{\sqrt{2}} \begin{pmatrix} 1 & 1 \\ 1 & -1 \end{pmatrix}. \tag{4.16}$$

Each step of the quantum walk is accomplished by the unitary operator $U$, a product of elemental operators, defined by

$$U = S(\mathbb{I} \otimes H), \tag{4.17}$$

which implements a 'coin' toss followed by a move. Let consider the internal states $|R\rangle$ and $|L\rangle$ as the spin 'up' $|\uparrow\rangle$ and $|\downarrow\rangle$ respectively. Suppose the walker is initially localized at the position $|n_0\rangle = |0\rangle$ and in an internal state $|\uparrow\rangle$ so that its overall state is $|\Psi_0\rangle = |0\rangle \otimes |\uparrow\rangle$. Then a one step application of the unitary operator $U$ results as follow

$$|\Psi_0\rangle \xrightarrow{H} \frac{1}{\sqrt{2}} |0\rangle \otimes (|\uparrow\rangle + |\downarrow\rangle), \tag{4.18a}$$

$$\xrightarrow{S} \frac{1}{\sqrt{2}} (|1\rangle \otimes |\uparrow\rangle + |-1\rangle \otimes |\downarrow\rangle). \tag{4.18b}$$

After this first step, a measurement of the coin state in the standard basis gives an equal probability of $\frac{1}{2}$ for the states $|\uparrow\rangle \otimes |1\rangle$ and $|\downarrow\rangle \otimes |-1\rangle$. For a three steps walk we have,

$$\begin{aligned} |\Psi_0\rangle &\xrightarrow{U} \frac{1}{\sqrt{2}} (|\rangle \otimes |\uparrow\rangle + |-1\rangle \otimes |\downarrow\rangle) \\ &\xrightarrow{U} \frac{1}{2} (|2\rangle \otimes |\uparrow\rangle + |0\rangle \otimes (|\uparrow\rangle + |\downarrow\rangle) + |-2\rangle \otimes |\downarrow\rangle) \\ &\xrightarrow{U} \frac{1}{2\sqrt{2}} (|3\rangle \otimes |\uparrow\rangle + |1\rangle \otimes (|\downarrow\rangle + 2|\uparrow\rangle) - |-1\rangle \otimes |\uparrow\rangle + |-3\rangle \otimes |\downarrow\rangle) \end{aligned} \tag{4.19}$$

The probability distribution after the third step shows a shift to right, influenced by the initial internal state ($|\uparrow\rangle$) of the walker. Figure 4.3 (panel b and c) illustrates the behavior of the probability distribution of the walker at $t = 100$ with an internal state $\frac{1}{\sqrt{2}}(|\uparrow\rangle + |\downarrow\rangle)$ (symmetric) and $|\uparrow\rangle$ (justified to right) respectively. Figure 4.3a shows the time evolution of the DTQW over $t = 100$ time steps for a walker starting initially at position $|0\rangle$ with an internal state in a symmetric superposition of the eigenstates of the internal state space. From Fig. 4.3, it is evident that the interference pattern of the quantum walk is much complex and absent in the Gaussian obtained in the classical walk. It is worth to note that the conditional shift operator $S$ is responsible for generating the entanglement between the coin and position degrees of freedom [65] Succinctly, the state of the walker after $t$ time steps is given by

$$|\Psi(t)\rangle = U^t |\Psi_0\rangle . \tag{4.20}$$

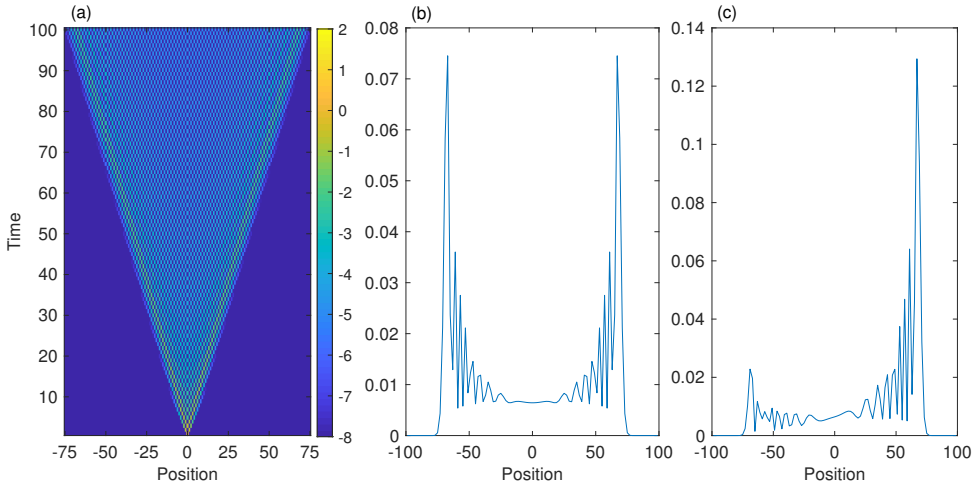


Fig. 4.3. (a) Probability distribution of a DTQW starting at $|\Psi_0\rangle = \frac{1}{\sqrt{2}}(|\uparrow\rangle + |\downarrow\rangle) \otimes |0\rangle$ using a Hadamard coin operator. (b) and (c) Probability distribution after $t = 100$ time steps of a DTQW starting at $|\Psi_0\rangle = (|\uparrow\rangle + \mathrm{i}\,|\downarrow\rangle) \otimes |0\rangle$ and $|\Psi_0\rangle = |\uparrow\rangle \otimes |0\rangle$ respectively. Only the probability at the even points is plotted, since the odd points have probability zero.

It is also possible to perform the quantum walk in the Fourier space [63]. Suppose the full state of the walker is defined by

$$|n,\uparrow\downarrow\rangle = \frac{1}{\mathcal{N}}\sum_{k=0}^{\mathcal{N}-1} e^{-\mathrm{i}\omega_k \mathrm{n}}\,|k,\uparrow\downarrow\rangle\,, \tag{4.21}$$

where $n = 0, 1, 2 \ldots \mathcal{N}-1$ and $\omega_k = 2\pi k/\mathcal{N}$. Using the Fourier shift theorem, the translation operator can be reduced to an eigenvalue problem

$$\hat{S}\,|k,\uparrow\rangle = e^{-\mathrm{i}\omega_k}\,|k,\uparrow\rangle\,, \tag{4.22a}$$

$$\hat{S}^\dagger\,|k,\downarrow\rangle = e^{\mathrm{i}\omega_k}\,|k,\downarrow\rangle\,, \tag{4.22b}$$

where $\hat{S} = \sum_n |n-1\rangle\langle n|$ and $\hat{S}^\dagger = \sum_n |n+1\rangle\langle n|$. Using the position independent Hadamard coin operator, one gets

$$\begin{aligned} U(\mathcal{F}|\Psi\rangle) &= U\sum_{k=0}^{\mathcal{N}-1}\sum_{c=\downarrow}^{\uparrow}\beta_{kc}\,|k,c\rangle \\ &= \sum_{k=0}^{\mathcal{N}-1}\left(|k\rangle\otimes\left(e^{-\mathrm{i}\omega_k}\,|\uparrow\rangle\langle\uparrow| + e^{\mathrm{i}\omega_k}\,|\downarrow\rangle\langle\downarrow|\right)C\sum_{c=\downarrow}^{\uparrow}\beta_{kc}\,|c\rangle\right) \\ &= \sum_{k=0}^{\mathcal{N}-1}\left(|k\rangle\otimes e^{-\mathrm{i}\sigma_3\omega_k}C\sum_{c=\downarrow}^{\uparrow}\beta_{kc}\,|c\rangle\right) \\ &= \sum_{k=0}^{\mathcal{N}-1}\left(|k\rangle\otimes C_k\sum_{c=\downarrow}^{\uparrow}\beta_{kc}\,|c\rangle\right). \end{aligned} \tag{4.23}$$

Equation 4.23 shows that the evolution of the quantum walk in Fourier space requires only the application of a modified coin $C_k$ at every node $k$ [62, 63].

## 4.3 Non-Unitary Quantum Walks

### 4.3.1 Non-Unitary CTQW

Typically a non-unitary CTQW is represented by a time-evolution operator of a non-Hermitian Hamiltonian. A sample case is described in [2] with an open boundaries system of $N$-site tight-binding lattice with gain and loss potentials $\pm i\gamma$ located

at parity symmetric sites $m_0 \leq N/2$ and $\bar{m}_0 = (N+1-m) > N/2$ respectively. From the parity of the size of the lattice the distance between the gain and the loss sites, $d = \bar{m}_0 - m_0$, ranges from $N-1$ to one or two whether $N$ is even or odd respectively. The non-Hermitian, $\mathcal{PT}$-symmetric effective Hamiltonian of system is given by

$$H_{PT} = H_0 + \Delta H, \tag{4.24}$$

where

$$H_0 = -J \sum_{n=1}^{N-1} (|n\rangle \langle n+1| + |n+1\rangle \langle n|) = H_0^\dagger, \tag{4.25a}$$

$$\Delta H = i\gamma(|m_0\rangle \langle m_0| - |\bar{m}_0\rangle \langle \bar{m}_0|) = -\Delta H^\dagger. \tag{4.25b}$$

$J > 0$ is the hoping energy of the Hermitian Hamiltonian and $|n\rangle$ is a single-particle state localized at lattice site $n$. The spectrum of the effective Hamiltonian $H_{\mathcal{PT}}$ is either purely real or complex conjugate pairs because it commutes with the antilinear operator $\mathcal{PT}$ [13, 14]. The $\mathcal{PT}$-phase marked by the reality of the spectrum happens when $\gamma \leq \gamma_{\mathcal{PT}}(m_0)$, where the gain-location dependent $\gamma_{\mathcal{PT}}$ is the $\mathcal{PT}$-symmetry breaking threshold. For an odd lattice size $N$, $\gamma_{\mathcal{PT}} \to J/2$ ($\gamma_{\mathcal{PT}} \to J$) when $d = 2$ ($d = N-1$). Figure 4.4 shows a case of a CTQW starting at $\Psi(n,0) = \delta_{n,0}$ on an odd size lattice $N = 81$ with a nearest gain and loss locations at $m_0 = 40$ and $\bar{m}_0 = 42$ respectively. Column (a) corresponds to Hermitian limit with $\gamma = 0$, columns (b) and (c) correspond to the transition region with $\gamma = 0.54J$ and $\mathcal{PT}$-broken region with $\gamma = 1.1J$ respectively where $\gamma_{\mathcal{PT}} = J/2$. For an even size lattice, the maximum threshold $\gamma_{\mathcal{PT}}$ occurs when the distance $d$ between the gain and loss potentials is minimum or maximum at $d = 1$ or $d = N-1$.

### 4.3.2 Non-Unitary DTQW

The dynamic of a non-unitary discrete-time quantum walk is governed by a propagator $\mathcal{G}$ described by

$$\mathcal{G} = SG\Phi C, \tag{4.26}$$

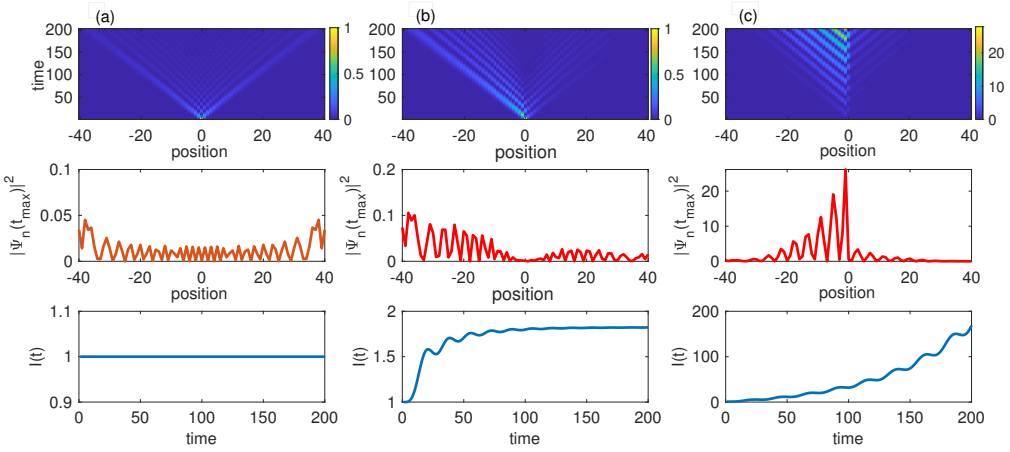


Fig. 4.4. Time-evolution for a CTQW; (a) $\gamma = 0$ (the unitary CTQW in $PT$-phase), (b) $\gamma = 0.54$ (the non-unitary CTQW at the exceptional points), (c) $\gamma = 1.1$ (the non-unitary CTQW in the $PT$-broken regime). (top panels) The contour maps of the logarithm of the norm of the wave function $\ln(|\psi(t)|^2)$ in the position and time plan. (middle panels) The norm of the wave function at maximum time $t$ $|\Psi_(n)(t_{max})|^2$. (bottom panels) The time dependence of the sum of the probability distribution I(t).

where $G$ and $\Phi$ represent the gain-loss operator and the phase operator respectively. Depending on the internal state of the walker, the gain-loss operator amplifies or damps the wave function while the phase operator adds a phase to the wave function amplitude. The gain-loss operator and phase operator can be defined by

$$G = \sum_n |n\rangle \langle n| \otimes \tilde{G}, \quad \tilde{G} = \begin{pmatrix} g_\uparrow(n) & 0 \\ 0 & g_\downarrow(n) \end{pmatrix}, \tag{4.27}$$

$$\Phi = \sum_n |n\rangle \langle n| \otimes \tilde{\Phi}_n, \quad \tilde{\Phi}_n = \begin{pmatrix} e^{\phi_\uparrow(n)} & 0 \\ 0 & e^{\phi_\downarrow(n)} \end{pmatrix}. \tag{4.28}$$

An example of the experimental realization of the nonunitary quantum walk implemented by two optical-fiber loops is depicted in Fig. 4.5 from [50]; in which case the nonunitary quantum walk can be represented by a two-steps time-evolution operator $\mathcal{G}$ defined by

$$\mathcal{G} = SG_2C(\theta_2)SG_1C(\theta_1), \tag{4.29}$$

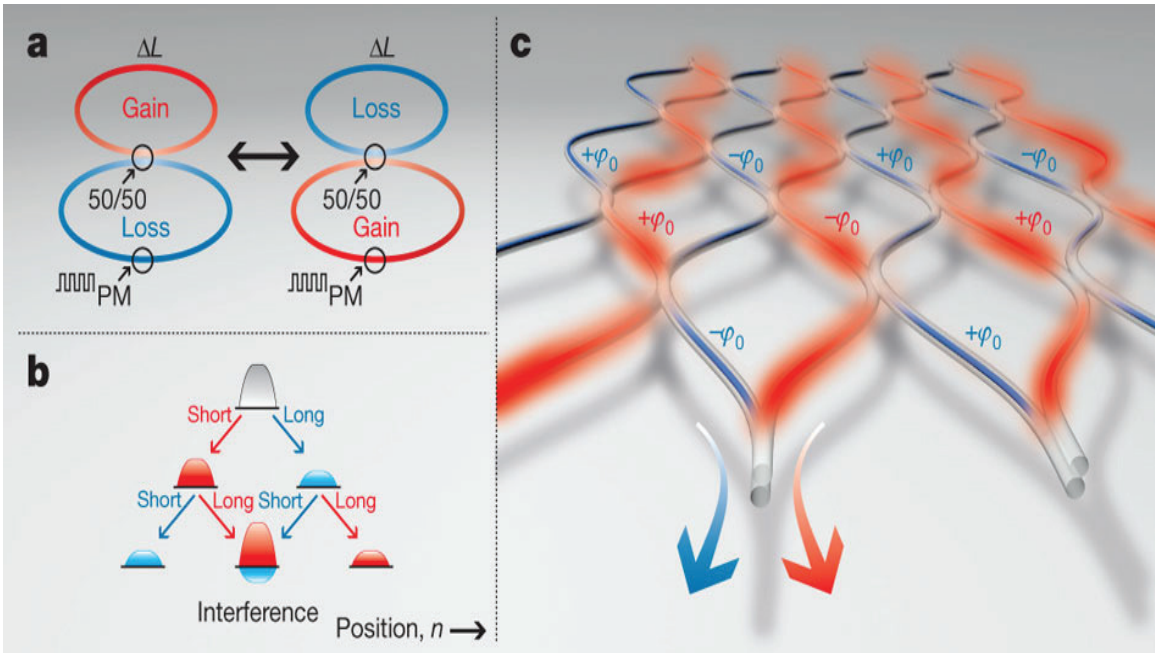


Fig. 4.5. From [50] (a) Two coupled fibre loops periodically switching between gain and loss. Pulses are delayed or advanced as a result of a length difference $\Delta L$ between the loops. PM, phase modulator. (b), Pulse evolution in the networks. Passages through short and long loops are indicated. (c) Equivalent $\mathcal{PT}$-symmetric network. Gain (red) and loss (blue) channels are positioned anti-symmetrically and are periodically coupled.

with

$$S = \sum_n \begin{pmatrix} |n-1\rangle\langle n| & 0 \\ 0 & |n+1\rangle\langle n| \end{pmatrix}, \tag{4.30}$$

$$G_i = \sum_n |n\rangle\langle n| \otimes \tilde{G}_{i,n}, \quad \tilde{G}_{i,n} = \begin{pmatrix} g_{i,L}(n) & 0 \\ 0 & g_{i,R}(n) \end{pmatrix}, \tag{4.31}$$

and

$$C(\theta_i) = \sum_n |n\rangle\langle n| \otimes \tilde{C}(\theta_{i,n}), \quad \tilde{C}(\theta_i(n)) = \begin{pmatrix} \cos[\theta_i(n)] & i\sin[\theta_i(n)] \\ i\sin[\theta_i(n)] & \cos[\theta_i(n)]. \end{pmatrix} \tag{4.32}$$

In the coin operator $C(\theta_i)$ and the gain-loss operator $G_i$, the subscript $i = 1$ or 2 distinguishes the parameter for the first or the second operator, respectively. Operator with a tilde on the top acts on the space of the internal states of the walker. Thus,

the operator $\tilde{C}(\theta_i, n)$ acts on the internal states of the walker at the position $n$ while the coin operator $C(\theta_i)$ mixes the walker's internal states, where the value of $\theta_i(n)$ determines the strength of the mixture at position $n$. The gain-loss operator $G_i$ multiplies the wave function amplitude by the factor $g_{i,\sigma}(n)$, where $\sigma =\uparrow$ or $\downarrow$. If $g_{i,\sigma}(n) \neq 1$, then $G_i$ and $\mathcal{G}$ are nonunitary operators. Suppose the walker was initially at the position $n = 0$ defined by the wave function $|\Psi(0)\rangle$, then after $t$ time steps it would be represented by

$$|\Psi(t)\rangle = \mathcal{G}^t |\Psi(0)\rangle = \sum_{n,\sigma=\uparrow,\downarrow} \psi_{n,\sigma}(t) |n\rangle \otimes |\sigma\rangle . \tag{4.33}$$

From the eigenvalue equation, the quasi-energy $\epsilon$ is defined by

$$\mathcal{G} |\Psi_\lambda\rangle = \lambda |\Psi_\lambda\rangle , \quad \lambda = e^{-i\varepsilon}, \tag{4.34}$$

where $|\Psi_\lambda\rangle$ is the eigenvector with eigenvalue $\lambda$. The quantum walk is unitary if $|\lambda| = 1$ and $\varepsilon$ is real with $2\pi$ periodicity, otherwise is nonunitary.

For an homogeneous nonunitary system in which all parameters are independent of the position $n$, the operators can be defined in momentum space where the coin operator $C(\theta_{i,n})$ and the gain-loss operator $G_{i,n}$ are both diagonal. Thus, the elemental operators of the time-evolution operator are given by

$$\tilde{G}_2 = \tilde{G}_1{}^{-1} = \tilde{G} = \begin{pmatrix} e^{\gamma} & 0 \\ 0 & e^{-\gamma} \end{pmatrix} = e^{\gamma\sigma_3}, \tag{4.35a}$$

$$\tilde{C}(\theta_i) = \begin{pmatrix} \cos[\theta_i] & i\sin[\theta_i] \\ i\sin[\theta_i] & \cos[\theta_i] \end{pmatrix} = e^{i\theta_i\sigma_1}, \tag{4.35b}$$

$$S = \sum_k |k\rangle \langle k| \otimes \tilde{S}(k), \quad \tilde{S}(k) = \begin{pmatrix} e^{+ik} & 0 \\ 0 & e^{-ik} \end{pmatrix} = e^{ik\sigma_3}, \tag{4.35c}$$

where $k$ is the wave number. In this context, the time-evolution operator is represented by

$$\mathcal{G} = \sum_k |k\rangle \langle k| \otimes \tilde{\mathcal{G}}(k), \tag{4.36a}$$

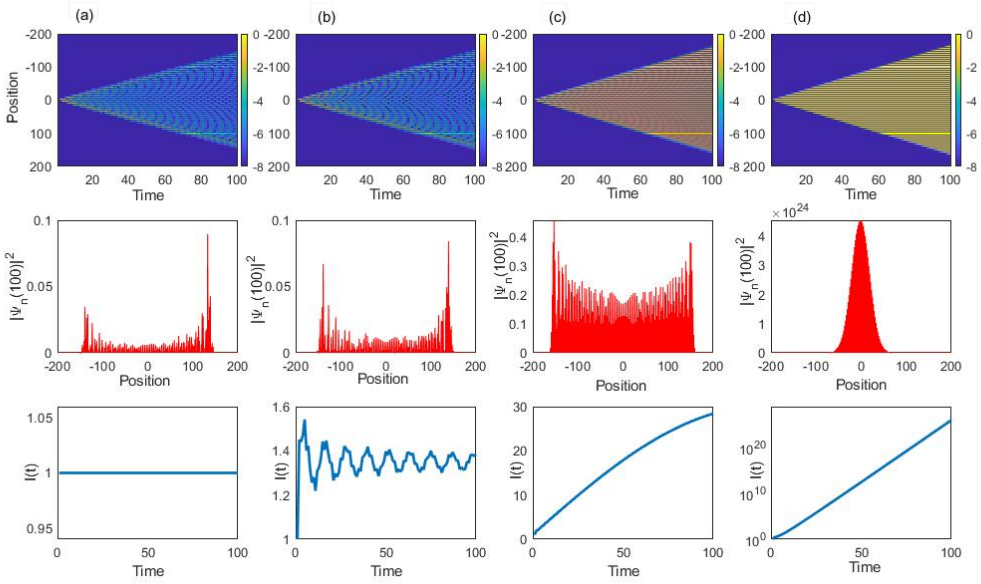


Fig. 4.6. Time-evolution of two-step DTQW in homogeneous system; (a) $e^{\gamma} = 1$ (unitary quantum walk),(b) $e^{\gamma} = 1.2$ (non-unitary quantum with all quasi-energy real), (c) $e^{\gamma} = 1.347$ (non-unitary quantum at the transition region),(d) $e^{\gamma} = 1.5$ (non-unitary quantum walk in the broken regime with complex quasi-energy). With $\theta_1 = -\pi/7$, $\theta_2 = \pi/4$ and $|\Psi_0\rangle = |\Psi(0)\rangle = |0\rangle \otimes |L\rangle$. Top panels: Contour maps of the logarithm of the norm of the wave function $\ln(|\Psi_n(t)|^2)$. Middle panels: The norm of the wave function after 100 time steps $|\Psi_n(t = 100)|^2$. Bottom panels: Sum of the weight of the wave function I(t) as a function of time steps.

$$\tilde{\mathcal{G}}(k) = \tilde{G}\tilde{C}(\theta_2)\tilde{S}(k)\tilde{G}^{-1}\tilde{C}(\theta_1). \tag{4.36b}$$

Figure 4.6 shows numerical results of the propagator for an homogeneous quantum walk defined in Eq. 4.36 with $C_1(-\pi/7)$ and $C_2(\pi/4)$. Column (a) represents a unitary quantum walk with $e^{\gamma} = 1$; column (b), a nonunitary quantum walk with entirely real quasi-energy when $e^{\gamma} = 1.2$; column (c) nonunitary quantum walk with exceptional point when $e^{\gamma} = 1.347$; and column (d), a nonunitary quantum walk with complex quasi-energy when $e^{\gamma} = 1.5$. The norm of the wave function at time step $T$ in columns (a) and (b) where the nonunitary quantum walk has entirely real quasi-

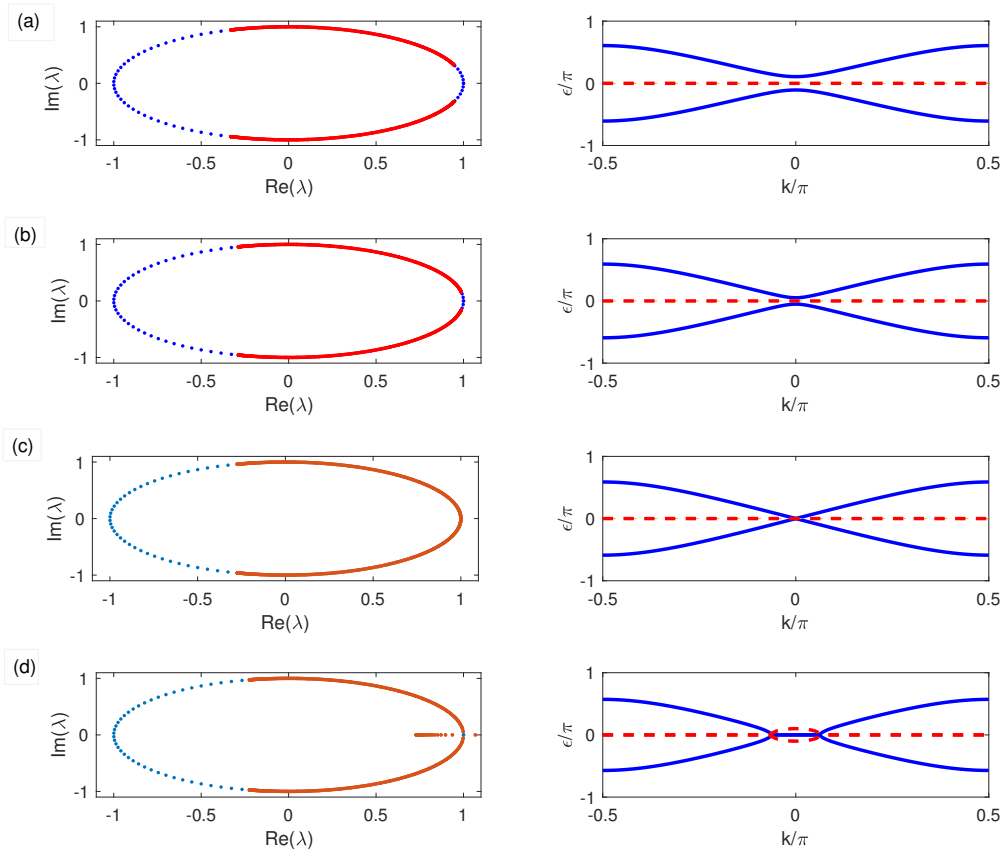


Fig. 4.7. Quasienergy and eigenvalues in two-step DTQW. The quasi-energy defined in Eq. 4.47 with different gain/loss parameters with $\theta_1 = -\pi/7$ and $\theta_2 = \pi/4$. The first column shows eigenvalue on a unit circle with $|\lambda| = 1$ on a complex plan. The second column shows the quasi-energy $\epsilon$ as a function of $k$ where the solid (dashed) curves are the real (imaginary) part of the quasi-energy.**(a)** (Fisrt row) For $e^{\gamma} = 1$, the quasi-energy are all real since the time-evolution operator is unitary. **(b)** For $e^{\gamma} = 1.3$, despite a non-unitary time-evolution operator the quasi-energy is entirely real, and there are open gaps of the quasi-energy around $\epsilon = 0, \pi$. (c) For $e^{\gamma} = 1.347$, with an entirely real quasi-energy, the gap around $\epsilon = 0$ closes. **(d)** For $e^{\gamma} = 1.5$, the quasi-energy becomes complex for $|k|/\pi = 0.1$, the gap closes.

energy is quite similar to the case of a unitary quantum walk in Fig. 4.3b. However the sum of the weight of the wave function $P(t)$ exhibits some small oscillations around $P(t) \approx 1$ when $e^{\gamma} \neq 1$.

Nonunitary DTQW has various symmetries and the most useful one, beside $\mathcal{PT}$ symmetry, are chiral symmetry ($\Gamma$) and particle hole symmetry ($\Xi$). In position and momentum spaces, the parity symmetry operator $\mathcal{P}$, time reversal symmetry operator $\mathcal{T}$, the chiral symmetry operator $\Gamma$ and the particle hole symmetry operator $\Xi$ are represented as follows,

$$\mathcal{P} = \sum_n |-n\rangle \langle n| \otimes \tilde{\mathcal{P}} = \sum_k |-k\rangle \langle k| \otimes \tilde{\mathcal{P}}, \tag{4.37}$$

$$\mathcal{T} = \sum_n |n\rangle \langle n| \otimes \tilde{\mathcal{T}} = \sum_k |-k\rangle \langle k| \otimes \tilde{\mathcal{T}}, \tag{4.38}$$

$$\Gamma = \sum_n |n\rangle \langle n| \otimes \tilde{\Gamma} = \sum_k |k\rangle \langle k| \otimes \tilde{\Gamma}, \tag{4.39}$$

$$\Xi = \sum_n |n\rangle \langle n| \otimes \tilde{\Xi} = \sum_k |-k\rangle \langle k| \otimes \tilde{\Xi}, \tag{4.40}$$

from which, the symmetry of the propagator $\mathcal{G}$ can be defined as,

$$(\mathcal{PT})\mathcal{G}(\mathcal{PT})^{-1} = \mathcal{G}^{-1}, \tag{4.41a}$$

$$(\tilde{\mathcal{P}}\tilde{\mathcal{T}})\tilde{\mathcal{G}(k)}(\tilde{\mathcal{P}}\tilde{\mathcal{T}})^{-1} = \tilde{\mathcal{G}}^{-1}(+k), \tag{4.41b}$$

$$\tilde{\Gamma}\tilde{\mathcal{G}}(k)\tilde{\Gamma}^{-1} = \tilde{\mathcal{G}}^{-1}(+k), \tag{4.41c}$$

$$\tilde{\Xi}\tilde{\mathcal{G}}(k)\tilde{\Xi}^{-1} = \tilde{\mathcal{G}}(-k). \tag{4.41d}$$

The appearance of the inverse of propagator in Eq. 4.41 makes its analytical solution challenging. To overcome the difficulty, it is necessary to apply the symmetry time frame; in which case for an homogeneous DTQW, the propagator becomes [66],

$$\mathcal{G}' = C(\theta_1/2)SG_2C(\theta_2)SG_1C(\theta_1/2). \tag{4.42}$$

A detailed analysis of the quasienergy of the propagator $\mathcal{G}$ can be easy carried out in momentum space by applying a Fourier transform on the propagator $\mathcal{G}$. Thus, we have:

$$\mathcal{G}'(k) = \sum_{i=0,1,2,3} d_i(k)\sigma_i \tag{4.43}$$

where $\sigma_i$ $(i = 1, 2, 3)$ are Pauli matrices and

$$d_0(k) = \cos\theta_1 \cos\theta_2 \cos 2k - \sin\theta_1 \sin\theta_2 \cosh 2\gamma, \tag{4.44a}$$

$$d_1(k) = \sin\theta_1 \cos\theta_2 \cos 2k + \cos\theta_1 \sin\theta_2 \cosh 2\gamma, \tag{4.44b}$$

$$d_2(k) = d_2 = -\sin\theta_2 \sinh 2\gamma, \tag{4.44c}$$

$$d_3(k) = \cos\theta_2 \sin 2k, \tag{4.44d}$$

with $d_0^2(k) + d_1^2(k) - d_2^2(k) + d_3^2(k) = 1$. The eigenvalues and eigenvectors of $\mathcal{G}'$ are

$$\lambda_\pm(k) = d_0(k) \pm i\sqrt{1 - d_0^2(k)}, \tag{4.45a}$$

$$|\psi_\pm(k)\rangle = \frac{1}{\sqrt{2\cos 2\omega_k}}(\mathrm{e}^{\pm i\omega_k}, \pm i\mathrm{e}^{\pm i\omega_k}\mathrm{e}^{-i\nu_k})^{\mathrm{T}}, \tag{4.45b}$$

with $\omega_k$ and $\nu_k$ defined as

$$|d(k)|\mathrm{e}^{i\nu_k} = d_3(k) + id_1(k), \tag{4.46a}$$

$$\cos 2\omega_k = \sqrt{1 - \left(\frac{d_2}{|d(k)|}\right)^2}. \tag{4.46b}$$

From Eq. 4.44a the quasienergy of the propagator is defined by

$$d_0(k) = \cos(\pm\epsilon) = \cos\theta_1 \cos\theta_2 \cos 2k - \sin\theta_1 \sin\theta_2 \cosh 2\gamma. \tag{4.47}$$

The plots of the eigenvalues and quasienergy of the propagator $\mathcal{G} = SG_2C(\pi/4)SG_1C(-\pi/7)$ on Fig. 4.7 illustrate the parity-time symmetric behavior by featuring the existence of a $\mathcal{PT}$-symmetry phase, panels (a)-(b) and a $\mathcal{PT}$-broken phase (Fig. 4.7, panels (c)-(d)). When the gain strength parameter $\gamma$ is not zero, the gain/loss operator $G_i$ becomes nonunitary, so does the propagator $\mathcal{G}$. The scenario is illustrated in Fig. 4.7b where $\gamma \neq 0$ but the quasienergy is still entirely real and the eigenvalues remain on a

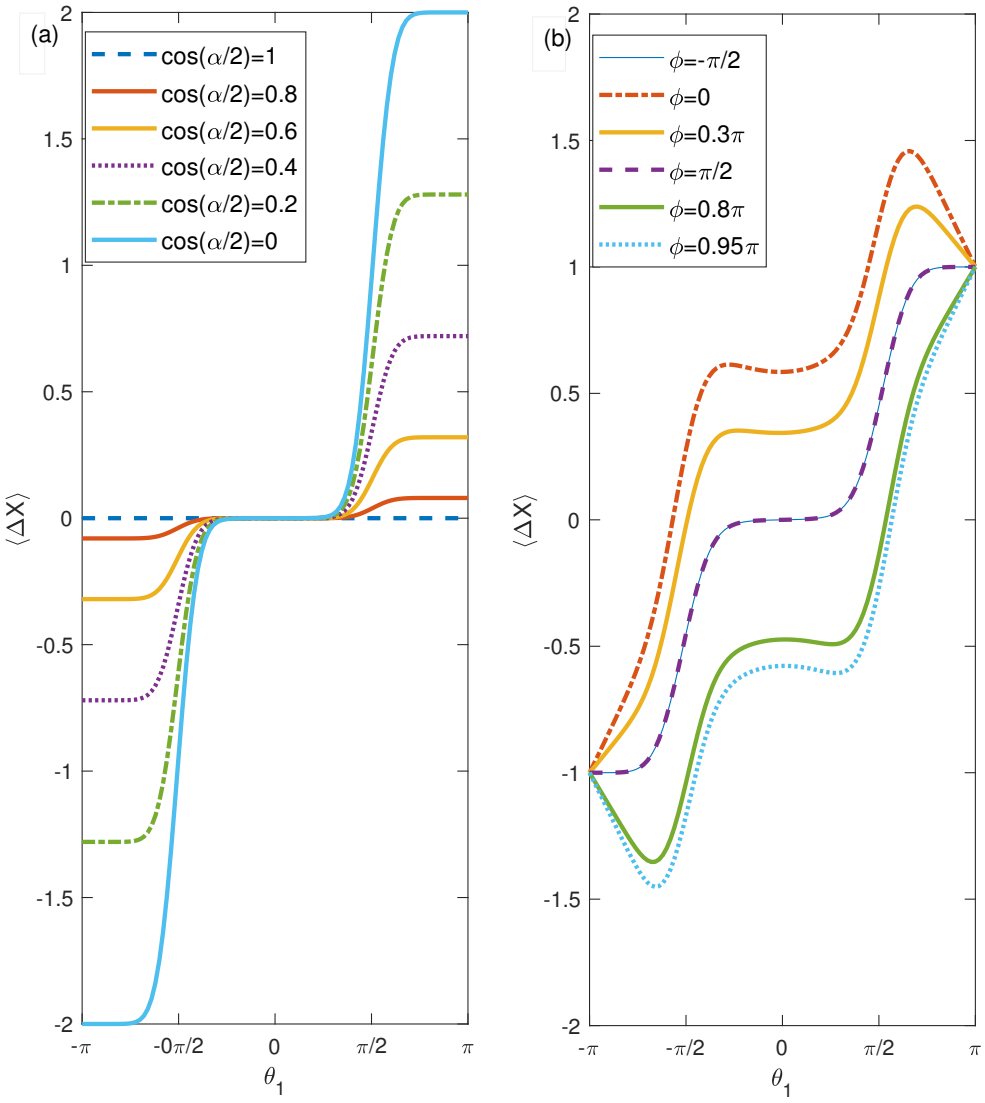


Fig. 4.8. Average displacement of the walker in the time frame symmetry of the coin parameter $\theta_1$. (a), For the measurement success parameter $p = 1$, $\phi = \pi/2$, and different values of $\alpha$, i.e different position of initial internal state on the Bloch sphere, the average displacement scale as $\langle \Delta x \rangle \propto (\cos(\alpha/2))^2$. (b) When $p = 1$ and $\alpha = \pi/4$, $\langle \Delta x \rangle$ is still discrete for different values of $\phi$.

unit circle ($\mathcal{PT}$-symmetric phase). Figure 4.7c shows the appearance of exceptional point when $\gamma \approx \gamma_{\mathcal{PT}}$ and the quasienergy becomes gapless at $\epsilon = 0$; while Fig. 4.7d corresponds to $\gamma > \gamma_{\mathcal{PT}}$ where the quasienergy becomes complex. Equation 4.44a and right column of Fig. 4.7 show that the quasienergy is symmetric with respect to $\epsilon = 0$. An increasing $\gamma$ changes drastically the behavior of the propagator manifested by a linear grow at exceptional point and an exponential increase in broken regime.

The ease of maintaining the symmetries in nonunitary operators makes DTQW an ideal platform to investigate and study topological properties. For example, the development of edge states that are robust under symmetry-preserving perturbations, which are also responsible for exponential amplification of wavefunction amplitudes at specific positions and times. The existence and the number of these edge states are dependent of the integer-value topological invariants characteristics of different phases of the system [67]. For a given Floquet topological phase there are two distinct topological invariant numbers, each associated with a specific symmetric time frame. These topological numbers are robust against perturbations which preserve symmetries. Figure 4.9 depicts different phases of the propagator of a nonunitary DTQW as a function of the parameters of the coin operators $\theta_1$ and $\theta_2$ with the gain/loss parameter $\gamma = \ln(1.1)$. The blue area corresponds to $\mathcal{PT}$-phase regime while the orange area represents the $\mathcal{PT}$-broken regime. Note that as expected the orange area extends as the gain parameter $\gamma$ increases further past the threshold. The first experimental observation of bulk topological invariants in nonunitary DTQW using single photon in a delayed choice scheme was conducted not too long ago by Zhan *et al.* [68]. Not only their work confirms the existing theory of the topological invariants, it also shows that with a specific setup a topological invariant can be detected by a measurement of the average displacement of the walker. Instead of a specific case of the initial internal state of the walker in their work, we generalize the computation of the average displacement $\langle \Delta x \rangle$ for an initial internal state on the Bloch sphere. Let consider a walker with an initial internal state given by $\cos(\alpha/2)\,|+\rangle + e^{i\phi}\sin(\alpha/2)\,|-\rangle$, where $|\pm\rangle = (|\uparrow\rangle \pm |\downarrow\rangle)/\sqrt{2}$. In analogy to [68], the gain-loss operations are implemented by

performing a partial measurement of the state of the walker at each time step with the probability of a successful measurement given by $0 < p \leq 1$; thus, the positive ($M_p$) and negative ($M_n$) partial measurement operators are given by

$$M_p = \sum_x |x\rangle\langle x| \otimes \sqrt{p}\,|-\rangle\langle -|\,, \tag{4.48a}$$

$$M_n = \sum_x |x\rangle\langle x| \otimes (|+\rangle\langle +| + \sqrt{1-p}\,|-\rangle\langle -|). \tag{4.48b}$$

In a case of successful measurement after $t$ time steps, the state of the coin walker is then given by $|\Psi_T\rangle = (M_p\mathcal{G}')(M_n\mathcal{G}')^{t-1}\,|\Psi_0\rangle$. With this setup, we numerically compute the average displacement of the walker with an initial internal state varying on the Bloch sphere. Not only the results in Fig. 4.8a confirm the discrete character of the average displacement, they show that for $p = 1$ and $\phi = \pi/2$, $\langle \Delta x \rangle$ scale as $\propto (\cos(\alpha/2))^2$. For $p = 1$ and $\alpha = \pi/4$, Fig. 4.8b also shows the quantization of the average displacement for different value of $\phi$. We believe there is a way to characterize the average displacement as function of the measurement success parameter $p$, the coordinates of initial internal state on the Bloch sphere ($\alpha$ and $\phi$), and the coin operators parameters $\theta_i$.

We also study a three-step DTQW whose dynamic is characterised by a combination of three coin/shift operations in a unit of time. For a unitary system, the time evolution operator $U$ is given by $U = SC(\theta_2)SC(\theta_0)SC(\theta_1)$, where $S$ and $C_{i=0,1,2}$ represent the shift operator and the coin operator respectively. A non-unitary system can be engineered in three-step DTQW for instance by symmetrically incorporating a gain/loss operator $G_i$ and its inverse into $U$. In which case, the non-unitary time evolution $\mathcal{G}$ is given by

$$\mathcal{G} = SGC(\theta_2)SC(\theta_0)SG^{-1}C(\theta_1). \tag{4.49}$$

Here also, the state of the walker evolves as $|\Psi(t+1)\rangle = \mathcal{G}\,|\Psi(t)\rangle$. In the homogeneous case of a quantum walk, the probability of finding the walker at position $n$ at

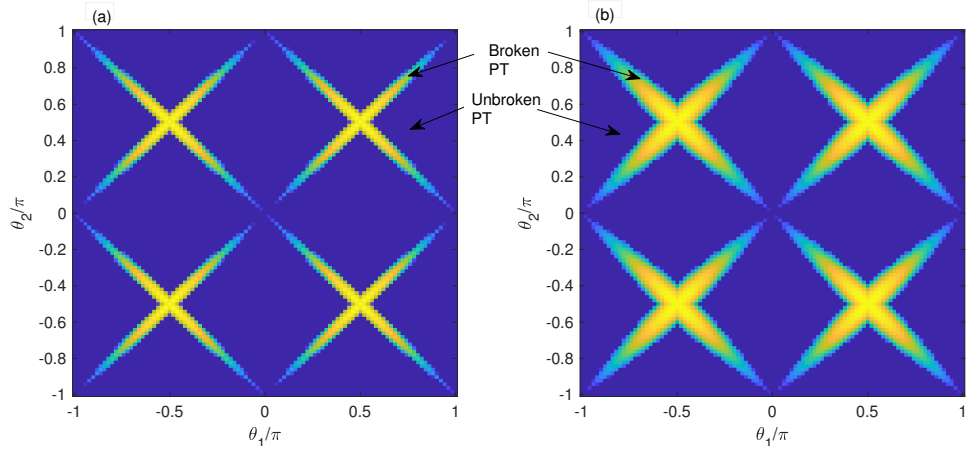


Fig. 4.9. Two-step DTQW. Phase diagram as a function of $\theta_1$ and $\theta_2$ when $e^{\gamma} = 1.1$ (a), and $e^{\gamma} = 1.2$ (b). The blue area corresponds to unbroken $\mathcal{PT}$-symmetry phase, while the orange area represents broken $\mathcal{PT}$-symmetry with complex eigenenergy whose real part is $Re(\epsilon) = 0$ or $\pi$.

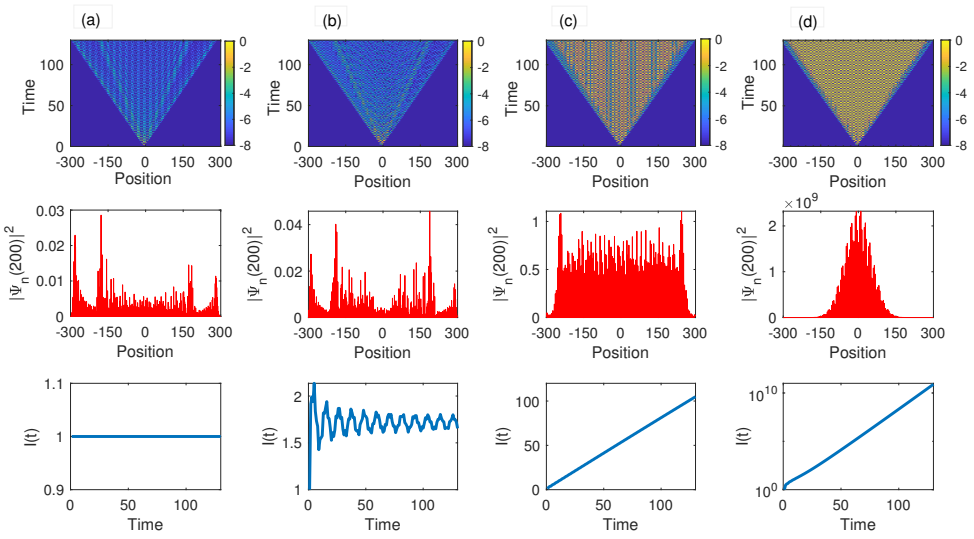


Fig. 4.10. The time evolution of a three-step quantum walk in homogeneous system, with $\theta_0 = \pi/4$, $\theta_1 = \pi/9$, $\theta_2 = -3\pi/4$ and the walker initial state $|\Psi_0\rangle = |0\rangle \otimes (|\uparrow\rangle + i\,|\downarrow\rangle)$. (a) For $\gamma = 0$, the time evolution $\mathcal{G}$ is unitary. (b) For $\gamma = \ln 1.3$, nonunitary quantum walk with all quasienergy real. (c) $\gamma = \ln 1.4805$, nonunitary quantum walk at $\mathcal{PT}$-breaking transition phase. (d) $\gamma = 1.5$, three-step nonunitary quantum walk in the broken regime with complex quasienergy. Top panels: Contour maps of the logarithm of the norm of the wave function $\ln(|\Psi_n(t)|^2)$. Middle panels: The norm of the wave function after 100 steps, $|\Psi_n(t = 100)|^2$. Bottom panels: Sum of the weight of the wave function as a function of time step, I(t).

time $t$ and the sum of the probability distributions over the position space are given respectively by

$$|\Psi_n(t)|^2 = |\Psi_{n,\uparrow}(t)|^2 + |\Psi_{n,\downarrow}(t)|^2, \tag{4.50a}$$

$$\mathrm{I}(t) = \sum_n |\psi_n(t)|^2. \tag{4.50b}$$

The bi-orthogonality (orthogonality defined on a combined vector space and its dual space) of the eigenvectors ($\langle\Psi_m|\Psi_n\rangle = \delta_{mn}$) guarantees $\mathrm{I}(t) = 1$ for a unitary DTQW (when $\gamma = 0$) Whereas it is expected to be different for a non-unitary case (when $\gamma \neq 0$).

Figure 4.10 shows the numerical results of the time evolution of an homogeneous three-step DTQW in a periodic boundary setting for $\theta_0 = \pi/4$, $\theta_1 = \pi/9$, and $\theta_2 = -3\pi/4$. In contrast to a single or two-step DTQW where the probability distribution (at a large specific time step $t$) shows a bi-modal character in a unitary regime ($\gamma = 0$),the probability distribution of a three-steps DTQW reveals a symmetric quad-modal distinction for a walker initially in a superposition of internal states and localized at site $n_0 = 0$, i.e $|\Psi_0\rangle = |0\rangle \otimes (|\uparrow\rangle + i\,|\downarrow\rangle)/\sqrt{(2)}$ (Fig. 4.10a, middle panel). A close analysis reveals that the variance of the inner extra pair of peaks in 3-step DTQW decreases as the central coin parameter $\theta_0$ goes from 0 to $\pi/2$ where it vanishes.

The quasienergy $\epsilon$ of the propagator can be derived from the eigenvalue equation and is given by

$$\begin{aligned} \mathcal{G}\,|\Psi_\lambda\rangle &= \lambda\,|\Psi_\lambda\rangle \\ \lambda &= e^{-i\epsilon}, \end{aligned} \tag{4.51}$$

where $\Psi_\lambda$ and $\lambda$ are eigenvector and corresponding eigenvalue respectively. The quasienergy $\epsilon$ is expected to be real for a unitary time-evolution when $|\lambda| = 1$. In similar way to Eq. 4.43 in the two-step DTQW, we apply a Fourier transform to $\mathcal{G}$ in order to analyse the relevant quasi-energies. We have,

$$\mathcal{G} = \sum_k |k\rangle\langle k| \otimes \tilde{\mathcal{G}}, \tag{4.52a}$$

$$\tilde{\mathcal{G}} = \sum_{i=0,1,2,3} n_i(k)\sigma_i, \tag{4.52b}$$

where,

$$\begin{aligned}
n_0(k) =& -\cos\theta_0\cos\theta_1\cos\theta_2\cos(3k) \\
&-\sin\theta_0\cos\theta_1\sin\theta_2\cos(k) \\
&+\cos\theta_0\sin\theta_1\sin\theta_2\cosh(2\gamma+ik) \\
&-\sin\theta_0\sin\theta 1\cos\theta 2\cosh(2\gamma-ik),
\end{aligned}$$

$$\begin{aligned}
n_1(k) =& i\cos\theta_0\cos\theta_2\sin\theta_1\cos(3k) \\
&-i\sin\theta_0\sin\theta_1\sin\theta_2\cos(k) \\
&+i\cos\theta_0\cos\theta_1\sin\theta_2\cosh(2\gamma+ik) \\
&+i\sin\theta_0\cos\theta_1\cos\theta_2\cosh(2\gamma-ik),
\end{aligned}$$

$$\begin{aligned}
n_2(k) =& -i\cos\theta_0\sin\theta_1\cos\theta_2\sin(3k) \\
&+i\sin\theta_0\sin\theta_1\sin\theta_2\sin(k) \\
&-\sin\theta_0\cos\theta_1\cos\theta_2\sinh(2\gamma-ik) \\
&-\cos\theta_0\sin\theta_1\sin\theta_2\sinh(2\gamma+ik),
\end{aligned}$$

$$\begin{aligned}
n_3(k) =& \cos\theta_0\cos\theta_1\cos\theta_2\sin(3k) \\
&-\sin\theta_0\cos\theta_1\sin\theta_2\sin(k) \\
&-\sin\theta_0\sin\theta_1\cos\theta_2\sinh(2\gamma-ik) \\
&-\cos\theta_0\sin\theta_1\sin\theta_2\sinh(2\gamma+ik).
\end{aligned}$$

A solution to the eigenvalue problem, Eq. 4.51 gives

$$\begin{aligned}
cos(\pm\epsilon) =& \cos\theta_0\cos\theta_1\cos\theta_2\cos(3k) \\
&-\sin\theta_0\cos\theta_1\sin\theta_2\cos(k) \\
&-\cos\theta_0\sin\theta_1\sin\theta_2\cosh(2\gamma+ik) \\
&-\sin\theta_0\sin\theta_1\cos\theta_2\cosh(2\gamma-ik).
\end{aligned} \tag{4.53}$$

From equation 4.53, the requirement for a finite non-zero $\mathcal{PT}$-breaking threshold is given by

$$\theta_1 = n\pi, \qquad \theta_0 - \theta_2 = n\pi. \tag{4.54}$$

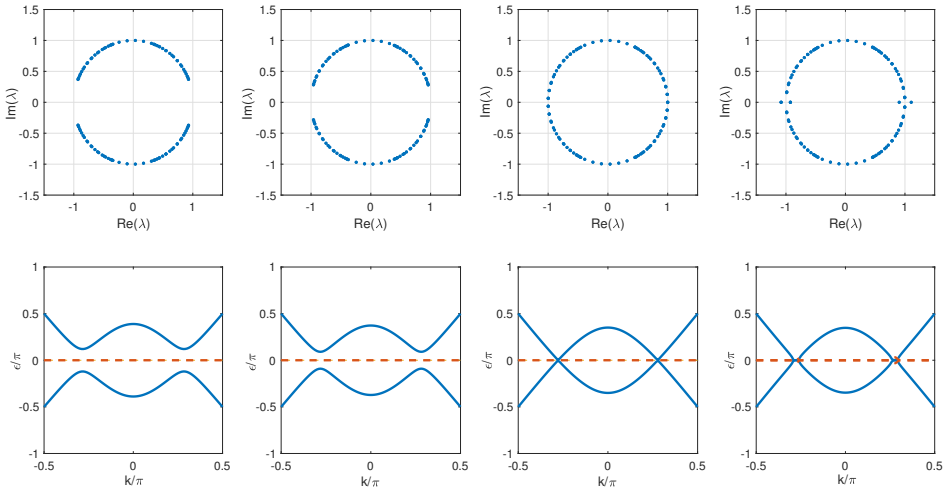


Fig. 4.11. Quasienergy and eigenvalues in three-step DTQW. The quasienergy defined in Eq. 4.53 with different gain/loss parameters with $\theta_0 = \pi/4$, $\theta_1 = \pi/9$ and $\theta_2 = -3\pi/4$. The top panel shows the eigenvalue on a unit circle with $|\lambda| = 1$ in the complex plane. The second panel shows the quasi-energy $\epsilon$ as a function of $k$ where the solid (dashed) curves are the real (imaginary) part of the quasi-energy. First column: $e^{\gamma} = 1$, the quasi-energy are all real since the time-evolution operator is unitary. Second column: $e^{\gamma} = 1.3$, despite a non-unitary time-evolution operator the quasi-energy is entirely real and there are open gaps of the quasi-energy around $\epsilon = 0, \pi$. Third column: $e^{\gamma} = 1.4805$ with an entirely real quasi-energy, the gap around $\epsilon = 0$ closes. Fourth column: $e^{\gamma} = 1.5$, the quasi-energy becomes complex for $|k|/\pi = 0.1$, the gap closes.

Figure 4.11 shows the results of a numerical study of the eigenvalues and the quasienergy of the propagator $\mathcal{G}$. Those results highlight, like in a two-step quantum walk, the existence of real quasienergy (Fig. 4.11) in a non-unitary regime; evidence that the three-step non-unitary time-evolution operator $\mathcal{G}$ possesses the parity-time symmetry. The top panel of Fig. 4.11 displays a plot of the eigenvalues of propagator $\mathcal{G}$ in a complex plane and the bottom panel features the plot of its quasienergy $\epsilon$ as a function of the wave vector $k$. When $\gamma = 0$, the propagator is unitary and its eigenvalues fit a complex unit circle as expected (first column). For $\gamma = \ln 1.3$, although the

propagator is nonunitary the eigenvalues still fit on a unit circle and the quasi-energy is entirely real with an open gap around $\epsilon = 0, \pi$ (second column),i.e. the propagator $\mathcal{G}$ is in a $\mathcal{PT}$ symmetry phase. At $\gamma = \ln 1.4805$, the quasienergy of the nonunitary propagator is still entirely real with a closure of the gap around $\epsilon = 0$; moreover, there is a coalescence of two pairs of eigenvalues in the complex plane, sign of development of exceptional points $\mathcal{PT}$-breaking transition (third column), meaning the $\mathcal{PT}$ symmetry threshold $\gamma_{\mathcal{PT}} \approx \ln 1.4805$. When the gain strength parameter $\gamma = \ln 1.5$, part of the quasienergy becomes complex and the gap closes, $\mathcal{PT}$-broken phase. In all cases the quasienergy spectrum shows a symmetrical feature with respect to $\epsilon = 0$.

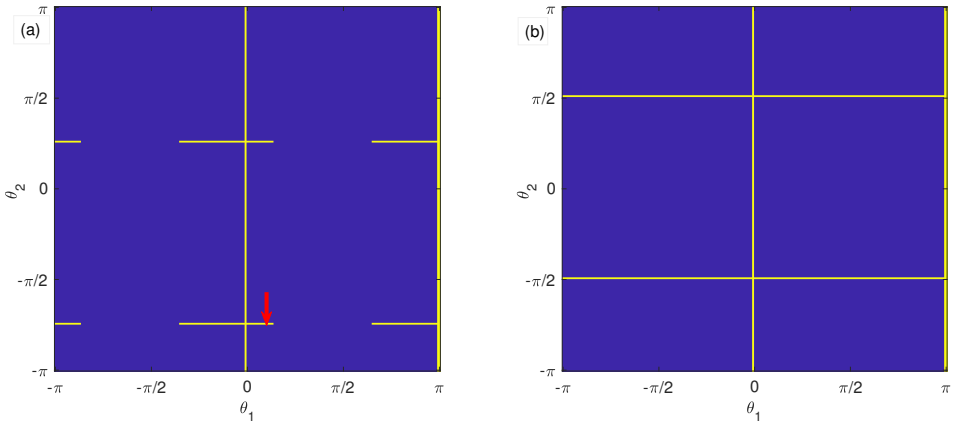


Fig. 4.12. Topological phase diagram of $\mathcal{G}$ for fixed center parameter $\theta_0$ and $e^{\gamma} = 1.1$ in PBC. (a) $\theta_0 = \pi/4$. The red arrow points to $(\theta_1, \theta_2) = (\pi/9, -3\pi/4)$. (b) $\theta_0 = \pi/2$.

To complete our work in three-step DTQW, we investigate the topological phase diagram of the time evolution in the plane of the coin operator parameters $\theta_1$ and $\theta_2$ at particular values of $\theta_0$. Although lacking a time frame symmetry due to its structure, the propagator of the three-step does exhibit some topological phase transition in a periodic boundary condition (PBC) as well in an open boundary condition (OBC) settings. In contrast the two-step quantum walk in PBC settings, the phase diagram of the propagator of the three-step revels a structure which is independent of the weight

of the gain/loss parameter $\gamma$; assertion we proved in Eqs. 4.53, 4.54. Figure 4.12 shows the phase diagram of the propagator $\mathcal{G}$ as a function of $\theta_1$ and $\theta_2$ for a fixed value of $\theta_0$ of the central coin parameter and gain/loss parameter $\gamma = \ln(1.1)$. For $\theta_0 = \pi/2$ (top panel), the thin orange strips along some finite values of other coin parameter denote the $\mathcal{PT}$-symmetric regime, characteristic of the reality of the eigenvalues of the time-evolution $\mathcal{G}$; the blue area corresponds to $\mathcal{PT}$-broken regime independently of the gain parameter $g$. For $\theta_0 = \pi/4$ (bottom panel), the singularity of the $\mathcal{PT}$-symmetric regime along some specific values of the coin operator parameters $\theta_1$ and $\theta_2$; the red arrow in Fig. 4.12b pinpoints a location in a $\mathcal{PT}$-symmetric regime corresponding to the values of the coin operator parameters used for the above numerical results.

A numerical study of the topological phase diagram of the time evolution operator $\mathcal{G}$ in OBC reveals an extended $\mathcal{PT}$-symmetric regime which depends on the gain-loss parameter $\gamma$ like in a two-step quantum walk with a PBC settings. As it is shown in Fig. 4.13, for a fixed value of the coin parameter $\theta_0 = \pi/2$ and gain-loss parameter $\gamma = \ln(1.1)$ (top panel), the $\mathcal{PT}$-symmetric regime (orange strips) extends symmetrically along the diagonal also along some specific values of the ends coin parameter at $\theta_{1,2} = \pm\pi/2$; the blue region corresponds to the $\mathcal{PT}$-broken phase. With the same middle coin operator parameter $\theta_0 = \pi/2$ and a larger value $\gamma = \ln(1.4)$ (bottom panel), the $\mathcal{PT}$-symmetric region exhibits the same symmetric structure but with a reduced area confirming the dependence of the topological phase transition of the gain-loss parameter $\gamma$.

Figure 4.12 shows the topological phase diagram of the 3-step DTQW for a fixed parameter ($\theta_0$) of the center coin, for $\theta_0 = \pi/2$ (a) and $\theta_0 = \pi/4$ (b). from equation [4.54], one expects for these fixed value of $\theta_0 = \pi/2$ and $\theta_0 = \pi/4$, $\theta_2$ to be $\pm\pi/2$ and $\theta_1 = \pm\pi$ $\theta_2 = \pi/4$ $(-3\pi/4)$ in $\mathcal{PT}$-regime respectively (yellow stripes in the figures).

Lastly, we consider DTQW models where gain and loss are localized to only two, reflection-symmetric sites, and investigate the dependence of the $\mathcal{PT}$ symmetry breaking transitions on other variables such as the gain-loss locations $m_0$ or the coin pa-

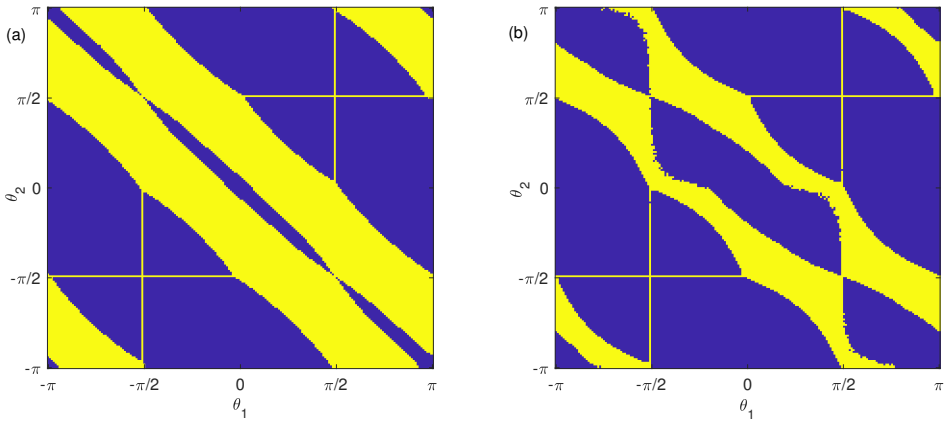


Fig. 4.13. Topological phase diagram of the propagator $\mathcal{G}$ for a fixed center coin parameter $\theta_0 = \pi/2$, different gain/loss parameter in OBC setting. (a) $\gamma = \ln(1.1)$ is marked by extended $\mathcal{PT}$-symmetric region (yellow area); (b) when $\gamma = \ln(1.4)$, the $\mathcal{PT}$-symmetric region is shrunk as expected.

rameter $\theta$. For that we choose a single-step DTQW whose propagator is given by $\mathcal{G} = SGC$, where $G$ is a square matrix with the main diagonal given by the column vector $L$ defined by,

$$L(k) = \begin{cases} e^{\gamma} & k = m_0 \\ e^{-\gamma} & k = \bar{m}_0 \\ 0 & \text{otherwise} \end{cases} \tag{4.55}$$

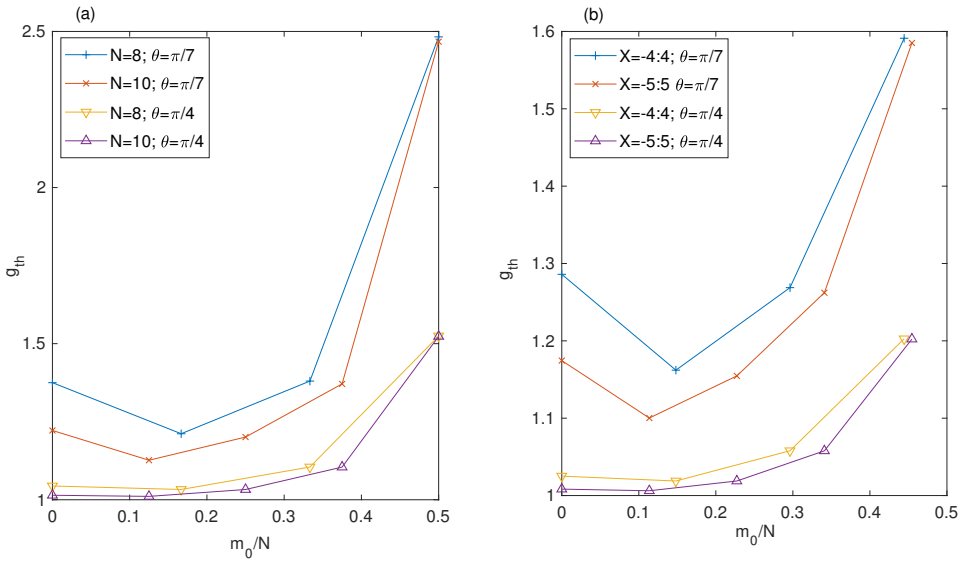


Fig. 4.14. Gain parameter $\mathcal{PT}$-breaking threshold $g_{th} = e^{\gamma_{\mathcal{PT}}}$ as a function of the gain location $m_0$ for even numbers of sites (a) and odd numbers of sites (b). For large coin parameter $\theta$, the $\mathcal{PT}$ gain threshold decreases monotonically with the gain location and it is strengthened again at small value of $\theta$.

The scheme describes a quantum walk on a line of integers $k$ where the walker only experiences a gain at site $k = m_0$ and a loss at site $k = \bar{m}_0 = N - m_0 + 1$ respectively ($N$ is the size of the lattice). In closed boundary condition setting, the $\mathcal{PT}$ gain threshold monotonically decreases as a function of the gain location for large coin parameter $\theta$ and it enhances again as the distance between gain and loss sites

increases for small value of $\theta$, Fig. 4.14. Also, we uncovered that for even lattice sizes, the gain parameter $\mathcal{PT}$-breaking threshold $g_{th}$ scales as $1/\sin\theta$ for both nearest and farthest gain-loss locations figure 4.15(a). whereas for odd lattice sizes $g_{th}$ scales as $1/\sin\theta$ for largest gain-loss separations, but scales as as $1/\sqrt{\sin\theta}$, Fig. 4.15b.

Moreover, we study the topological phase transitions of a non-homogeneous system with site dependent coin parameter $\theta$. Our result reveals, in open boundary conditions (OBC), a finite gain $\mathcal{PT}$-breaking threshold for certain periodical structure of the coin operator. For instance, let us consider a site-dependent coin with periodicity $p = 2$ given by

$$C(\theta_1, \theta_2) = \mathrm{diag}(X, C_2(\theta_1), C_2(\theta_2), C_2(\theta_1), C_2(\theta_2), \ldots, X), \tag{4.56}$$

where $C_2(\theta)$=exp$(iX\theta)$ is the 2x2 unitary coin operator, and the open boundary conditions are imposed by choosing the coin operator $X = \sigma_1$ (Pauli matrix) at the two ends of the lattice. This DTQW approximates the finite Su-Schrieffer-Heeger Hamiltonian for a CTQW. Figure 4.16 shows the $\mathcal{PT}$ symmetry threshold for an even lattice with different locations of the gain and the loss. For closest and farthest away gain and loss locations the $g_{\mathcal{PT}}$ is robust for $\theta_1 \simeq \theta_2$ (left and right panels), whereas $g_{\mathcal{PT}}$ is weakened for a gain location at midway location on the lattice (center panel). The phase diagram behaves differently for an odd lattice size where $g_{\mathcal{PT}}$ seems to strengthen as the gain location transfers from the beginning to the end of the lattice, see Fig. 4.17.

Although lacking a $\mathcal{PT}$-symmetric structure, the following periodical structure coins operators also lead to a positive threshold,

$$\begin{aligned} C &= XC_2(\theta_1)C_2(\theta_2)C_2(\theta_2)\ldots X \qquad (N = 0 \mod 3) \\ C &= XC_2(\theta_1)C_2(\theta_1)C_2(\theta_2)\ldots X \qquad (N = 1 \mod 3). \end{aligned} \tag{4.57}$$

Thus, through this analysis we have expanded the class of DTQW models that show $\mathcal{PT}$ symmetry breaking transition even though the underlying Hermitian DTQW is not reflection symmetric.

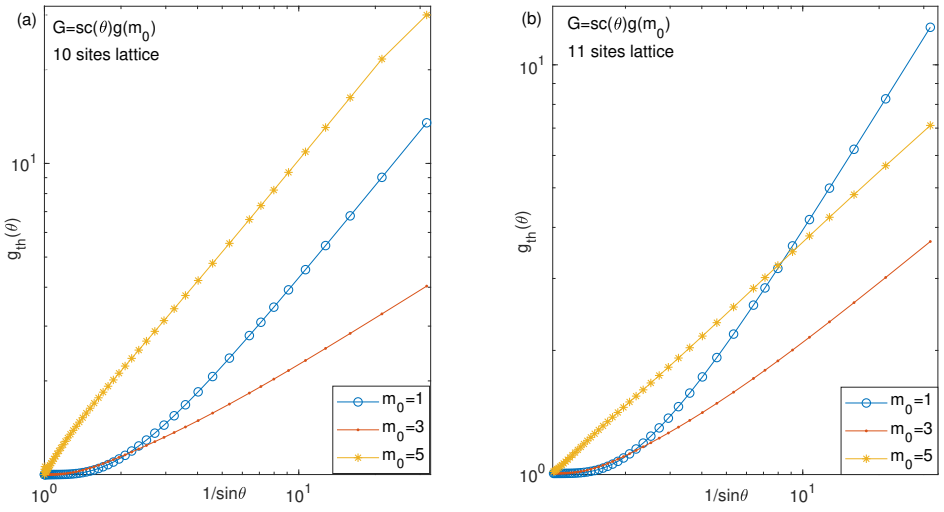


Fig. 4.15. Gain parameter $\mathcal{PT}$-breaking threshold $g_{th}$ as a function of the coin parameter $\theta$. (a) For an even number of lattice size, $g_{th}$ scales as $1/\sin\theta$ for both nearest ($m_0 = 5$) and farthest ($m_0 = 1$) gain-loss locations. (b) For an odd number of lattice size, $g_{th}$ scales as $1/\sin\theta$ for largest gain-loss locations ($m_0 = 1$), but scales as $1/\sqrt{\sin\theta}$ when gain and loss are closest to each other ($m_0 = 5$).

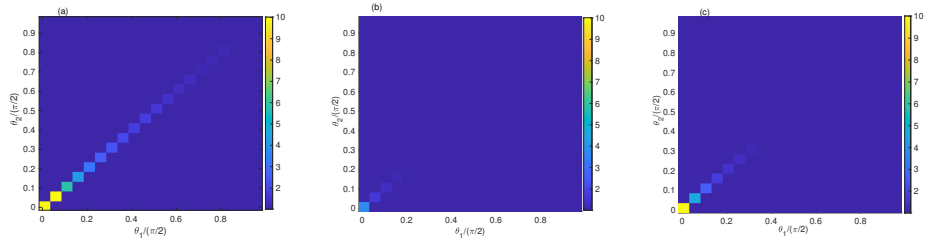


Fig. 4.16. Phase diagram of single step DTQW for an even lattice size. The blue area corresponds to $\gamma_{\mathcal{PT}} = 0$. When the distance $d$ between the gain location and the loss location is maximum (a). When $d$ is about a half the lattice size (b). when $d$ is minimum (c).

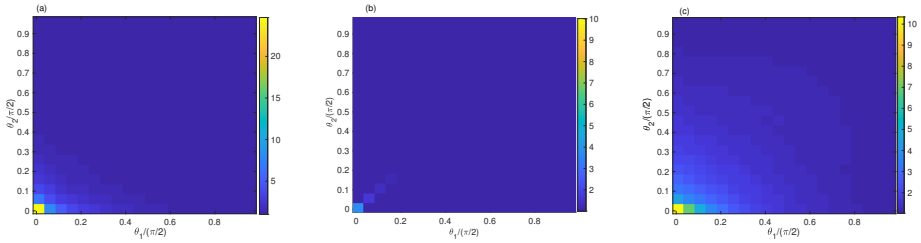


Fig. 4.17. Phase diagram of single step DTQW for an odd lattice size. The blue area corresponds to $\gamma_{\mathcal{PT}} = 0$. When the distance $d$ between the gain location and the loss location is maximum (a). When $d$ is about a half the lattice size (b). when $d$ is minimum (c).

# 5. SUMMARY

In this thesis, we investigated variant features of non-Hermitian $\mathcal{PT}$-symmetric systems in continuous time and discrete time settings. In chapter two, we studied the effects of random, periodic, long-range hopping disorder on the fate of the $\mathcal{PT}$-symmetric phase in uniform lattice with a single gain and single loss located at mirror symmetric sites. Mathematically, the lattice models considered correspond to tridiagonal matrices with Hermitian, random, periodic entries, combined with a non-Hermitian, fixed, gain-loss potential entries along the main diagonal. While, in general, $\mathcal{PT}$-symmetric systems are fragile to random disorder we uncovered that for some set of random disorder of period $p$, gain location $m_0$ and lattice size $N$ such that $\{m_0 = 0, N + 1 = 0\}$ mod $p$, there exists a positive $\mathcal{PT}$ threshold. These results hold as well for next-nearest-neighbor or higher hopping processes, consequently suggest that there exists an hidden symmetry, which preserves the positive $\mathcal{PT}$ symmetry breaking threshold of the clean lattice. Experimentally, the models studied can be realized in coupled waveguide arrays with one gain waveguide and one lossy waveguide. Preferably, if the on-site potentials or tunneling amplitudes are tunable; for example, via voltage-controlled top-gate heaters. In chapter three, we investigated the fate of phase differences between wave-function amplitudes on nearest-neighbor sites in $\mathcal{PT}$-symmetric lattice models and other time-invariants quantities of $\mathcal{PT}$-symmetric Hamiltonian. For a wide range of open chains, deep in the $\mathcal{PT}$-broken phase, we numerically found that the phase differences between adjacent sites, located before the gain site, saturate at $3\pi/2$ while the rest of the phase difference of the chain saturate at $\pi/2$. However the trending disappears for lattice chains with periodic boundary conditions but the saturation phenomenon is still valid. We presented an analytical solution for all time invariants of a broad class of $\mathcal{PT}$-symmetric Hamiltonians. Our results were confirmed using a single-photon interferometry by simulating

the quantum dynamics of a $\mathcal{PT}$-symmetric qudit across a fourth-order exceptional point. The observed enhanced sensitivity at the fourth-order exceptional point and phase locking signal the abundant and complex dynamics of $\mathcal{PT}$-symmetric systems with higher-order EPs that is potentially useful in developing ultrasensitive detection devices such as whispering-gallery mode (WGM) sensors. In chapter four, we studied the properties of random walks. On one hand, we contrasted and compared the classical walk with the quantum walk, and then investigated the different features of quantum walk in the continuous and discrete time settings. We explored the time evolution of DTQW embedded with $\mathcal{PT}$ symmetry in closed and open boundary conditions. We derived the analytical and numerical solutions of the eigenvalue problem for two-steps and three-steps of a one-dimensional DTQW, in finding the limit of $\mathcal{PT}$ symmetry threshold. Additionally, we investigated the topological properties of the non-unitary DTQW and.... The one-dimensional DTQW quantum walk (in which the movement is only allowed on a line) has been experimentally implemented in a number of different physical systems, ranging from neutral atoms in spin-dependent optical lattices [69] to ions in a linear ion trap [70], from photons in arrays of evanescently coupled waveguides [71] to optical setups with a fibre network, where additional optical amplifiers make it possible to control the effects of gain and loss [50]. We believe that the results obtained in our study of the DTQW stimulate further developments on $\mathcal{PT}$ symmetry of non-unitary time evolution operators, which has not been studied enough yet, compared with non-Hermitian Hamiltonians systems.

# REFERENCES


[1] A. K. Harter, F. A. Onanga, and Y. N. Joglekar, "PT symmetry breaking in the presence of random, periodic, long-range hopping," in *Active Photonic Materials VIII*, vol. 9920. International Society for Optics and Photonics, 2016, p. 99201O.

[2] ——, "Veiled symmetry of disordered parity-time lattices: protected PT-threshold and the fate of localization," *Scientific reports*, vol. 8, no. 1, p. 44, 2018.

[3] Y. N. Joglekar, F. A. Onanga, and A. K. Harter, "Time-invariant PT product and phase locking in PT-symmetric lattice models," *Physical Review A*, vol. 97, no. 1, p. 012128, 2018.

[4] Z. Bian, L. Xiao, K. Wang, X. Zhan, F. A. Onanga, F. Ruzicka, W. Yi, Y. N. Joglekar, and P. Xue, "Time invariants across a fourth-order exceptional point in a parity-time-symmetric qudit," *arXiv preprint arXiv:1903.09806*, 2019.

[5] P. M. Chaikin and T. C. Lubensky, *Principles of condensed matter physics*. Cambridge university press Cambridge, 2000, vol. 1.

[6] A. Aspuru-Guzik and P. Walther, "Photonic quantum simulators," *Nature physics*, vol. 8, no. 4, p. 285, 2012.

[7] K. Leung, "Two-electron reduction of ethylene carbonate: A quantum chemistry re-examination of mechanisms," *Chemical Physics Letters*, vol. 568, pp. 1–8, 2013.

[8] K. A. Olive, K. Agashe, C. Amsler, M. Antonelli, J.-F. Arguin, D. M. Asner, H. Baer, H. R. Band, R. Barnett, T. Basaglia *et al.*, "Review of particle physics," *Chinese physics C*, vol. 38, no. 9, p. 090001, 2014.

[9] A. V. Pinheiro, D. Han, W. M. Shih, and H. Yan, "Challenges and opportunities for structural dna nanotechnology," *Nature nanotechnology*, vol. 6, no. 12, p. 763, 2011.

[10] J. J. Sakurai and E. D. Commins, "Modern quantum mechanics, revised edition," 1995.

[11] C. M. Bender and S. Boettcher, "Real spectra in non-hermitian hamiltonians having PT symmetry," *Physical Review Letters*, vol. 80, no. 24, p. 5243, 1998.

[12] C. Bender, "Cm bender, rep. prog. phys. 70, 947 (2007)." *Rep. Prog. Phys.*, vol. 70, p. 947, 2007.

[13] C. M. Bender, "Cm bender, dc brody, and hf jones, phys. rev. lett. 89, 270401 (2002)." *Phys. Rev. Lett.*, vol. 89, p. 270401, 2002.

[14] A. Mostafazadeh, "Pseudo-hermiticity versus pt symmetry: the necessary condition for the reality of the spectrum of a non-hermitian hamiltonian," *Journal of Mathematical Physics*, vol. 43, no. 1, pp. 205–214, 2002.

[15] K. G. Makris, R. El-Ganainy, D. Christodoulides, and Z. H. Musslimani, "Beam dynamics in PT symmetric optical lattices," *Physical Review Letters*, vol. 100, no. 10, p. 103904, 2008.

[16] Z. Musslimani, K. G. Makris, R. El-Ganainy, and D. N. Christodoulides, "Optical solitons in PT periodic potentials," *Physical Review Letters*, vol. 100, no. 3, p. 030402, 2008.

[17] A. Guo, G. Salamo, D. Duchesne, R. Morandotti, M. Volatier-Ravat, V. Aimez, G. Siviloglou, and D. Christodoulides, "Observation of PT-symmetry breaking in complex optical potentials," *Physical Review Letters*, vol. 103, no. 9, p. 093902, 2009.

[18] C. E. Rüter, K. G. Makris, R. El-Ganainy, D. N. Christodoulides, M. Segev, and D. Kip, "Observation of parity–time symmetry in optics," *Nature physics*, vol. 6, no. 3, p. 192, 2010.

[19] A. Ruschhaupt, F. Delgado, and J. Muga, "Physical realization of-symmetric potential scattering in a planar slab waveguide," *Journal of Physics A: Mathematical and General*, vol. 38, no. 9, p. L171, 2005.

[20] M. Lawrence, N. Xu, X. Zhang, L. Cong, J. Han, W. Zhang, and S. Zhang, "Manifestation of PT symmetry breaking in polarization space with terahertz metasurfaces," *Physical review letters*, vol. 113, no. 9, p. 093901, 2014.

[21] B. Zhen, C. W. Hsu, Y. Igarashi, L. Lu, I. Kaminer, A. Pick, S.-L. Chua, J. D. Joannopoulos, and M. Soljačić, "Spawning rings of exceptional points out of dirac cones," *Nature*, vol. 525, no. 7569, p. 354, 2015.

[22] L. Feng, Y.-L. Xu, W. S. Fegadolli, M.-H. Lu, J. E. Oliveira, V. R. Almeida, Y.-F. Chen, and A. Scherer, "Experimental demonstration of a unidirectional reflectionless parity-time metamaterial at optical frequencies," *Nature materials*, vol. 12, no. 2, p. 108, 2013.

[23] L. Feng, Z. J. Wong, R.-M. Ma, Y. Wang, and X. Zhang, "Single-mode laser by parity-time symmetry breaking," *Science*, vol. 346, no. 6212, pp. 972–975, 2014.

[24] Z. Lin, H. Ramezani, T. Eichelkraut, T. Kottos, H. Cao, and D. N. Christodoulides, "Unidirectional invisibility induced by PT-symmetric periodic structures," *Physical Review Letters*, vol. 106, no. 21, p. 213901, 2011.

[25] S. Longhi, "Optical realization of relativistic non-hermitian quantum mechanics," *Physical review letters*, vol. 105, no. 1, p. 013903, 2010.

[26] Y. Chong, L. Ge, and A. D. Stone, "PT-symmetry breaking and laser-absorber modes in optical scattering systems," *Physical Review Letters*, vol. 106, no. 9, p. 093902, 2011.

[27] L. Ge and A. D. Stone, "Parity-time symmetry breaking beyond one dimension: the role of degeneracy," *Physical Review X*, vol. 4, no. 3, p. 031011, 2014.

[28] L. Ge, K. G. Makris, D. N. Christodoulides, and L. Feng, "Scattering in PT- and RT-symmetric multimode waveguides: Generalized conservation laws and spontaneous symmetry breaking beyond one dimension," *Physical Review A*, vol. 92, no. 6, p. 062135, 2015.

[29] H. Schomerus, "Quantum noise and self-sustained radiation of PT-symmetric systems," *Physical review letters*, vol. 104, no. 23, p. 233601, 2010.

[30] C. M. Bender, "Pt symmetry in quantum physics: From a mathematical curiosity to optical experiments," *Europhysics News*, vol. 47, no. 2, pp. 17–20, 2016.

[31] T. Kato, *Perturbation theory for linear operators*. Springer Science & Business Media, 2013, vol. 132.

[32] D. N. Christodoulides, F. Lederer, and Y. Silberberg, "Discretizing light behaviour in linear and nonlinear waveguide lattices," *Nature*, vol. 424, no. 6950, p. 817, 2003.

[33] U. Peschel, T. Pertsch, and F. Lederer, "Optical bloch oscillations in waveguide arrays," *Optics letters*, vol. 23, no. 21, pp. 1701–1703, 1998.

[34] M. Segev, Y. Silberberg, and D. N. Christodoulides, "Anderson localization of light," *Nature Photonics*, vol. 7, no. 3, p. 197, 2013.

[35] R. El-Ganainy, K. Makris, D. Christodoulides, and Z. H. Musslimani, "Theory of coupled optical pt-symmetric structures," *Optics letters*, vol. 32, no. 17, pp. 2632–2634, 2007.

[36] Y. N. Joglekar, C. Thompson, D. D. Scott, and G. Vemuri, "Optical waveguide arrays: quantum effects and pt symmetry breaking," *The European Physical Journal-Applied Physics*, vol. 63, no. 3, 2013.

[37] M. D. Wheeler, "For integrated photonics, a tale of two materials," *Photonics Spectra*, vol. 50, no. 8, pp. 38–45, 2016.

[38] Z. Gong, Y. Ashida, K. Kawabata, K. Takasan, S. Higashikawa, and M. Ueda, "Topological phases of non-hermitian systems," *Physical Review X*, vol. 8, no. 3, p. 031079, 2018.

[39] E. Farhi and S. Gutmann, "Quantum computation and decision trees," *Physical Review A*, vol. 58, no. 2, p. 915, 1998.

[40] Y. Aharonov, L. Davidovich, and N. Zagury, "Quantum random walks," *Physical Review A*, vol. 48, no. 2, p. 1687, 1993.

[41] L. Jin and Z. Song, "Solutions of p t-symmetric tight-binding chain and its equivalent hermitian counterpart," *Physical Review A*, vol. 80, no. 5, p. 052107, 2009.

[42] D. D. Scott and Y. N. Joglekar, "Pt-symmetry breaking and ubiquitous maximal chirality in a pt-symmetric ring," *Physical Review A*, vol. 85, no. 6, p. 062105, 2012.

[43] Y. N. Joglekar, D. Scott, M. Babbey, and A. Saxena, "Robust and fragile pt-symmetric phases in a tight-binding chain," *Physical Review A*, vol. 82, no. 3, p. 030103, 2010.

[44] C. M. Bender, D. C. Brody, and H. F. Jones, "Must a hamiltonian be hermitian?" *American Journal of Physics*, vol. 71, no. 11, pp. 1095–1102, 2003.

[45] A. Mostafazadeh, "Exact pt-symmetry is equivalent to hermiticity," *Journal of Physics A: Mathematical and General*, vol. 36, no. 25, p. 7081, 2003.

[46] A. Mostafazadeh and A. Batal, "Physical aspects of pseudo-hermitian and pt-symmetric quantum mechanics," *Journal of Physics A: Mathematical and General*, vol. 37, no. 48, p. 11645, 2004.

[47] A. Mostafazadeh, "Pseudo-hermitian representation of quantum mechanics," *International Journal of Geometric Methods in Modern Physics*, vol. 7, no. 07, pp. 1191–1306, 2010.

[48] S. Klaiman, U. Günther, and N. Moiseyev, "Visualization of branch points in p t-symmetric waveguides," *Physical review letters*, vol. 101, no. 8, p. 080402, 2008.

[49] L. Feng, M. Ayache, J. Huang, Y.-L. Xu, M.-H. Lu, Y.-F. Chen, Y. Fainman, and A. Scherer, "Nonreciprocal light propagation in a silicon photonic circuit," *Science*, vol. 333, no. 6043, pp. 729–733, 2011.

[50] A. Regensburger, C. Bersch, M.-A. Miri, G. Onishchukov, D. N. Christodoulides, and U. Peschel, "Parity–time synthetic photonic lattices," *Nature*, vol. 488, no. 7410, p. 167, 2012.

[51] B. Peng, Ş. K. Özdemir, F. Lei, F. Monifi, M. Gianfreda, G. L. Long, S. Fan, F. Nori, C. M. Bender, and L. Yang, "Parity–time-symmetric whispering-gallery microcavities," *Nature Physics*, vol. 10, no. 5, p. 394, 2014.

[52] M. Brandstetter, M. Liertzer, C. Deutsch, P. Klang, J. Schöberl, H. Türeci, G. Strasser, K. Unterrainer, and S. Rotter, "Reversing the pump dependence of a laser at an exceptional point," *Nature communications*, vol. 5, p. 4034, 2014.

[53] B. Peng, Ş. Özdemir, S. Rotter, H. Yilmaz, M. Liertzer, F. Monifi, C. Bender, F. Nori, and L. Yang, "Loss-induced suppression and revival of lasing," *Science*, vol. 346, no. 6207, pp. 328–332, 2014.

[54] H. Hodaei, M.-A. Miri, M. Heinrich, D. N. Christodoulides, and M. Khajavikhan, "Parity-time–symmetric microring lasers," *Science*, vol. 346, no. 6212, pp. 975–978, 2014.

[55] I. Barashenkov, D. Pelinovsky, and P. Dubard, "Dimer with gain and loss: Integrability and-symmetry restoration," *Journal of Physics A: Mathematical and Theoretical*, vol. 48, no. 32, p. 325201, 2015.

[56] H. Hodaei, A. U. Hassan, S. Wittek, H. Garcia-Gracia, R. El-Ganainy, D. N. Christodoulides, and M. Khajavikhan, "Enhanced sensitivity at higher-order exceptional points," *Nature*, vol. 548, no. 7666, p. 187, 2017.

[57] W. Su, J. Schrieffer, and A. J. Heeger, "Solitons in polyacetylene," *Physical review letters*, vol. 42, no. 25, p. 1698, 1979.

[58] A. J. Heeger, S. Kivelson, J. Schrieffer, and W.-P. Su, "Solitons in conducting polymers," *Reviews of Modern Physics*, vol. 60, no. 3, p. 781, 1988.

[59] P. G. Harper, "Single band motion of conduction electrons in a uniform magnetic field," *Proceedings of the Physical Society. Section A*, vol. 68, no. 10, p. 874, 1955.

[60] S. Aubry and G. André, "Analyticity breaking and anderson localization in incommensurate lattices," *Ann. Israel Phys. Soc*, vol. 3, no. 133, p. 18, 1980.

[61] J. Kempe, "Quantum random walks: an introductory overview," *Contemporary Physics*, vol. 44, no. 4, pp. 307–327, 2003.

[62] A. Nayak and A. Vishwanath, "Quantum walk on the line," *arXiv preprint quant-ph/0010117*, 2000.

[63] J. Wang and K. Manouchehri, *Physical implementation of quantum walks*. Springer, 2013.

[64] A. M. Childs, E. Farhi, and S. Gutmann, "An example of the difference between quantum and classical random walks," *Quantum Information Processing*, vol. 1, no. 1-2, pp. 35–43, 2002.

[65] G. Abal, R. Siri, A. Romanelli, and R. Donangelo, "Quantum walk on the line: Entanglement and nonlocal initial conditions," *Physical Review A*, vol. 73, no. 4, p. 042302, 2006.

[66] K. Mochizuki, D. Kim, and H. Obuse, "Explicit definition of PT symmetry for nonunitary quantum walks with gain and loss," *Physical Review A*, vol. 93, no. 6, p. 062116, 2016.

[67] D. Kim, M. Ken, N. Kawakami, and H. Obuse, "Floquet topological phases driven by PT- symmetric nonunitary time evolution," *arXiv preprint arXiv:1609.09650*, 2016.

[68] X. Zhan, L. Xiao, Z. Bian, K. Wang, X. Qiu, B. C. Sanders, W. Yi, and P. Xue, "Detecting topological invariants in nonunitary discrete-time quantum walks," *Physical review letters*, vol. 119, no. 13, p. 130501, 2017.

[69] O. Mandel, M. Greiner, A. Widera, T. Rom, T. W. Hänsch, and I. Bloch, "Coherent transport of neutral atoms in spin-dependent optical lattice potentials," *Physical review letters*, vol. 91, no. 1, p. 010407, 2003.

[70] F. Zähringer, G. Kirchmair, R. Gerritsma, E. Solano, R. Blatt, and C. Roos, "Realization of a quantum walk with one and two trapped ions," *Physical review letters*, vol. 104, no. 10, p. 100503, 2010.

[71] D. T. Nguyen, D. A. Nolan, and N. F. Borrelli, "Localized quantum walks in quasi-periodic fibonacci arrays of waveguides," *Optics express*, vol. 27, no. 2, pp. 886–898, 2019.

# A. PHASE LOCKING IN ADJACENT SITES

```
% For the observation of the phase locking phenomenon,
   this code plots
% the phase difference of wave functions in adjacent sites
% and of the norm of the wavefunctions on each site.

clear;
tic

N=8; % number of sites
j=1; % tunneling parameter
gamma = 1.2*j; % gain strength parameter
tmax = 12;
m0=1; % gain location

m1=2*pi;
% Define a random initial state
r=rand(N,1);
psi0=exp(2i*pi*rand(N,1));
psi=r.*psi0;

% define the Hamiltonian
H1=zeros(N);
H1(m0,m0)=1i*gamma;
H1(N-m0+1,N-m0+1)=-1i*gamma;
```

```
H2=full(gallery('tridiag',N,-1,0,-1));
H = H1 + H2;
t=0:0.1:tmax;
A=zeros(N,length(t));

for k=1:length(t)
    u=expm(-1i*H*t(k))*psi;
    A(:,k)=u;
    prob=abs(A).^2;
end
A1=angle(A);
B=diff(A1);
B=mod(B,m1);
% plot of the norms
figure
hold on;
plot(t,abs(A(:,:)));
xlim([0 tmax]);
ylim([0 1000]);
title('Norm of the wave functon per site');
xlabel('time t');
ylabel('u(:)');
prob = abs(A).^2;
plot(t,abs(A(4,:)));
plot(t,abs(A(3,:)));

%plot of the phase difference of adjacent sites
figure
hold on;
```

```
plot(t,(1./pi)*(B(:,:)));
title('Phase difference between consecutive entry of u(t)'
   );
xlabel('Normalized time Jt');
ylabel('\theta_i_+_1 - \theta_i');
toc
```

# B. AVERAGE DISPLACEMENT IN DTQW

```
% This is the code for the plots of the average
   displacement of the walker
% in different times frame symmetry, Fig. 4.8.


% Label x corresponds to the site index.
% Time evolution: U'=R(theta_1/2)SR(\theta_2)SR(\theta_1
   /2).

clear;
tic;

% Defining DTQW lattice parameters, coin-space basis and
   projectors.
T=31;
N=31; % number of sites: choose odd for a symmetric
   lattice.
xx=-(N-1)/2:1:(N-1)/2;%
vf=zeros(2*N,T); % DTQW state of the walker.
wf=zeros(2*N,T); % create ancilliary tracking for B=0.5
   case.

X=[0 1;1 0];
Y=[0 -1i;+1i 0];
```

```
Z=[1 0;0 -1];
up=[1;0]; % basis element of the internal state
down=[0;1]; % basis element of the internal state
up1=(eye(2)+Z)/2;
down1=(eye(2)-Z)/2;
plus=(up+down)/sqrt(2); % symmetric state, eigenstate of X
   .
minus=(up-down)/sqrt(2); % antisymmetric state, eigenstae
   of X.

% The walker is localized on the central cell, and has a
   coin-space
% wavefunction.
v=zeros(N,1);
v(floor((N+1)/2))=1;
% state of the walker in the coin-space is arbitrary.
A=1/sqrt(2);
B=0;
psicoin=A*plus+exp(1i*B*pi)*sqrt(1-A^2)*minus;
v1=kron(v,psicoin);
vf(:,1)=v1;

psitrack=A*plus+exp(1i*0.5*pi)*sqrt(1-A^2)*minus;
w1=kron(v,psitrack);
wf(:,1)=w1;

% Defining the shif operator that moves the walker to
   right or left. Use
% PBC for a unitary shift operator.
```

```
a=ones(N-1,1);
a1=diag(a,1);
a2=diag(a,-1);
a11=zeros(N);
a11(1,N)=1;
a22=a11';
s=kron(a2+a11,up1)+kron(a1+a22,down1);

% Define the measurement-loss operator with 0<=p<=1. The
   plus-initial
% coin-state may be needed for the loss protocol to work.
p=1;
g=sqrt(1-p);
g00=(plus*plus')+g*(minus*minus');
g0e=sqrt(p)*(minus*minus');
g0=kron(eye(N),g00);
gf=kron(eye(N),g0e);

% Coin operator is defined by two angles. Vary theta_1
   only for PX work.
% U'=R(theta_1/2)SR(\theta_2)SR(\theta_1/2).
theta2=pi/2;
coin2=expm(1i*theta2*Y/2);
c2=kron(eye(N),coin2);

tt1=-1:0.01:1; % theta_1 range in units of pi, for the
   coin operator.
deltax=zeros(length(tt1),1);
dwellt=zeros(length(tt1),1);
```

```
deltatrackx=zeros(length(tt1),1);
dwelltrackt=zeros(length(tt1),1);

%time-evolve the wavefunction for T steps and then extract
    various weights
%for ranging over all values of theta_1.
 for aa=1:length(tt1)
        theta1=tt1(aa)*pi;
        coin1=expm(1i*theta1*Y/4);
        c1=kron(eye(N),coin1);
        u=g0*c1*s*c2*s*c1; % Propagator of negative
           measurement
        uf=gf*c1*s*c2*s*c1; % Propagator that defines the
           final state

        for bb=2:T
             vf(:,bb)=u*vf(:,bb-1);
             wf(:,bb)=u*wf(:,bb-1);
        end
        vf1=uf*vf;
        wf1=uf*wf;

        vff=abs(kron(eye(N),down)'*vf1).^2+abs(kron(eye(N)
           ,up)'*vf1).^2;
        wff=abs(kron(eye(N),down)'*wf1).^2+abs(kron(eye(N)
           ,up)'*wf1).^2;
        % add the coin-space down and up weights.
```

```
        % calculate space-time averages for N and L
           sectors.
        deltax(aa)=sum(sum(xx'.*vff));
        dwellt(aa)=sum(sum((1:1:T)'.*vff'));

        deltatrackx(aa)=sum(sum(xx'.*wff));
        dwelltrackt(aa)=sum(sum((1:1:T)'.*wff'));
 end

 diffx=deltax-deltatrackx;
 difft=dwellt-dwelltrackt;

toc;
```

# C. PHASE DIAGRAM OF THE PT-BREAKING THRESHOLD

```
% Code for the phase diagram of the PT-breaking threshold
   as a function of
% the gain location.

clear;
tic;

J=1; % tunneling parameter
Loc=1; % location of the gain
N=110; % number of lattice sites

all=zeros(1,floor(N/2));

% take a loop over all possible location of the gain
for m0=Loc:Loc:floor(N/2)
    m0bar=N+1-m0;   % location of the loss
    d=zeros(N,1);
    d(m0,1)=1i;
    d(m0bar,1)=conj(d(m0,1));

    H0=full(gallery('tridiag',N,-J,0,-J));

        CHAT=0;
```

```
        gamma=0;
        deltagamma=1.e-3;
        while(CHAT==0)
            gamma=gamma+deltagamma; %gain/loss parameter
            H=gamma*diag(d)+H0;
            D=eig(H);
            maxerror=max(abs(imag(D)));
            if(maxerror>1.e-8)
                CHAT=1;
            end
        end
        index=m0;
    all(:,m0)=gamma;
    x=linspace(0,m0/N,floor(N/2));
end

plot(x,all)
 toc;
```

# VITA

## Education

- **Doctor of Philosophy**, Physics. Expected: December 2019
  Purdue University, Indianapolis, IN Dissertation: *Parity-Time Symmetry in Non-Hermitian Quantum Walks*
- **Master of Science**, Physics, May 2014
  Purdue University, Indianapolis, IN
- **Bachelor of Science**, Mathematics, August 2011
  Purdue University, Indianapolis, IN

## Teaching Experience

- **Recitation Instructor, Laboratory Instructor, Recitation Mentor**
  Indiana University-Purdue University Indianapolis, Indianapolis, IN 2011 - 2019

## Publications

- A. K. Harter, F. Assogba Onanga & Y. N. Joglekar, "Veiled Symmetry of Disordered Parity-Time Lattices," Scientific report **8**, 44 (2018)
- Y. N. Joglekar, F. Assogba Onanga & A. K. Harter, "Time-Invariant PT-Product and Phase-Locking in PT-Symmetric Lattice Models," Phys. Rev. **97**, 012128 (2018)
- Z. Bian, et *al*, "Time Invariant Across a Fourth-Order Exceptional Point in a Parity-Time-Symmetric Qudit," arXiv:1903.09806v1

- A. K. Harter, F. Assogba Onanga & Y. N. Joglekar, "PT-Symmetry Breaking in the Presence of Random, Periodic, Long Range Hopping," Proc. of SPIE, Vol. 9920, 99201O-1 (2016)

**Presentations**

- "PT-Symmetry Breaking in the Presence of Random, Periodic, Long-Range Hopping,"
  (Contributed coauthor) SPIE Nanoscience & Engineering, San Diego, CA (USA), August 2016
- "Parity-Time Breaking in Discrete-Time Quantum Walk"
  (Contributed poster), 642 WH-Heraeus-Seminar "Non-Hermitian Hamiltonian in Physics," Bad Honnef (Germany) May 2017
- "Time Invariant PT-Product and Phase Locking in PT-Symmetric Systems"
  (Invited talk) "PT Symmetry and Physics with Non-Hermitian," Sanya (China) March 2019

**Honors**

- Dean's List, Spring 2011, IUPUI
- Alpha Sigma Lambda, July 2010
- Golden Key International, December 2009
- Scholars List, Fall 2009, IUPUI
- Dean's List, Fall 2007, Ivy Tech